MB 2026-17

Volcanic-hosted mineral systems and Pinwarian–Grenvillian magmatism in the western Pinware terrane, Grenville Province, Québec: Part 2, geochronology

Documents complémentaires

Additional Files





Licence



License

Cette première page a été ajoutée au document et ne fait pas partie du rapport tel que soumis par les auteurs.

Ressources naturelles et Forêts
Québec



Volcanic-hosted mineral systems and Pinwarian–Grenvillian magmatism in the western Pinware terrane, Grenville Province, Québec: Part 2, geochronology

Louise Corriveau, Anne-Laure Bonnet et Isabelle Lafrance

MB 2026-17

Québec

Avertissement

Ce document est une copie fidèle du manuscrit soumis par l'auteur, sauf pour une vérification sommaire destinée à assurer une qualité convenable de diffusion.

Volcanic-hosted mineral systems and Pinwarian–Grenvillian magmatism in the western Pinware terrane, Grenville Province, Québec: Part 2, geochronology

Louise Corriveau (Geological Survey of Canada, Natural Resources Canada), Anne-Laure Bonnet (Polytechnique Montréal), Isabelle Lafrance (Ministère des Ressources naturelles et des Forêts, Québec)

Recommended citation: Corriveau, L., Bonnet, A.-L., and Lafrance, I., 2026, Volcanic-hosted mineral systems and Pinwarian–Grenvillian magmatism in the western Pinware terrane, Grenville Province, Québec: Part 2, geochronology: Ministère des Ressources naturelles et des Forêts, Québec, MB-2026-17, 78 p.

ABSTRACT

The Pinware continental magmatic arc in the eastern Grenville Province of Québec comprises extensive hydrothermal systems within thin, partly dismembered volcano-sedimentary basins interpreted as the southeastern extension of the Wakeham Group. Their 1.51 Ga supracrustal sequences have been metamorphosed up to granulite facies and intruded by a large, multi-phase granitic to granodioritic batholith whose Pinwarian ages remained to be confirmed. An older belt of tonalitic to dioritic orthogneisses outcrops farthest south along the coast and the archipelagos, as do sporadic plutons inland.

This report publishes legacy U-Pb geochronological data from an argillic-altered lapillistone, a hydrothermally altered amphibolite, a metagabbroic amphibolite and an aluminous gneiss of uncertain origin in the La Romaine supracrustal belt. A series of granitoids across the study area, from D'Auteuil Lake through La Romaine and to Baie des Loups, and the Musquaro mafic-ultramafic layered intrusion were also dated.

Four plutonic units at Musquaro and D'Auteuil lakes yielded U-Pb zircon ages of 1505 ± 12 Ma, 1499.8 ± 6.1 Ma, 1497 ± 12 Ma and 1494 ± 12 Ma. These ages overlap previously reported ages of 1511 Ma to 1491 Ma obtained on their metavolcanic hosts. To the southeast, in the La Romaine area, an age of 1502 ± 22 Ma on a least-altered lapillistone further supports broadly coeval volcanic activity in the La Romaine supracrustal belt, the Musquaro-D'Auteuil sector and the intervening Coude Complex north-west of Kegaska. The maximum age of 1516.0 ± 6.9 Ma for hydrothermal activity obtained from an argillic altered lapillistone, and the Pinwarian age of granitoids that host enclaves of hydrothermally altered units, indicate that the hydrothermal activity is Pinwarian. In the La Romaine supracrustal belt, both dated amphibolites contain spongy, inclusion-rich zircons anomalously rich in uranium that are typical of zircon growth in a hydrothermal environment. Their ages were reset, yielding dates in the 1325 Ma to 1032 Ma range, none of which provides a crystallization age.

At La Romaine, igneous zircon ages of 1502 +9/-8 Ma and 1487 ± 19 Ma from granitic to granodioritic gneisses further support field and geochemical data for coeval plutonism and volcanism. The age range of the Musquaro-La Romaine granitoids falls within the currently documented 1.51–1.46 Ga age range of Pinwarian granitoids in the Grenville Province. The 1529 +7/-6 Ma U-Pb age obtained on the laterally extensive belt of tonalitic gneiss with interference fold patterns south of the La Romaine supracrustal belt and a recently published age of 1582 Ma for a tonalitic gneiss north-west of the belt records Wakamian magmatism.

No rocks of Labradorian age have been found yet in the area. The presence of zircon xenocrysts in the 1660–1554 Ma range and peaking at 1.59 Ga as well as Nd model ages indicate that the western Pinwarian continental magmatic arc was built on Labradorian and Wakamian crust.

Along the coast, the sub-vertically layered ultramafic-to-mafic Musquaro intrusion yielded an age of 1063 ± 13 Ma while a large granitic dyke yielded an age of 1031 ± 8 Ma. U-Pb SHRIMP analysis of metamorphic zircons and U-Pb TIMS analyses of metamorphic titanites and monazites yielded Grenvillian ages between 1.06 to 0.99 Ga.

RÉSUMÉ

L'arc magmatique continental de Pinware, dans l'est de la Province de Grenville au Québec, renferme un vaste système hydrothermal au sein de bassins volcano-sédimentaires étroits et partiellement démantelés interprétés comme la poursuite vers le sud-est du Groupe de Wakeham. Ces séquences, datées à 1,51 Ga, ont subi un métamorphisme atteignant le faciès des granulites et ont été recoupées par un vaste batholite granitique à granodioritique multiphasé dont l'âge pinwarien reste à confirmer. Une ceinture d'orthogneiss tonalitiques à dioritiques, antérieure au dépôt des roches supracrustales, affleure plus au sud, le long de la côte du golfe du Saint-Laurent et dans les archipels, ainsi qu'à l'intérieur des terres.

Ce rapport présente des données de géochronologie U-Pb inédites provenant d'échantillons de lapillistone peu altéré, de lapillistone avec altération argileuse, d'amphibolite ayant subi une altération hydrothermale, d'amphibolite métagabbroïque et de gneiss alumineux d'origine incertaine de la ceinture supracrustale de La Romaine. Une variété de granitoïdes de la zone d'étude, du lac D'Auteuil à La Romaine jusqu'à la baie des Loups, ainsi que l'intrusion litée mafique-ultramafique de Musquaro ont aussi été datées.

Quatre unités plutoniques de la région des lacs Musquaro et D'Auteuil ont livré des âges U-Pb sur zircons de 1505 ±12 Ma, 1499,8 ±6,1 Ma, 1497 ±12 Ma et 1494 ±12 Ma. Ces âges sont similaires à ceux compris entre 1511 Ma et 1491 Ma obtenus antérieurement pour les roches métavolcaniques encaissantes de ces intrusions. Plus au sud-est, dans la région de La Romaine, un âge de 1502 ±22 Ma provenant d'un lapillistone peu altéré semble démontrer que le volcanisme dans la ceinture supracrustale de La Romaine et le secteur de Musquaro–D'Auteuil, ainsi que dans le Complexe de Coude, situé au nord-ouest de Kegaska, entre ces deux secteurs, sont contemporains. L'âge de 1516,0 ± 6,9 Ma d'un lapillistone altéré fournit une limite d'âge supérieure à l'activité hydrothermale. Cette contrainte, combinée aux âges pinwariens des granitoïdes contenant des enclaves de roches altérées, indique que cette activité est pinwarienne. Dans la ceinture supracrustale de La Romaine, deux échantillons d'amphibolite contiennent des zircons spongieux, anormalement riches en uranium et en inclusions, caractéristiques d'une croissance en contexte hydrothermal. Aucun de ces échantillons n'a fourni d'âge de cristallisation, mais les données démontrent que les âges ont été réinitialisés entre 1325 et 1029 Ma.

À La Romaine, les âges des zircons ignés compris entre 1502 +9/-8 Ma et 1487 ±19 Ma des gneiss granitiques à granodioritiques corroborent les données de terrain et de lithogéochimie qui indiquent que le plutonisme et le volcanisme sont en partie contemporains. Les âges des granitoïdes de Musquaro-La Romaine s'inscrivent dans la fourchette d'âges de 1,51 à 1,46 Ga des granitoïdes pinwariens de la Province de Grenville. L'âge U-Pb de 1529 +7/-6 Ma obtenu pour la ceinture de gneiss tonalitiques au sud de la ceinture supracrustale de La Romaine et un âge récemment publié de 1582 Ma pour un gneiss tonalitique au nord-ouest mettent en évidence l'existence d'un magmatisme wakamien dans la région.

Aucune unité d'âge labradorien n'a encore été reconnue dans la région. La présence de xénocristaux de zircon, dont les âges s'échelonnent principalement entre 1660 et 1554 Ma avec un mode à 1,59 Ga, ainsi que les âges modèles Nd indiquent que la portion occidentale de l'arc magmatique continental pinwarien s'est édifié sur une croûte labradorienne et wakamienne.

Le long de la côte du golfe du Saint-Laurent, l'intrusion ultramafique à mafique de Musquaro, caractérisée par un litage subvertical, a été datée à 1063 ±13 Ma, tandis qu'un large dyke granitique a été daté à 1031 ±8 Ma. Les analyses U-Pb SHRIMP réalisées sur des zircons métamorphiques et les analyses U-Pb TIMS de titanites et monazites métamorphiques ont livré des âges grenvilliens compris entre 1,06 et 0,99 Ga.

1. Introduction

Between 2000 and 2009, the Geological Survey of Canada conducted a geological transect eastward from the Wakeham Group through its extension into restricted and partly dismembered volcano-sedimentary basins of the Pinware terrane in the eastern Grenville Province of Québec (Fig. 1). The project took place under the Targeted Geoscience Initiative (TGI) program of Natural Resources Canada in collaboration with academia and the ministère des Ressources naturelles et des Forêts du Québec. The geology of the study area is provided in the complementary Part 1 report (Corriveau et al., 2026) and summarized herein and in Figure 2.

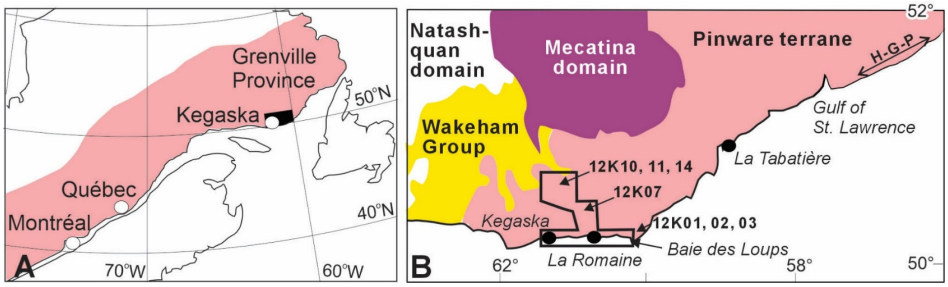


Figure 1. The Wakeham Group and its extension into the Musquaro-D'Auteuil lakes area in the western Pinware terrane (Gobeil et al., 2003; Corriveau and Bonnet, 2005). **A.** Location of the studied area in the Grenville Province. **B.** Location of the studied area in the western Pinware terrane. H-G-P: Geochronological transect by Heaman et al. (2004) along the coast, between longitudes 58°W and 56°W.

During the TGI project, in addition to the geochronological data published by van Breemen and Corriveau (2005), Dr. Otto van Breemen dated eight granitoids and orthogneisses, two lapillistones (one least-altered, the other significantly hydrothermally altered), one aluminous gneiss interpreted as a metapelite, two hydrothermally altered mafic units and one late-stage gabbro. The results were written up in an unpublished manuscript. Additional samples were also dated and written up in the unpublished manuscript of Bonnet et al. (2009) in the second author's PhD thesis. These rocks belong to the former *Aguanish complex* (Fig. 2; Gobeil et al., 2003; Corriveau and Bonnet, 2005; Bonnet, 2009) and to the La Romaine supracrustal belt (Corriveau and Bonnet, 2005). The original key references for the geochronological data processing and interpretation have been kept as reported in the preliminary manuscripts, acknowledging that a lot more research in U-Pb geochronology, especially on hydrothermal zircon is now available. The U-Pb analyses were carried out by isotope dilution-thermal ionization mass spectrometry (ID-TIMS) on zircon, monazite and titanite and by sensitive high-resolution ion microprobe (SHRIMP) on zircon. The legacy data provided herein are linked with previously published ages and the geochronological and geological data of Lafrance and Daoudene (2024), Daoudene and Lafrance (2025), David et al. (2026a, b), Lafrance et al. (2026) and Rochín-Bañaga and Davis (in press).

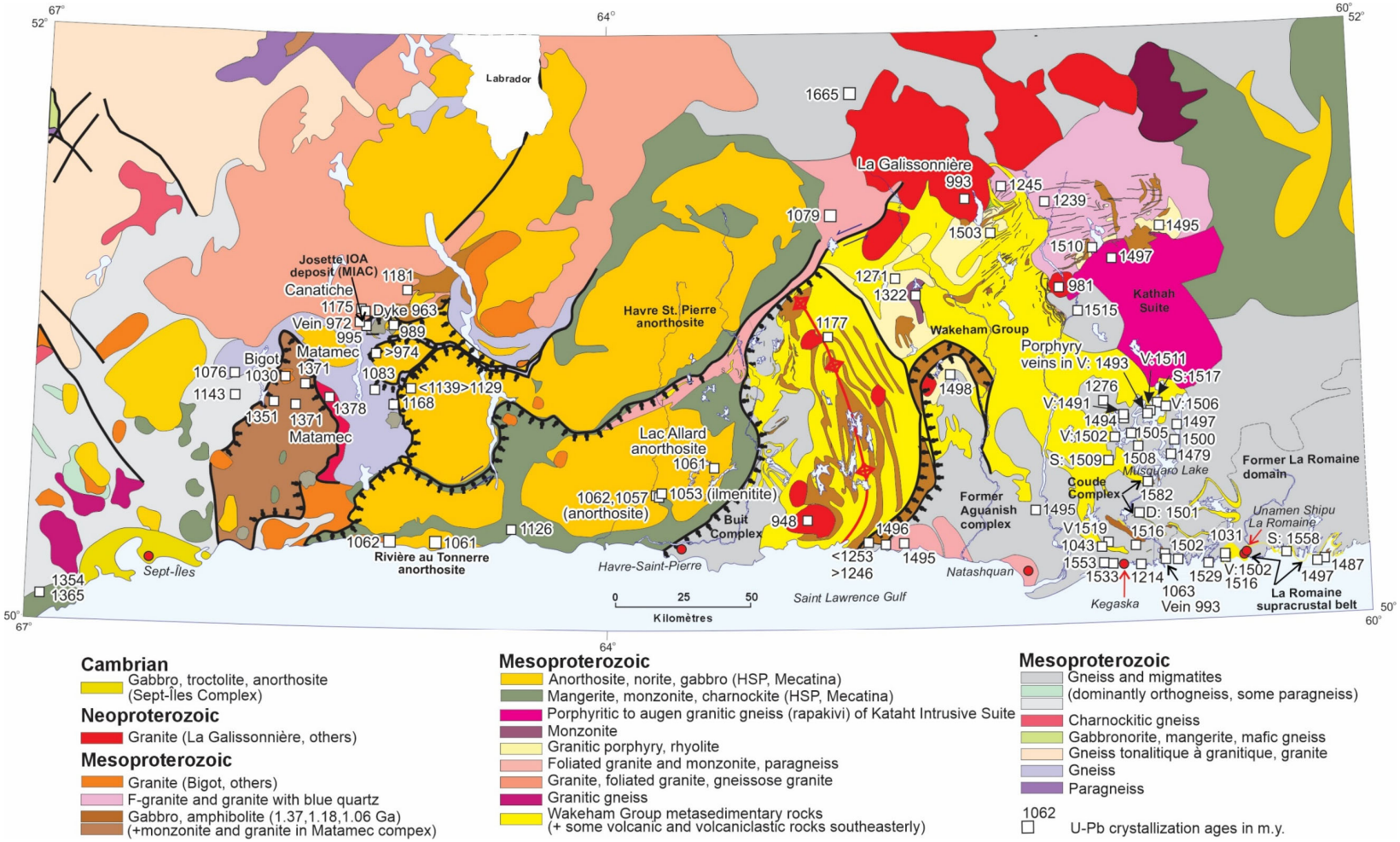


Figure 2. Simplified geological map of the Sept-Îles to Baie des Loups area modified and expanded from Figures 3 of Gobeil et al. (2003) and Wodicka et al. (2003) published in the appendix of Brisebois and Clark (2003). V and S: volcanic/volcaniclastic and sedimentary rocks dated. Ages are from Fowler and Doig (1983); Loveridge (1986); Emslie and Hunt (1990); Martignole et al. (1992, 1994); Indares and Martignole (1993); van Breemen and Higgins (1993); Clark and Machado (1995); Madore et al. (1997a, b); Verpaelst et al. (1997a, b); Chevé et al. (1999, 2001); Gobeil et al. (1999); Wodicka et al. (2003); van Breemen and Corriveau (2005); Morisset et al. (2009); David et al. (2026a, b); Rochín-Bañaga and Davis (in press); and the present study.

This complementary Part 2 geochronological report to Corriveau et al. (2026) throws light on the age of the Pinwarian continental intra-arc magmatism documented in the western Pinware terrane by Corriveau and Bonnet (2005), Bonnet et al. (2005) and Lafrance et al. (2026). Age constraints are placed on a broad zone of Pinwarian magmatic rocks along the north shore of the St. Lawrence Gulf and at Musquaro and D'Auteuil lakes in Québec, Canada. The nature of the substrate is investigated by dating zircon xenocrysts and obtaining Nd isotopic data from igneous rocks. We also place age constraints on the regional Grenvillian magmatism and metamorphism. The maps presented in this report retain the lithological and stratigraphic nomenclature used during the original fieldwork (Bonnet and Corriveau, 2009; Corriveau and Bonnet 2009a–c) and described in Corriveau et al. (2026); subsequent MRNF mapping has revised the assignment and subdivision of several supracrustal and intrusive units, as discussed below and in Corriveau et al. (2026).

2. Geological Summary and Previous Geochronology

2.1. The Wakeham Group and its Southeastern Extension at Musquaro and D'Auteuil Lakes

The dominantly arenaceous Wakeham Group metasedimentary rocks (Fig. 2) provide the main tectonostratigraphic marker in the Natashquan domain (Gobeil et al., 2003) of the western Pinware terrane. The time of deposition of the sediments —within the main outcrop of the Group and at least for part of the succession— had been bracketed between 1630 Ma and 1500 Ma (Wodicka et al., 2003). Metamorphism of the Wakeham Group increases from greenschist facies near the centre of the Group, to amphibolite facies along the margin of the Group.

The history of definitions of the Wakeham Group is available in a MRNF lexicon (MRNF a). The description of its southeastern volcanosedimentary extension in the D'Auteuil and Musquaro lakes region is provided by Corriveau and Bonnet (2001, 2005), Corriveau et al. (2002, 2003, 2026), Bonnet and Corriveau (2003), Bonnet et al. (2005, 2009), Bonnet (2009) and Lafrance et al. (2026). Units representing the potential extension of the Wakeham Group as lenses within the dominant granitoids and orthogneisses of the Kegaska region (12K03) have been assigned to the Coude Complex (Lafrance and Daoudene, 2024). Lafrance et al. (2026) extended the Coude Complex to the D'Auteuil and Musquaro lakes region to comply with the North American Stratigraphic Code. Supracrustal rocks in this sector were dated by van Breemen and Corriveau (2005), David et al. (2026a, b), Rochín-Bañaga and Davis (in press) and herein.

During the TGI project, Pinwarian volcanism was identified in the southeastern extension of the Wakeham Group at Musquaro and D'Auteuil lakes (Fig. 3) (Corriveau and Bonnet, 2001, 2005; Corriveau et al., 2002). The oldest ages are from intermediate lapillistones (samples CQA-00-111P and CQA-00-1032M) at Musquaro Lake and a felsic volcanic rock slightly north of Kegaska (sample 23-IL-3135-B). Both are associated with the sedimentary rocks in their vicinity. In contrast younger felsic volcanic and volcaniclastic rocks —specifically, an ash tuff (CQA-00-295A) and a banded rhyolite (sample CQA-00-273A)— are younger and not associated with exposed sedimentary rocks. A rhyolite is also cut by an intricate network of anastomosing porphyry veins with an age of 1497 +15/-9 Ma interpreted as marking the end of volcanism in the region (sample CQA-00-105; van Breemen and Corriveau, 2005; illustrated in the discussion section).

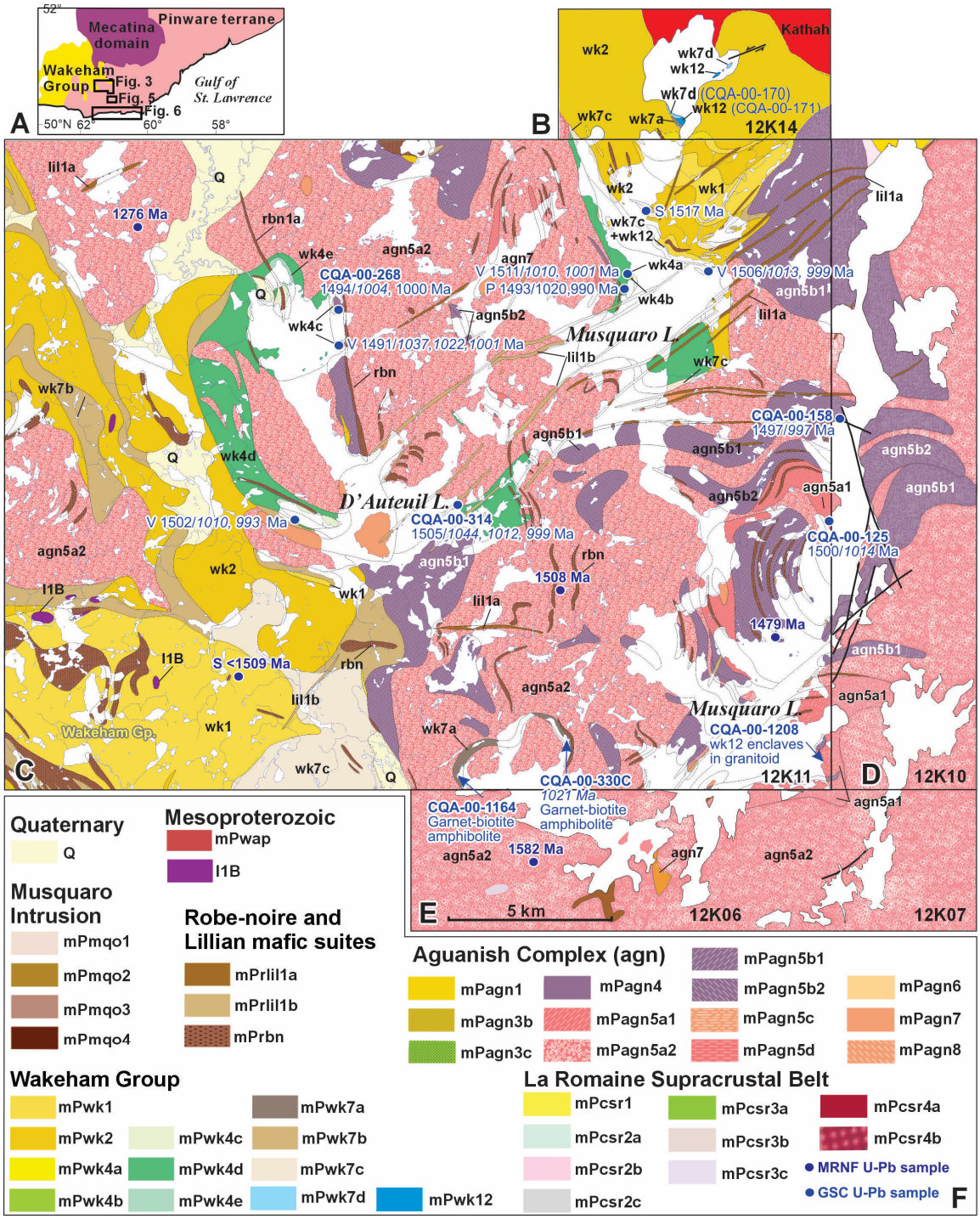


Figure 3. Geological map of the metamorphosed extension of the Wakeham Group into the Musquaro-D'Auteuil lakes area. The map units are listed and described in Appendix 1 and in Corriveau et al. (2026). **A.** Location of the study area. **B.** Geology of NTS map sheet 12K14. **C.** Geology of the NTS map sheet 12K11. **D.** Geology of the NTS map sheet 12K10. **E.** Geology of the NTS map sheet 12K07. **F.** Legend for the Wakeham Group (mPwk) as applied to its extension in the Musquaro and D'Auteuil lakes area, the La Romaine supracrustal belt (mPcsr), the *Aguanish complex* (mPagn), the Lillian and Robe Noire suites (mPlil and mPrbn), the Musquaro mafic-ultramafic intrusion (mPmqo), the Wapitagun intrusion (mPwap) and the Quaternary sediments (Q).

At Musquaro Lake, field relationships described by van Breemen and Corriveau (2005) suggest that the volcanic rocks are slightly younger than the stratigraphically underlying metasedimentary units (see stratigraphic sections in Corriveau and Bonnet, 2001, also reproduced as Figure 4 in Corriveau et al., 2026). A sedimentary rock at outcrop CQA-00-006 dated by van Breemen and Corriveau (2005) has a maximum age of deposition of 1517 Ma. Within analytical uncertainties, this age overlaps the age range of the stratigraphically higher volcanic succession, constrained between 1519 and 1491 Ma by U-Pb zircon in that sector (van Breemen and Corriveau, 2005; David et al., 2026a). A maximum deposition age of 1509 Ma was obtained on a sedimentary sample from the D'Auteuil Lake area (Fig. 3C); this age indicates that the relationship between sedimentation and volcanism may not be uniform throughout the supracrustal succession (Lafrance et al., 2026). It should be noted that in the data table of van Breemen and Corriveau (2005) for sample CQA-00-006, two detrital zircon analysis yielded an age of 1491 Ma. These analyses were considered too imprecise (1σ at 10 and 11 Ma) to be interpreted in isolation as the maximum age of sediment deposition. These analyses were thus grouped with other young zircons to obtain the more robust maximum depositional age of 1517 Ma (see Table 2 in van Breemen and Corriveau, 2005). In this sample, the age spectrum of the detrital zircons is dominated by Paleoproterozoic populations (~1.95 to 1.75 Ga, including a population of metamorphic zircons dated at 1864 ± 17 Ma. Neo- and Mesoarchean zircon populations also occur in the 2280–2520 Ma and 2647–2744 Ma ranges respectively. Only one Labradorian age, at 1621 Ma, was identified in this sample.

Metamorphism reaches mid- to upper-amphibolite facies in the Musquaro-D'Auteuil lakes area (Bonnet, 2009; Corriveau et al., 2026; Lafrance et al., 2026).

2.2. The La Romaine Supracrustal Belt

To the southeast, a Cu-mineralized, ≤10 km wide by >60 km long Pinwarian 1.5 Ga continental intra-arc volcano-sedimentary belt, the La Romaine supracrustal belt was identified from Kegaska to Baie des Loups (Figs. 4, 5). The La Romaine supracrustal belt was first identified by Corriveau et al. (2003) and defined by Corriveau and Bonnet (2005). It was renamed the La Romaine Complex by Daoudene and Lafrance (2025). The belt is surrounded by the rocks of the *Aguanish complex* that prevail along the St-Lawrence Gulf coast (Fig. 4).

The stratigraphic sequence of the belt consists, from the base to the top, of metasedimentary rocks (meta-arenite, calc-silicate rocks and aluminous gneiss of uncertain origin), felsic-dominated volcanic, felsic to intermediate volcaniclastic rocks, and a composite amphibolite unit. Lapilli- and bomb-size fragments with a pumiceous texture are abundant in the volcaniclastic units and accretionary lapilli and shattered lapilli occur locally (Corriveau et al., 2002, 2026; Corriveau and Bonnet, 2005). The composite amphibolite unit has a significant lateral extension forming a narrow zone of layers concordant with the regional structural grain. It is interpreted as volcanic-related and polygenic, with volcanic flows, metagabbroic sills and amphibolite of uncertain intrusive or extrusive origin (Corriveau and Bonnet, 2005). A cogenetic relationship is indicated also by the similar calc-alkaline arc-like affinity of the felsic-to-mafic volcanic rocks, suggesting fractional crystallization from a common parental magma (Bonnet et al., 2005). Metagabbros from the composite amphibolite unit have a higher degree of alkalinity from that of the felsic to mafic metavolcanic rocks and display within-plate affinity (Bonnet et al., 2005). Field relationship suggests that the metagabbros are coeval or slightly younger than the 1.5 Ga arc-related magmatic activity (Bonnet et al., 2005).

Ages are presented in this report for two lapillistones, one least-altered and one pervasively affected by argillic alteration; two amphibolite one interpreted as a potential mafic lava replaced

by high-temperature Ca-Fe alteration; and one metagabbro. In addition, the MRNF dated one paragneiss to the east of La Romaine (Fig. 4D). Additional volcano-sedimentary rocks have been characterized between the Musquaro-D'Auteuil lakes area and the La Romaine supracrustal belt and have been grouped within the Coude Complex (Fig. 2) by Lafrance and Daoudene (2024) and Lafrance et al. (2026).

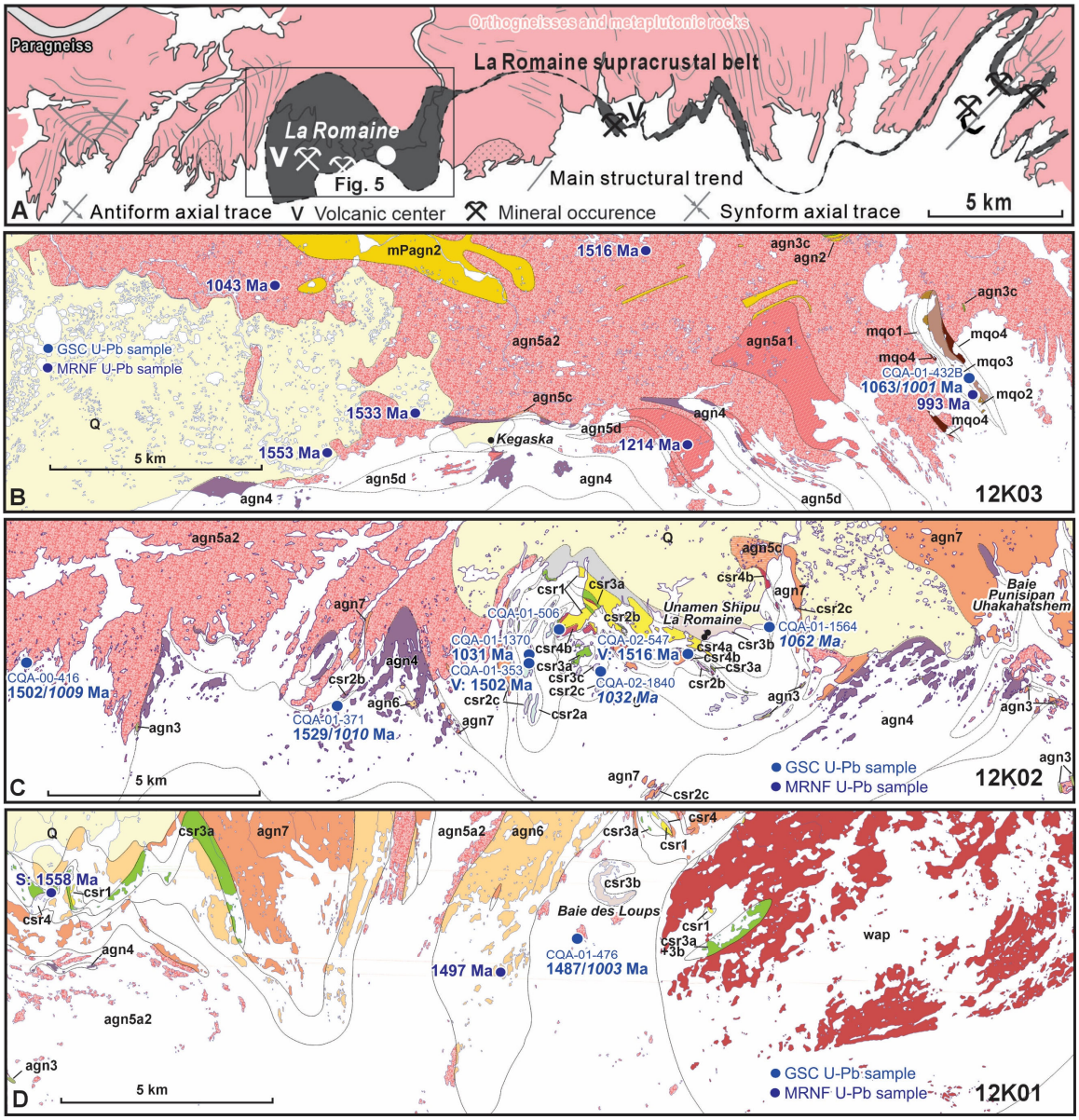


Figure 4. Geology of the Kegaska, La Romaine-Unamen Shipu, Baie Punisipan Uhakahatshem and Baie des Loups areas mapped along the shore of the St Lawrence Gulf and in the archipelago during the TGI project. The map units are listed and described in Appendix 1 and in Corriveau et al. (2026). **A.** Location of the La Romaine supracrustal belt and structural interpretation of the area for the TGI project. **B.** Geology of NTS map sheet 12K03 in the Kegaska area as mapped by Bonnet and Corriveau (2009). **C.** Geology of NTS map sheet 12K02 in the La Romaine area as mapped by Corriveau and Bonnet (2009b). The map sheet includes the main outcrop of the La Romaine supracrustal belt (see Fig. 5). V and S: volcanic/volcaniclastic and sedimentary rocks dated. **D.** Geology of NTS map sheet 12K01 in the Baie des Loups area as mapped by Corriveau and Bonnet (2009a).

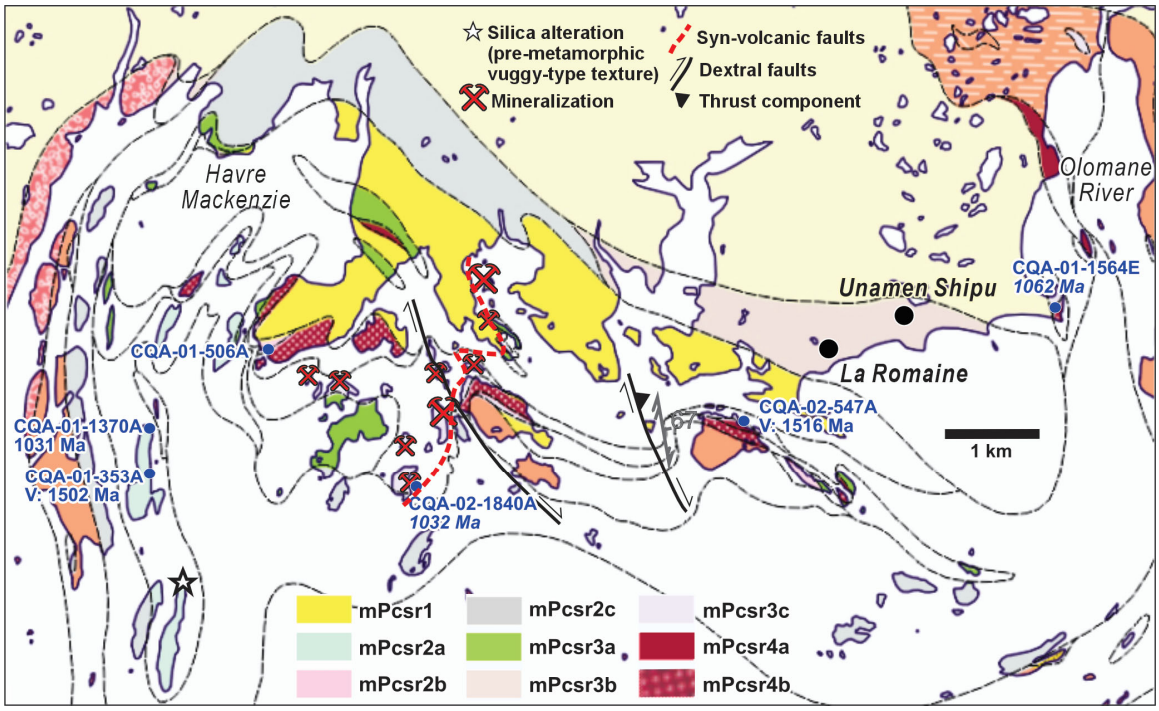


Figure 5. Geology of the La Romaine supracrustal belt in NTS map sheet 12K02, in the La Romaine area, as mapped by Corriveau and Bonnet (2005, 2009b) and Bonnet and Corriveau (2003). Localized mineralization is described in Corriveau et al. (2003), Bonnet (2009) and in section 3.5.7 of Corriveau et al. (2026). U-Pb geochronology samples are listed with their crystallization age in bold normal and their metamorphic age in bold italic; V is for the volcaniclastic rocks dated.

2.3. The Hydrothermal System at La Romaine

The La Romaine supracrustal belt, the volcanic center at Musquaro and D'Auteuil lakes and the additional volcano-sedimentary units of the Coude Complex between these two areas are extensively hydrothermally altered and form large-scale mineral systems (Corriveau and Bonnet, 2005; Corriveau et al., 2026; Lafrance et al., 2026). A high-sulphidation volcanic-hosted massive sulphide deposit model has been proposed by Bonnet et al. (2005). Renewed mapping has significantly expanded the understanding of the hydrothermal alteration in the Musquaro-D'Auteuil lakes area (Lafrance et al., 2026). Regionally, alteration consists of albitization, high-temperature Ca-Fe, Ca-K-Fe and K-Fe alteration, widespread sericitic, argillic and advanced argillic alteration and localized silicic alteration (Bonnet et al., 2005; Bonnet, 2009; Lafrance and Daoudene, 2024; Corriveau et al., 2026; Lafrance et al., 2026). A metasomatic iron and alkali-calcic (MIAC) mineral system model may explain this range of alteration types (Corriveau et al., 2026; Lafrance et al., 2026) but a high-sulphidation mineral system cannot be discarded entirely as discussed in Corriveau et al. (2026).

At La Romaine, the quartzofeldspathic gneisses interpreted as rhyolitic tuffs have quartz-muscovite-sillimanite-iron oxide nodules and veins derived from sericitic alteration. None were dated. A migmatized aluminous gneiss with well-preserved volcanic fragments was dated (CQA-02-547A); its protolith is an argillic-altered lapillistone. Grey lapilli tuffs with discontinuous trains of quartz and cordierite correspond to extreme advanced argillic alteration leading to vuggy silica (not dated). Heterogeneous layered packages of ironstone, metacarbonate and calc-silicate rock, garnetite, diopsidite, epidosite and sulphide-bearing or magnetite- and magnetite-biotite-rich amphibolite derived from Ca-Fe and K-Fe alteration are closely associated with copper sulphide

mineralization (Corriveau et al., 2026). These heterogeneous units are the altered equivalents of calc-alkaline metavolcanic rocks and metagabbro of within-plate affinity (Bonnet et al., 2005).

The Ca-Fe alteration zone is cut by centimetre-wide, anastomosing veins of fluorite-bearing calc-silicate rocks. Fluids involved in the formation of the various alteration zones have been interpreted as F-rich, hot and strongly acidic to neutral (Bonnet et al., 2005). Leaching zones (argillic alteration and vuggy silica alteration) occurred preferentially within felsic to intermediate metavolcaniclastic rocks in the central part of the volcanic centre. The fluid discharge is achieved along contact zones between the permeable volcaniclastic units and the impermeable layer of composite amphibolite unit with the mafic lava flows and gabbroic sills acting as a physical cap (Bonnet et al., 2005).

2.4. Pinwarian Metaplutonic Rocks

The supracrustal rocks occur among Pinwarian sub-volcanic felsic porphyritic intrusions and granitic to granodioritic intrusions of coeval to slightly younger age, all of which are of calc-alkaline affinity (Bonnet et al., 2005; Corriveau and Bonnet, 2005). These belong to the former *Aguanish complex* defined by Gobeil et al. (2003) and extended eastward by Corriveau and Bonnet (2005). They were mapped according to the subdivision in use at the time (Appendix 1; Figs. 2–5).

The following ages for metaplutonic rocks within this complex were available prior to this study and the studies by Lafrance and Daoudene (2024), Daoudene and Lafrance (2025) and Lafrance et al. (2026): 1495 ± 2 Ma for a granitic gneiss (Clark and Machado, 1995), 1496 +8/-7 Ma for a granitic orthogneiss (Wodicka et al., 2003) and 1498 ± 3 Ma for a porphyritic granite that cuts the sedimentary rocks of the Wakeham Group (Wodicka et al., 2003); they are reported in Figure 2.

Along the northern margin of the Wakeham Group, a granitic gneiss of the Boulain igneous complex yielded a U-Pb age of 1515 ± 30 Ma (Wodicka et al., 2003), while three porphyries and a rapakivi granite of the hypabyssal Kataht felsic igneous suite yielded ages between 1510 Ma and 1495 Ma (Wodicka et al., 2003), including one dated at 1503 +6/-4 Ma that cuts the sedimentary rocks of the Wakeham Group. Younger granites along the northern margin of the Wakeham Group and within it, yielded ages of 1245 ± 3 Ma and 1239 ± 3 Ma (Martignole et al., 1994), 1322 ± 7 Ma (Martignole et al., 1992) and 1271 +13/-3 Ma (Loveridge, 1986). These ages are reported in Figure 2.

In the Musquaro-D'Auteuil lakes, Kegaska and Coacoachou Lake regions, the *Aguanish complex* was mapped at a scale of 1:50,000 by Lafrance and Daoudene (2024), Daoudene and Lafrance (2025) and Lafrance et al. (2026). This work led to the definition or revision of several metaplutonic lithodemic units, including the L'Aigle Complex (1582 Ma); the D'Auteuil (1494 Ma), Kegaska (~1553–1529 Ma), Marie-Claire (1505–1479 Ma), Grand Priant (1502 Ma), Coacoachou (1497–1487 Ma), Blacklands, Foucher (1494–1487 Ma), Coconipi, Mantuh (~1088 Ma), Musquanousse, Wapitagun (1053 Ma) and Washicoutai (1043–1031 Ma) intrusive suites; the Grand Portage Granodiorite (1499.8 Ma); and the Grozieux (1516 Ma), Dabin (1276 Ma), Parsons (1215 Ma) and Mukanipan intrusions (David et al., 2026a, b; Rochín-Bañaga and Davis, in press; this work). These units are described individually in the MRNF stratigraphic lexicons (MRNF b).

The *Aguanish complex*, as mapped between 2000 and 2003 in the study area, grouped all the felsic to intermediate metaplutonic rocks and orthogneisses in the study area as well as the amphibolite dykes, before some of these rocks were recognized as Grenvillian in age, as now documented by David et al. (2026a, b) and Rochín-Bañaga and Davis (in press). The mPagn7 unit described in Appendix 1 differs from the granitic dyke with magmatic layering affiliated with the Washicoutai Intrusive Suite that is dated herein and described in Corriveau et al. (2002, 2026). The thickness of the dykes prevents them from being shown on the maps. In NTS map sheet 12K01, the mPagn7

unit of Corriveau and Bonnet (2009a) was remapped in detail by Daoudene and Lafrance (2025), dated at 1088 Ma, and defined as the Mantuh Intrusive Suite (see also MRNF c).

2.5. Grenvillian Intrusions

The ages of Grenvillian intrusions are reported in Figure 2. In the Musquaro and D'Auteuil sector, amphibolite dykes were mapped and subdivided into the Lillian and Robe Noire suites in Figure 3 and Appendix 1 (see discussion in Corriveau et al., 2026). Gabbro and amphibolite dykes and sills from the Lillian and Robe Noire mafic suites intrude the Wakeham Group and the surrounding Pinwarian plutons and gneiss complexes, masking many contact zones (Verpaelst et al. 1997a, b; Corriveau and Bonnet, 2001; Gobeil et al., 2003). The two suites have nearly identical geochemical signatures (Scherrer, 2003). Although a Robe Noire gabbro sill has been dated at 1177 +5/-4 Ma (Martignole et al., 1994), it is unclear whether this age applies to the entire suite. Several other periods of mafic magmatism are known to occur in the Natashquan and adjacent domains.

Within and along the western margin of the Natashquan domain extends the Buit Complex composed mainly of foliated granite and granite gneiss, for which a 1079 ± 5 Ma zircon age was obtained (Loveridge, 1986). To the west, the Havre St. Pierre anorthosite complex formed in the 1.13–1.06 Ga age range (van Breemen and Higgins, 1993; Wodicka et al., 2003).

The Musquaro ultramafic to mafic, subvertically layered intrusion (NTS map sheet 12K03) was defined, described and subdivided into four main units by Corriveau et al. (2002) and was subsequently explored by Robillard (2003). Lafrance and Daoudene (2024) further mapped the intrusion, took extensive photographs of its field geology and refined the interpretation of previous work. These authors also completed a stratigraphic glossary formally referring to the Musquaro Gabbroic Intrusion (MRNF d). The age of a pegmatitic gabbro coeval with the main intrusion is provided herein. A younger pegmatitic gabbro that sharply cut the intrusion has been dated by the MRNF, and the field geology of this dyke is illustrated herein.

The Wapitagun Intrusion (NTS map sheet 12K01) was defined and mapped by Bourne et al. (1978) and briefly documented during this project along the St Lawrence Gulf coast and on its islands. The intrusion was remapped at 1:50,000 and subdivided into two units by Daoudene and Lafrance (2025) and dated by the MRNF. The Washicoutai Intrusive Suite was mapped as part of the *Aguanish complex* during the TGI project and dated herein. Unfoliated granites were emplaced at 993 ± 3 Ma (Loveridge, 1986) and 981 ± 2 Ma (Wodicka et al., 2003), north and south of the main Wakeham Group outcrop (Fig. 2). These youngest intrusions, part of the La Galissonnière felsic suite, mark the last stage of orogenic activity in the eastern Grenville Province.

2.6. Remaining Questions Addressed Through Geochronology

Despite all the previous U-Pb geochronological dating, questions remained concerning the nature and age of some supracrustal rocks —notably whether zircon populations could help determine if an aluminous gneiss is a metapelite with detrital zircon or a hydrothermally altered volcanic rock with igneous zircons—, and the timing of hydrothermal activity, intrusive events and high-grade metamorphism.

Mapping of the lapillistone units in the La Romaine supracrustal belt showed that with increasing pre-metamorphic sericitic, argillic and advanced argillic hydrothermal alteration, volcanic rocks subsequently metamorphosed under granulite facies conditions became increasingly similar to metapelites (Bonnet et al., 2005). In most cases, atypical mineral abundances facilitated the identification of hydrothermally altered protoliths based on the identification criteria of Bonnet

and Corriveau (2007a, b) and Corriveau and Spry (2014). In some cases, however, the possibility remained that bona fide metapelites were present or that sedimentary rocks were altered as well.

Zircon morphology and age distribution can provide robust evidence for a volcanic or a sedimentary origin (McFarlane et al., 2007). In addition, new zircon growth and partial zircon dissolution can occur through hydrothermal alteration or metasomatism (Yeats et al., 1996; Hartmann et al., 2000; Hoskin, 2005; Lawrie et al., 2007), including during intense albitization to albitite in MIAC systems (Pelleter et al., 2007; Davis et al., 2011).

U-Pb Sensitive High Resolution Ion MicroProbe (SHRIMP) geochronology of hydrothermally altered rocks is a powerful technique for dating the internal components of zircon grains and thereby clarifying the geological history and constraining genetic models of ore formation in high-grade metamorphic terranes (Claoué-Long et al., 1990; Yeats et al., 1996; Williams, 1998; Hartmann et al., 2000; Giles and Nutman, 2003). In the present case, it can help more precisely constrain the timing of hydrothermal activity. Field relationships indicate that this activity was coeval with or slightly postdated volcanism but predated the gneissic intrusions. Acquiring U-Pb dates on such rocks is relatively straightforward but interpreting them in terms of meaningful ages requires detailed investigation of zircon internal structures and compositions together with a well-documented regional temporal framework on which to base their interpretation. This was undertaken on a suite of amphibolite units in the La Romaine supracrustal belt as well as on a K-Fe altered amphibolite dyke at Musquaro Lake.

Near the Québec and Labrador border (Fig. 1), the Pinwarian continental magmatic arc was emplaced into mid- to late-Labradorian granitic to granodioritic granitoids and orthogneisses with local supracrustal rocks along the coast of the St Lawrence Gulf. In that area, the Pinware terrane also hosts Paleo- or Mesoproterozoic mafic intrusions as well as late- to post-Grenvillian mafic and felsic intrusions (Wasteneys et al., 1997; Heaman et al., 2004). As both Pinwarian and Labradorian rocks occur throughout the Grenville Province (Indares et al., 2022), an important question was how far west Labradorian crust is exposed within the Pinware terrane of the eastern Grenville Province. Resolving this question required extensive U-Pb geochronology because the Labradorian and Pinwarian granitoids are notoriously similar in Labrador and could easily have been overlooked in the study area.

3. U–Pb Geochronology: Methods and Results

U-Pb geochronology is presented from nine intrusive units of the *Aguanish complex* across the study area, one amphibolite interpreted as a K-Fe altered mafic dyke at Musquaro Lake, and one metagabbro sill, one amphibolite interpreted as a Ca-Fe and K-Fe altered mafic lava, two volcaniclastic rocks, one argillic altered, and one aluminous gneiss of uncertain origin from the La Romaine supracrustal belt. Sample coordinates in NAD 83 UTM zone 20 are provided for each sample dated. The full dataset is provided in the Supplementary file.

The representative samples were collected, broken into small pieces and bagged at the sampled outcrop to avoid contamination. The samples were then crushed and the minerals separated at the Geochronology Laboratories of the Geological Survey of Canada (Ottawa, Ontario) using standard crushing, grinding, and separation on a Wilfley™ table and by heavy liquid techniques. Mineral separates were sorted by magnetic susceptibility using a Frantz™ isodynamic separator, then hand-picked using a binocular microscope and analyzed using an scanning electron microscope (SEM) and imaged using a secondary backscattered electron mode.

In most cases, zircons were first analyzed using U-Pb ID-TIMS (Isotope Dilution-Thermal Ionization Mass Spectrometry) techniques, but because of their complexity, it was not always possible to obtain precise ages, and these samples were reanalyzed using U-Pb SHRIMP (Sensitive High Resolution Ion Microprobe) techniques, which provide better spatial resolution at the grain scale. Titanite and monazite analyses reported from these samples were performed using ID-TIMS techniques. Zircon morphology, internal zoning and core-rim relationships were used to distinguish between igneous and metamorphic origins (cf. Poldervaart, 1956; van Breemen et al., 1986; Vavra et al., 1999; Corfu et al., 2003; Hoskin and Schaltegger, 2003). Th/U ratios also provided a guide to the zircon growth environment when interpreting geochronological results. Values in the range of 0.1 to 1 are typical of igneous zircons from most source rock types and crystallization environments, except for carbonatites and nepheline syenite, for which the ratios can reach 100 to 1000 (Belousova et al., 2002). Th/U ratios below 0.07 are generally indicative of metamorphic zircon or zircon grown in equilibrium with partial melts or leucosomes (Williams and Claesson, 1987; Rubatto, 2002); Th/U ratios may increase under granulite-facies conditions to values characteristic of many igneous zircons (Vavra et al., 1999). Low Th/U ratios (below 1) can also occur at the lower range of values of some S-type granites (Artemieva et al., 2017; Regelous et al., 2021).

3.1. TIMS Techniques and Data

Isotope dilution and thermal ionisation techniques for measuring U–Pb isotopes in zircon at the Geological Survey of Canada are summarized by Parrish et al. (1987) and are based on Krogh (1973). Prior to analysis, all zircon fractions were strongly abraded until the crystals assumed a well-rounded shape (Krogh, 1982). Abrasion was used to minimize the effects of peripheral lead loss and/or to remove rims inferred to have grown during later metamorphism. Mass spectrometry, data reduction, and the propagation of analytical uncertainties of the relevant components used in calculating isotopic ratios and ages followed the numerical procedure of Roddick (1987). A modified form of York's (1969) method for linear regression analysis was used (see Parrish et al., 1987). U–Pb TIMS isotopic data are presented in Table 1 and plotted on concordia diagrams using a $^{238}U/^{235}U$ ratio of 137.88.

All TIMS age uncertainties are given at the 95% confidence level. U-Pb TIMS ages for zircon are defined by the intercepts of discordia lines with concordia. For titanite analyses, the $^{206}Pb/^{238}U$ ages are generally presented, as these ages are considered likely to be least sensitive to common Pb corrections. If the analysis is discordant, however, the $^{207}Pb/^{206}Pb$ age is used. For monazite, the $^{207}Pb/^{235}U$ model age is chosen because of the possibility that the $^{206}Pb/^{238}U$ age is affected by unsupported ^{206}Pb (Schärer, 1984).

3.2. SHRIMP Techniques and Data

For U–Pb analysis using the Geological Survey of Canada SHRIMP facility, approximately 150 grains were selected at random from the least-magnetic fraction, with an average size of approximately 100 microns. Zircon grains were mounted in a 2.5 cm epoxy disk (#IP207) along with fragments of the international SHRIMP zircon standard BR 266. The polished zircons were imaged using a scanning electron microscope (SEM) in secondary backscattered electron or cathodoluminescence mode for the purpose of guiding the placement of ion probe analyses.

Selected areas of the zircons were sputtered using a mass-filtered O_2^- primary beam operating in Kohler mode. Primary beam currents ranged from 2-6 nA, generating elliptical pits of 20 microns in diameter. Pits were <1 micron deep after completion of the 10-minute analyses. Details of

analytical procedures using the SHRIMP II ion microprobe at the Geological Survey of Canada are available in Stern (1997) and Stern and Amelin (2003).

Table 1. U-Pb TIMS isotopic data for zircon, monazite and titanite from Musquaro and D'Auteuil lakes and the transect along the St. Lawrence Gulf coast between Kegaska and Baie des Loups. Spreadsheet in the supplementary file.

Fraction[1]	Wt[2]	U	Pb[3]	$^{206}Pb/^{204}Pb$[4]	Pb[5]	$^{208}Pb/^{206}Pb$[6]	$^{207}Pb/^{235}U$[6]	$^{206}Pb/^{238}U$[6]	$^{207}Pb/^{206}Pb$[6]	$^{207}Pb/^{235}U$[7]	$^{206}Pb/^{238}U$[7]	$^{207}Pb/^{206}Pb$[7]	Disc[8]
	mg	ppm	ppm		pg								
Musquaro and D'Auteuil lakes													
Hornblende-biotite quartz-syenite gneiss (CQA-00-314A; GSC laboratory number 6718)													
T1 (T)	50	234	50	345	375	0.40	1.668±0.50	0.1673±0.16	0.07227±0.41	996.2±6.4	997.4±2.9	994±17	-0.41
T2 (T)	51	224	48	335	379	0.41	1.692±0.59	0.1682±0.16	0.07299±0.49	1005.7±7.5	1002.1±3.0	1014±20	1.22
T3 (T)	112	259	57	475	657	0.44	1.676±0.46	0.1674±0.27	0.07258±0.30	999.3±5.9	998.0±5.1	1002±12	0.45
Porphyritic granite (CQA-00-125A; GSC laboratory number 6719)													
M1 (M)	10	1575	2199	29414	6	8.39	1.716±0.11	0.1703±0.09	0.07307±0.04	1014.4±1.5	1013.7±1.7	1016±2	0.24
M2 (M)	3	1234	1231	14272	3	5.75	1.689±0.12	0.1688±0.10	0.07256±0.05	1004.4±1.5	1005.7±1.8	1002±2	-0.43
M3 (M)	6	2199	2496	11387	11	6.61	1.712±0.11	0.1705±0.09	0.07282±0.05	1012.9±1.5	1014.7±1.7	1009±2	-0.61
Foliated hornblende-biotite granite (CQA-00-158A; GSC laboratory number 6720)													
A1 (Z)	22	73	21	1716	15	0.23	3.257±0.15	0.2549±0.11	0.09266±0.09	1470.8±2.4	1463.7±2.9	1481±3	1.30
A2 (Z)	18	125	33	10262	3	0.18	2.987±0.13	0.2400±0.11	0.09028±0.06	1404.4±2.0	1386.7±2.8	1431±2	3.47
A3 (Z)	17	146	40	7209	5	0.19	3.156±0.12	0.2490±0.09	0.09191±0.05	1446.5±1.8	1433.5±2.3	1466±2	2.44
A4 (Z)	17	179	50	31539	2	0.20	3.167±0.15	0.2501±0.13	0.09184±0.05	1449.2±2.3	1439.0±3.5	1464±2	1.91
T1 (T)	37	115	30	489	97	0.69	1.738±0.39	0.1711±0.16	0.07369±0.31	1022.8±5.1	1018.1±3.0	1033±13	1.55
T2 (T)	35	166	35	575	110	0.35	1.719±0.47	0.1701±0.19	0.07330±0.38	1015.8±6.0	1012.8±3.6	1022±15	0.99
T3 (T)	45	135	26	672	97	0.25	1.718±0.91	0.1695±0.15	0.07351±0.82	1015.4±11.	1009.6±2.9	1028±33	1.93
Augen granitic orthogneiss (CQA-00-268A; GSC laboratory number 6721)													
T1 (T)	43	144	32	228	301	0.48	1.647±0.74	0.1666±0.22	0.07169±0.61	988.5±9.4	993.6±4.0	977±25	-1.81
T2 (T)	44	173	39	212	411	0.48	1.676±0.84	0.1691±0.23	0.07187±0.70	999.3±10.7	1007.1±4.3	982±28	-2.73
T3 (T)	41	158	34	456	155	0.43	1.679±0.39	0.1678±0.16	0.07257±0.31	1000.7±5.0	1000.1±3.0	1002±12	0.20
Transect Kegaska–La Romaine-Unamen Shipu–Baie des Loups													
Multiply folded tonalitic gneiss (CQA-01-371A; GSC laboratory number z7091)													
B1 (Z)	15	176	51	8660	5	0.20	3.323±0.12	0.2576±0.10	0.09357±0.05	1486.5±1.9	1477.4±2.6	1500±2	1.65
C1 (Z)	13	242	66	14926	3	0.17	3.162±0.12	0.2488±0.11	0.09220±0.06	1448.0±1.9	1432.0±2.8	1472±2	2.99
C2 (Z)	15	281	72	15263	1	0.11	3.146±0.13	0.2481±0.10	0.09197±0.04	1444.1±2.0	1428.7±2.7	1467±2	2.89
D1 (Z)	15	227	55	5032	10	0.15	2.794±0.14	0.2289±0.12	0.08856±0.06	1354.1±2.1	1328.5±2.8	1395±2	5.25
Granitic augen/lenticular gneiss (CQA-01-416; GSC laboratory number z7092)													
A1 (Z)	19	158	37	11055	4	0.10	2.797±0.14	0.2298±0.12	0.08826±0.05	1388±2	1333.6±2.9	1354.7±2.1	4.35
B1 (Z)	14	210	46	7037	5	0.09	2.547±0.13	0.2160±0.11	0.08552±0.05	1328±2	1260.6±2.6	1285.5±2.0	5.55
C2 (Z)	12	239	57	6446	6	0.10	2.847±0.14	0.2325±0.11	0.08883±0.05	1400±2	1347.4±2.8	1368.0±2.0	4.20
D1 (Z)	16	153	39	2955	12	0.12	3.039±0.13	0.2431±0.10	0.09067±0.06	1440±2	1402.7±2.5	1417.5±2.0	2.85

[1]N = non-magnetic at a side slope given in degrees on a Frantz isodynamic magnetic separator operating at 1.8 amps; Sizes in μm before abrasion; [2]error on weight = ±1 μg; [3]radiogenic Pb; [4]measured ratio corrected for spike and Pb fractionation of 0.09 ± 0.03 percent per AMU; [5]total common Pb on analysis corrected for fractionation and spike; [6]corrected for blank Pb and U, common Pb, errors quoted are one sigma in percent; [7]age errors quoted are 2 SE in Ma; [8]discordance in per cent along a discordia to origin.

Age estimates and error calculations, mean square of weighted deviates (MSWD) and probability of fit (POF) were calculated using Isoplot/Ex version 2.2 (Ludwig, 2000). U-Pb SHRIMP isotopic data for samples in section 3.3 to 3.12 are presented in Tables 2 and 3 and shown on concordia diagrams. Age uncertainties are given at the 68% confidence level in the tables but are presented at the 95% confidence level in the concordia plots and in the text. Since all the analyses in this study were concordant to slightly discordant, weighted mean $^{207}Pb/^{206}Pb$ ages were used for estimating

ages for zircons older than 1.4 Ga. For zircons younger than 1.1 Ga, which are invariably concordant, weighted mean $^{206}Pb/^{238}U$ age were used. These younger ages mostly record metamorphic zircon growth. Zircon grains were also separated and analyzed from five other samples (sections 3.13 to 3.17). Sample locations are illustrated in Figures 3 to 5.

Table 2. U-Pb SHRIMP zircon isotopic data for samples from Musquaro and D'Auteuil lakes in a format following Stern (1997). Uncertainties are reported at 1s (absolute) and calculated by numerical propagation of all known sources of error. $f206^{204}$ refers to mole fraction of total ^{206}Pb that is due to common Pb, calculated using the ^{204}Pb-method; common Pb composition used is the surface blank. Spreadsheet in the supplementary file.

																	Apparent ages				
Sample	U	Th	Th	Pb	^{204}Pb	^{204}Pb	±1s	f^{206}	^{208}Pb	±1s	^{207}Pb	±1s	^{206}Pb	±1s	^{207}Pb	±1s	^{206}Pb	±1s	^{207}Pb	±1s	Conc.
Spot #*	(ppm)	(ppm)	U	(ppm)	(ppb)	^{206}Pb			^{206}Pb		^{235}U		^{238}U		^{206}Pb		^{238}U		^{206}Pb		(%)
Hornblende-biotite quartz-syenite gneiss (CQA-00-314A; GSC laboratory number 6718)																					
6718-49.2	1002	75	0.08	162	3	2.33E-05	9.55E-06	0.0004	0.0237	0.0011	1.731	0.0216	0.1721	0.0019	0.073	0.0004	1023	10	1012	10	101.1
6718-25.2	682	70	0.11	109	1	7.52E-06	2.14E-05	0.0001	0.0291	0.0020	1.717	0.0288	0.1681	0.0020	0.074	0.0008	1002	11	1044	22	96.0
6718-25.1	355	289	0.84	104	1	1.00E-05	1.00E-05	0.0002	0.2580	0.0035	3.231	0.0454	0.2515	0.0030	0.093	0.0006	1446	16	1492	11	96.9
6718-35.1	200	163	0.84	60	1	2.95E-05	2.64E-05	0.0005	0.2485	0.0046	3.342	0.0555	0.2592	0.0032	0.094	0.0009	1486	16	1499	18	99.1
6718-95.1	218	176	0.83	65	4	7.96E-05	4.36E-05	0.0014	0.2501	0.0066	3.347	0.0661	0.2588	0.0033	0.094	0.0013	1484	17	1504	26	98.7
6718-93.1	268	184	0.71	77	1	2.03E-05	2.24E-05	0.0004	0.2124	0.0045	3.310	0.0585	0.2559	0.0035	0.094	0.0009	1469	18	1504	19	97.6
6718-8.1	425	144	0.35	111	2	1.79E-05	1.44E-05	0.0003	0.0968	0.0021	3.310	0.0472	0.2558	0.0030	0.094	0.0006	1468	16	1505	12	97.6
6718-64.1	248	71	0.30	63	1	1.00E-05	1.00E-05	0.0002	0.0868	0.0024	3.248	0.0582	0.2489	0.0033	0.095	0.0010	1433	17	1521	20	94.2
6718-65.1	253	108	0.44	69	1	8.95E-06	1.92E-05	0.0002	0.1341	0.0043	3.388	0.0491	0.2593	0.0030	0.095	0.0007	1486	15	1523	14	97.6
6718-74.1	108	50	0.47	32	2	6.30E-05	5.65E-05	0.0011	0.1375	0.0048	3.656	0.0746	0.2750	0.0037	0.096	0.0013	1566	18	1556	26	100.7
6718-31.1	109	70	0.66	34	1	5.33E-05	6.34E-05	0.0009	0.1958	0.0057	3.730	0.0754	0.2767	0.0036	0.098	0.0014	1575	18	1582	26	99.5
6718-49.1	255	158	0.64	78	1	1.00E-05	1.00E-05	0.0002	0.1880	0.0037	3.780	0.0836	0.2781	0.0041	0.099	0.0015	1582	21	1598	28	99.0
6718-48.1	175	103	0.61	53	2	3.92E-05	3.86E-05	0.0007	0.1835	0.0043	3.756	0.0736	0.2724	0.0038	0.100	0.0012	1553	19	1624	23	95.6
Porphyritic granite (CQA-00-125A; GSC laboratory number 6719)																					
6719-45.1	1306	33	0.03	253	2	1.00E-05	1.00E-05	0.0002	0.0084	0.0005	2.382	0.0367	0.2066	0.0025	0.084	0.0007	1210	14	1284	15	94.3
6719-2.1	1148	130	0.12	295	3	1.12E-05	6.87E-06	0.0002	0.0334	0.0007	3.394	0.0465	0.2649	0.0033	0.093	0.0004	1515	17	1486	8	101.9
6719-47.2	1266	518	0.42	358	3	1.10E-05	4.96E-06	0.0002	0.1237	0.0012	3.468	0.0464	0.2702	0.0033	0.093	0.0004	1542	17	1490	8	103.5
6719-49.1	569	83	0.15	146	0	1.11E-06	1.25E-05	0.0000	0.0435	0.0011	3.389	0.0412	0.2628	0.0028	0.094	0.0004	1504	14	1499	9	100.3
6719-8.1	843	352	0.43	225	1	7.44E-06	5.49E-06	0.0001	0.1292	0.0033	3.279	0.0397	0.2541	0.0028	0.094	0.0004	1460	14	1500	7	97.3
6719-50.1	1571	876	0.58	454	2	5.42E-06	5.47E-06	0.0001	0.1704	0.0013	3.435	0.0582	0.2654	0.0038	0.094	0.0007	1517	19	1506	15	100.8
6719-40.1	976	406	0.43	268	3	1.53E-05	7.55E-06	0.0003	0.1288	0.0014	3.386	0.0413	0.2613	0.0028	0.094	0.0004	1496	14	1508	8	99.2
6719-46.1	1290	446	0.36	353	3	1.18E-05	6.01E-06	0.0002	0.1033	0.0011	3.448	0.0413	0.2660	0.0028	0.094	0.0004	1520	14	1508	9	100.8
6719-39.1	949	473	0.51	260	13	6.30E-05	1.48E-05	0.0011	0.1523	0.0024	3.306	0.0403	0.2549	0.0027	0.094	0.0005	1464	14	1510	9	97.0
6719-50.2	76	55	0.74	23	1	4.10E-05	8.72E-05	0.0007	0.2129	0.0069	3.689	0.1169	0.2704	0.0041	0.099	0.0026	1543	21	1604	49	96.2
6719-55.1	176	110	0.64	53	1	2.95E-05	3.64E-05	0.0005	0.1880	0.0043	3.754	0.0690	0.2742	0.0039	0.099	0.0010	1562	20	1611	19	96.9
6719-31.1	67	48	0.75	20	1	8.86E-05	7.04E-05	0.0015	0.2179	0.0148	3.701	0.0878	0.2632	0.0039	0.102	0.0017	1506	20	1660	31	90.7
6719-47.1	112	72	0.67	57	1	3.16E-05	4.65E-05	0.0006	0.1964	0.0073	10.318	0.1741	0.4349	0.0062	0.172	0.0013	2328	28	2578	13	90.3
Foliated hornblende-biotite granite (CQA-00-158A; GSC laboratory number 6720)																					
6720-59.1	83	43	0.54	23	1	5.41E-05	8.84E-05	0.0009	0.1469	0.0064	3.227	0.0802	0.2574	0.0036	0.091	0.0017	1477	19	1445	36	102.2
6720-15.1	122	74	0.62	34	3	1.00E-04	5.44E-05	0.0017	0.1794	0.0074	3.257	0.0678	0.2558	0.0037	0.092	0.0012	1469	19	1474	25	99.6
6720-6.1	163	155	0.98	49	2	5.92E-05	4.08E-05	0.0010	0.2878	0.0084	3.220	0.0560	0.2511	0.0032	0.093	0.0009	1444	17	1488	19	97.0
6720-8.1	81	48	0.61	23	1	4.10E-05	8.98E-05	0.0007	0.1788	0.0062	3.332	0.0874	0.2597	0.0038	0.093	0.0019	1488	20	1489	38	99.9
6720-35.1	90	62	0.71	26	2	1.02E-04	6.34E-05	0.0018	0.2147	0.0064	3.317	0.0731	0.2585	0.0037	0.093	0.0014	1482	19	1489	29	99.5
6720-36.1	556	230	0.43	150	1	1.18E-05	1.34E-05	0.0002	0.1236	0.0018	3.325	0.0425	0.2585	0.0028	0.093	0.0005	1482	15	1494	10	99.2
6720-55.1	151	164	1.12	46	0	9.58E-06	7.14E-05	0.0002	0.3134	0.0110	3.237	0.0674	0.2512	0.0031	0.093	0.0014	1445	16	1497	29	96.5
6720-3.1	44	19	0.44	11	2	2.60E-04	1.04E-04	0.0045	0.1278	0.0077	3.201	0.1312	0.2474	0.0047	0.094	0.0032	1425	24	1505	66	94.7
6720-51.1	289	153	0.55	81	1	1.00E-05	1.00E-05	0.0002	0.1626	0.0030	3.345	0.0455	0.2583	0.0029	0.094	0.0006	1481	15	1507	12	98.3
6720-30.1	114	68	0.62	32	2	7.21E-05	5.58E-05	0.0013	0.1815	0.0051	3.335	0.0660	0.2559	0.0034	0.095	0.0013	1469	17	1518	25	96.7
6720-21.1	98	69	0.73	27	1	2.68E-05	4.43E-05	0.0005	0.2269	0.0059	3.220	0.0687	0.2466	0.0038	0.095	0.0012	1421	20	1522	24	93.3
Augen granitic orthogneiss (CQA-00-268A; GSC laboratory number 6721)																					
6721-45.1	980	69	0.07	152	0	2.68E-06	6.34E-06	0.0001	0.0211	0.0007	1.647	0.0237	0.1650	0.0021	0.072	0.0004	985	12	997	11	98.7
6721-27.2	1172	65	0.06	185	2	1.00E-05	1.00E-05	0.0002	0.0176	0.0007	1.691	0.0238	0.1688	0.0019	0.073	0.0005	1005	11	1004	14	100.1
6721-36.1	1498	46	0.03	241	2	1.00E-05	1.00E-05	0.0002	0.0094	0.0005	1.738	0.0209	0.1732	0.0019	0.073	0.0003	1030	10	1007	8	102.3
6721-27.1	155	105	0.70	44	2	6.36E-05	9.58E-05	0.0011	0.2206	0.0059	3.179	0.0807	0.2523	0.0037	0.091	0.0018	1450	19	1454	37	99.7
6721-51.1	293	209	0.74	85	1	8.43E-06	1.24E-05	0.0002	0.2190	0.0058	3.272	0.0453	0.2578	0.0029	0.092	0.0006	1479	15	1468	13	100.7
6721-34.1	151	116	0.80	44	2	5.89E-05	3.70E-05	0.0010	0.2416	0.0055	3.232	0.0574	0.2539	0.0034	0.092	0.0009	1458	17	1474	20	98.9
6721-49.1	388	159	0.42	107	0	4.28E-06	1.36E-05	0.0001	0.1263	0.0020	3.349	0.0452	0.2619	0.0030	0.093	0.0006	1500	15	1483	11	101.1
6721-40.1	304	119	0.41	82	2	2.52E-05	3.27E-05	0.0004	0.1210	0.0025	3.317	0.0483	0.2586	0.0029	0.093	0.0007	1482	15	1489	15	99.6
6721-31.1	193	150	0.80	58	1	3.24E-05	1.52E-05	0.0006	0.2361	0.0066	3.362	0.0680	0.2614	0.0042	0.093	0.0010	1497	22	1494	20	100.2
6721-44.1	417	235	0.58	118	1	1.00E-05	1.00E-05	0.0002	0.1734	0.0024	3.338	0.0462	0.2592	0.0030	0.093	0.0006	1486	15	1496	12	99.3
6721-47.1	351	157	0.46	96	1	1.28E-05	1.67E-05	0.0002	0.1355	0.0022	3.342	0.0437	0.2587	0.0028	0.094	0.0006	1483	15	1502	11	98.7
6721-36.2	405	179	0.46	110	0	5.30E-07	5.91E-06	0.0000	0.1394	0.0039	3.339	0.0497	0.2570	0.0028	0.094	0.0008	1474	14	1513	17	97.4
6721-22.1	190	153	0.83	57	0	1.00E-05	1.00E-05	0.0002	0.2555	0.0042	3.369	0.0501	0.2591	0.0031	0.094	0.0007	1485	16	1514	15	98.1
6721-9.1	205	187	0.94	65	1	1.10E-05	3.09E-05	0.0002	0.2891	0.0047	3.471	0.0530	0.2659	0.0032	0.095	0.0008	1520	16	1522	16	99.9

Table 3. U-Pb SHRIMP zircon isotopic data, Kegaska to Baie des Loups transect (see Table 2 for additional information). Spreadsheet in the supplementary file.

																		Apparent ages				
Sample	U	Th	Th	Pb	^{204}Pb	^{204}Pb	±1s	f^{206}	^{208}Pb	±1s	^{207}Pb	±1s	^{206}Pb	±1s	^{207}Pb	±1s	^{206}Pb	±1s	^{207}Pb	±1s	Conc.
Spot #*	(ppm)	(ppm)	U	(ppm)	(ppb)	^{206}Pb			^{206}Pb		^{235}U		^{238}U		^{206}Pb		^{238}U		^{206}Pb		(%)
Lapillistone, La Romaine Supracrustal Belt (CQA-01-353A; GSC laboratory number 7090)																					
7090-116.1	290	140	0.50	81	6	9.92E-05	2.16E-05	0.00172	0.14637	0.00408	3.3976	0.0513	0.26199	0.00312	0.09406	0.0008	1500	16	1509	15	99.4
7090-103.1	195	80	0.42	53	7	0.000153	4.04E-05	0.00265	0.12370	0.00256	3.3565	0.0503	0.26081	0.00297	0.09334	0.0008	1494	15	1495	16	99.9
7090-105.1	354	200	0.58	102	6	8.00E-05	2.07E-05	0.00139	0.16794	0.00181	3.5918	0.0454	0.26600	0.00286	0.09793	0.0005	1521	15	1585	10	95.9
7090-56.1	205	69	0.35	64	4	7.53E-05	2.06E-05	0.0013	0.10484	0.00176	4.4406	0.0623	0.29952	0.00363	0.10753	0.0006	1689	18	1758	10	96.1
7090-43.1	318	379	1.23	175	8	7.25E-05	1.34E-05	0.00126	0.35137	0.00403	9.3138	0.1344	0.42424	0.00460	0.15922	0.0013	2280	21	2447	14	93.1
Biotite granitic gneiss, Baie des Loups map sheet (CQA-01-476A: GSC laboratory number z7093)																					
7093-102.1	1379.4	484.7	0.36	235	7	3.58E-05	1.06E-05	0.00062	0.1101	0.00136	1.6583	0.0223	0.16738	0.00199	0.07185	0.0004	997.7	11	982	10	101.6
7093-30.1	1227.4	427.1	0.36	214	4	2.26E-05	7.86E-06	0.00039	0.1089	0.00115	1.7109	0.0216	0.17198	0.00197	0.07215	0.0003	1023	11	990	8	103.3
7093-90.1	1070.2	363.7	0.35	188	2	1.49E-05	1.38E-05	0.00026	0.10969	0.00156	1.7249	0.0236	0.17239	0.00198	0.07257	0.0004	1025	11	1002	12	102.3
7093-15.1	1199.4	405.9	0.35	208	6	3.24E-05	9.74E-06	0.00056	0.10649	0.00152	1.7079	0.0228	0.1706	0.00205	0.07261	0.0003	1015	11	1003	9	101.2
7093-73.1	979.5	147.9	0.16	158	6	4.26E-05	1.19E-05	0.00074	0.04627	0.00094	1.6798	0.0221	0.16773	0.00193	0.07263	0.0004	999.6	11	1004	10	99.6
7093-107.1	1170.4	392.9	0.35	200	7	3.91E-05	1.16E-05	0.00068	0.10524	0.00125	1.6927	0.0236	0.16899	0.00205	0.07265	0.0004	1007	11	1004	11	100.2
7093-25.1	1200.3	395	0.34	204	2	1.37E-05	1.16E-05	0.00024	0.10494	0.00165	1.6825	0.0217	0.16792	0.00192	0.07267	0.0003	1001	11	1005	10	99.6
7093-4.1	706.8	318.2	0.47	123	13	0.000126	2.56E-05	0.00218	0.14076	0.00456	1.67679	0.0241	0.16729	0.00188	0.0727	0.0006	997.2	10	1005	16	99.2
7093-85.1	996.9	348.2	0.36	172	4	2.47E-05	1.47E-05	0.00043	0.10872	0.00149	1.7045	0.0233	0.16995	0.00204	0.07274	0.0004	1012	11	1007	11	100.5
7093-93.1	983.6	442.5	0.46	174	4	2.49E-05	1.19E-05	0.00043	0.13791	0.00233	1.7097	0.0227	0.16965	0.00195	0.07309	0.0004	1010	11	1017	11	99.4
7093-76.1	791.4	209.5	0.27	136	3	2.42E-05	1.72E-05	0.00042	0.0806	0.00167	1.7574	0.0240	0.17348	0.00201	0.07347	0.0004	1031	11	1027	12	100.4
7093-6.1	70.8	25.67	0.37	15	4	0.000341	0.000136	0.00592	0.10593	0.00697	2.47601	0.1070	0.20992	0.00483	0.08555	0.0029	1228	26	~~1328~~	~~67~~	92.5
7093-22.1	109.0	57.43	0.54	30	17	0.000708	0.000278	0.01228	0.14884	0.01107	3.15348	0.1688	0.25812	0.00342	0.08861	0.0045	1480	18	~~1396~~	~~100~~	106.1
7093-12.1	210.0	96.11	0.47	54	6	0.000148	4.52E-05	0.00257	0.14588	0.0033	3.00808	0.0535	0.24146	0.00292	0.09035	0.0011	1394	15	~~1433~~	~~22~~	97.3
7093-16.1	110.6	64.58	0.60	31	10	0.000402	0.000135	0.00697	0.18606	0.0074	3.19183	0.1074	0.25446	0.00336	0.09098	0.0027	1461	17	~~1446~~	~~57~~	101.1
7093-21.1	139.7	84.6	0.63	40	12	0.000378	6.88E-05	0.00655	0.17768	0.00536	3.259	0.0694	0.25969	0.00341	0.09102	0.0014	1488	17	~~1447~~	~~29~~	102.9
7093-2.1	67.0	29.42	0.45	17	9	0.000609	0.000192	0.01055	0.1197	0.00857	3.11349	0.1261	0.24568	0.00369	0.09191	0.0033	1416	19	1466	70	96.6
7093-82.1	161.9	85.86	0.55	45	9	0.000252	6.34E-05	0.00437	0.16704	0.00416	3.31489	0.0742	0.25836	0.0037	0.09306	0.0014	1481	19	1489	30	99.5
7093-101.2	206.3	107.7	0.54	56	11	0.000251	6.32E-05	0.00435	0.1535	0.00425	3.23689	0.0594	0.2516	0.00305	0.09331	0.0012	1447	16	1494	24	96.8
7093-28.1	199.1	67.36	0.35	54	10	0.000227	5.13E-05	0.00393	0.1102	0.00403	3.37708	0.0581	0.26175	0.00313	0.09357	0.0010	1499	16	1500	21	100.0
7093-2.2	453.3	197.8	0.45	125	5	4.54E-05	1.74E-05	0.00079	0.12957	0.00233	3.3824	0.0525	0.26177	0.00338	0.09372	0.0007	1499	17	1502	14	99.8
7093-45.1	186.1	63.04	0.35	48	3	8.06E-05	3.9E-05	0.0014	0.10881	0.00448	3.20933	0.0787	0.24756	0.00309	0.09402	0.0018	1426	16	1509	37	94.5
7093-86.1	92.4	48.04	0.54	26	7	0.000336	9.9E-05	0.00582	0.16062	0.00643	3.43501	0.1186	0.26144	0.00396	0.09529	0.0028	1497	20	~~1534~~	~~56~~	97.6
7093-72.1	132.7	43.8	0.34	36	5	0.000181	0.000175	0.00314	0.10427	0.00706	3.44192	0.1147	0.25913	0.00322	0.09634	0.0028	1485	16	~~1554~~	~~56~~	95.6
7093-57.1	83.7	39.65	0.49	23	5	0.000243	0.000112	0.00422	0.15324	0.00624	3.54953	0.0897	0.25994	0.00323	0.09903	0.0020	1490	17	~~1606~~	~~39~~	92.7
7093-51.1	73.4	41.67	0.59	21	6	0.000389	0.000114	0.00673	0.1799	0.0084	3.63402	0.1189	0.26383	0.00346	0.0999	0.0028	1509	18	~~1622~~	~~54~~	93.0
Pegmatitic gabbro, Musquaro ultramafic to mafic layered intrusion (CQA-01-432B2; GSC laboratory number z7089)																					
7089-31.1	248	35	0.15	39	8	2.31E-04	4.76E-05	0.00401	0.04492	0.00436	1.62842	0.0286	0.16290	0.00184	0.07250	0.0009	973	10	1000	25	97.3
7089-99.2	153	44	0.30	26	2	9.65E-05	8.10E-05	0.00167	0.09365	0.00390	1.70944	0.0436	0.16651	0.00251	0.07446	0.0014	993	14	1054	38	94.2
7089-106.1	270	121	0.46	47	7	1.76E-04	4.05E-05	0.00304	0.13448	0.00324	1.67953	0.0376	0.16709	0.00264	0.07290	0.0010	996	15	1011	29	98.5
7089-4.1	277	78	0.29	46	1	3.71E-05	2.74E-05	0.00064	0.08787	0.00186	1.70847	0.0282	0.16735	0.00220	0.07404	0.0006	998	12	1043	17	95.7
7089-13.1	564	62	0.11	90	5	5.87E-05	2.03E-05	0.00102	0.03446	0.00105	1.68399	0.0229	0.16793	0.00186	0.07273	0.0005	1001	10	1006	13	99.4
7089-101.1	222	29	0.13	36	6	1.76E-04	4.10E-05	0.00304	0.04286	0.00206	1.71303	0.0299	0.16799	0.00200	0.07396	0.0008	1001	11	1040	23	96.2
7089-96.1	260	28	0.11	42	6	1.49E-04	8.25E-05	0.00259	0.03453	0.00334	1.73480	0.0421	0.16897	0.00210	0.07446	0.0014	1006	12	1054	39	95.5
7089-45.1	282	62	0.23	46	10	2.37E-04	3.95E-05	0.00410	0.06112	0.00204	1.66135	0.0275	0.16903	0.00195	0.07128	0.0008	1007	11	966	22	104.3
7089-7.1	258	87	0.35	44	5	1.42E-04	3.29E-05	0.00245	0.10258	0.00221	1.66447	0.0265	0.16950	0.00198	0.07122	0.0007	1009	11	964	19	104.7
7089-103.1	210	23	0.11	34	11	3.47E-04	8.31E-05	0.00601	0.02716	0.00334	1.68269	0.0410	0.16953	0.00208	0.07199	0.0014	1010	11	986	40	102.4
7089-47.1	212	9	0.04	34	2	6.71E-05	3.97E-05	0.00116	0.01804	0.00170	1.74731	0.0285	0.17070	0.00192	0.07424	0.0008	1016	11	1048	21	96.9
7089-41.1	133	70	0.55	25	5	2.29E-04	6.29E-05	0.00396	0.16756	0.00417	1.82883	0.0417	0.17524	0.00209	0.07569	0.0014	1041	11	1087	36	95.8
7089-18.1	434	278	0.66	84	4	5.71E-05	1.66E-05	0.00099	0.19971	0.00217	1.83594	0.0233	0.17657	0.00189	0.07541	0.0004	1048	10	1079	11	97.1
7089-100.1	137	50	0.38	25	11	5.41E-04	9.66E-05	0.00938	0.10589	0.00655	1.77538	0.0482	0.17671	0.00217	0.07287	0.0017	1049	12	1010	47	103.8
7089-33.1	268	165	0.64	52	11	2.77E-04	5.47E-05	0.00480	0.18974	0.00345	1.80243	0.0413	0.17762	0.00280	0.07360	0.0011	1054	15	1030	30	102.3
7089-53.1	142	55	0.40	26	4	1.80E-04	6.45E-05	0.00312	0.11807	0.00410	1.87276	0.0380	0.17976	0.00209	0.07556	0.0012	1066	11	1083	31	98.4
7089-116.1	109	39	0.37	20	7	3.95E-04	8.68E-05	0.00684	0.10540	0.00448	1.79693	0.0495	0.17991	0.00231	0.07244	0.0017	1067	13	998	47	106.8
7089-120.1	250	106	0.44	47	5	1.23E-04	3.20E-05	0.00213	0.13235	0.00476	1.85930	0.0303	0.18039	0.00217	0.07475	0.0007	1069	12	1062	20	100.7
7089-99.1	192	101	0.54	37	9	3.15E-04	6.03E-05	0.00546	0.15535	0.00361	1.81854	0.0401	0.18058	0.00263	0.07304	0.0011	1070	14	1015	30	105.4
7089-93.1	137	47	0.35	25	7	3.25E-04	7.39E-05	0.00563	0.10209	0.00451	1.85262	0.0429	0.18069	0.00231	0.07436	0.0013	1071	13	1051	36	101.8
7089-114.1	430	185	0.44	81	6	9.15E-05	4.44E-05	0.00159	0.13366	0.00231	1.87787	0.0305	0.18096	0.00204	0.07526	0.0008	1072	11	1076	21	99.7
7089-29.1	365	162	0.46	69	5	9.32E-05	2.49E-05	0.00162	0.13450	0.00195	1.87497	0.0271	0.18265	0.00206	0.07445	0.0006	1081	11	1054	16	102.6
Granite dyke (CQA-01-1370A; GSC laboratory number z7094)																					
7094-33.1	173.61	202.8	1.21	38	10	0.000399	0.0001	0.00691	0.37457	0.00734	1.69058	0.0648	0.17432	0.00265	0.07034	0.0023	1036	15	938	70	110.4
7094-26.1	157.7	143.2	0.94	31	7	0.000323	0.000105	0.00559	0.27241	0.00659	1.67271	0.0503	0.17013	0.00228	0.07131	0.0018	1013	13	966	53	104.8
7094-96.1	2611.74	85.6	0.03	428	6	1.55E-05	4.74E-06	0.00027	0.0096	0.00029	1.7594	0.0228	0.1763	0.00211	0.07238	0.0003	1047	12	997	8	105.0
7094-81.1	362.37	345.8	0.99	75	7	0.000129	3.8E-05	0.00223	0.301	0.00426	1.74168	0.0292	0.17417	0.00203	0.07253	0.0008	1035	11	1001	22	103.4
7094-37A.2	288.24	304.6	1.09	60	7	0.000167	5.4E-05	0.00289	0.32715	0.00473	1.72015	0.0346	0.17199	0.0022	0.07254	0.0010	1023	12	1001	29	102.2
7094-49.1	2144.44	92.1	0.04	348	8	2.52E-05	7.56E-06	0.00044	0.01314	0.00041	1.74055	0.0238	0.17361	0.00215	0.07271	0.0003	1032	12	1006	9	102.6
7094-54.1	1020.54	41.0	0.04	166	6	3.88E-05	1.22E-05	0.00067	0.01096	0.00075	1.74786	0.0258	0.17432	0.00208	0.07272	0.0005	1036	11	1006	15	103.0
7094-88.1	2847.24	95.4	0.03	456	7	1.59E-05	1.65E-05	0.00028	0.0101	0.00068	1.72476	0.0249	0.17199	0.00204	0.07273	0.0005	1023	11	1007	14	101.6
7094-44.1	2285.25	81.0	0.04	373	3	7.34E-06	4.64E-06	0.00013	0.01102	0.00031	1.75799	0.0222	0.17505	0.00204	0.07284	0.0003	1040	11	1009	7	103.0
7094-94.1	2199.53	163.9	0.08	363	5	1.56E-05	7.68E-06	0.00027	0.02268	0.00047	1.7631	0.0225	0.17531	0.00202	0.07294	0.0003	1041	11	1012	9	102.9
7094-58.1	2261.27	100.9	0.05	362	10	3.04E-05	7.74E-06	0.00053	0.01432	0.00045	1.72488	0.0238	0.17138	0.00199	0.07299	0.0005	1020	11	1014	13	100.6
7094-101.1	2328.58	305.4	0.14	400	12	3.35E-05	7.06E-06	0.00058	0.04472	0.00123	1.79756	0.0240	0.17854	0.00211	0.07302	0.0004	1059	12	1015	10	104.4
7094-63.1	2831.61	92.1	0.03	461	10	2.32E-05	5.29E-06	0.0004	0.00977	0.00031	1.76193	0.0239	0.17491	0.00203	0.07306	0.0004	1039	11	1016	12	102.3
7094-37A.1	165.46	134.7	0.84	31	6	0.000258	9.38E-05	0.00447	0.24163	0.00606	1.68776	0.0473	0.16679	0.00231	0.07339	0.0017	~~994~~	~~13~~	1025	47	97.0
7094-21.1	211.38	179.8	0.88	42	5	0.000176	6.48E-05	0.00306	0.26761	0.00588	1.72958	0.0388	0.17086	0.0022	0.07342	0.0012	1017	12	1025	34	99.2
7094-42.1	217.32	192.0	0.91	43	6	0.000194	7.59E-05	0.00337	0.2741	0.00575	1.72111	0.0411	0.16986	0.00221	0.07349	0.0014	1011	12	1027	38	98.4
7094-41.1	2363.39	225.2	0.10	404	4	1.2E-05	8.61E-06	0.00021	0.03305	0.00054	1.82032	0.0239	0.17953	0.00212	0.07354	0.0003	1064	12	1029	9	103.5
7094-73.1	298.12	367.0	1.27	65	0	7.4E-06	5.42E-05	0.00013	0.38819	0.00857	1.76763	0.0335	0.17219	0.00208	0.07445	0.0010	1024	11	1054	27	97.2
7094-3A.1	269.82	302.2	1.16	56	5	0.000128	4.84E-05	0.00222	0.34473	0.00482	1.75719	0.0329	0.16836	0.002	0.0757	0.0010	1003	11	1087	26	92.3
7094-29.1	96.22	118.7	1.27	21	5	0.000314	0.00015	0.00545	0.39506	0.00993	1.83935	0.0691	0.17502	0.00237	0.07622	0.0025	1040	13	1101	68	94.4
7094-54.2	182.99	238.5	1.35	41	3	9.93E-05	5.7E-05	0.00172	0.39951	0.00804	1.84562	0.0383	0.17474	0.00222	0.0766	0.0011	1038	12	1111	30	93.5
7094-72.1	48.78	22.3	0.47	14	9	0.000836	0.000456	0.0145	0.13033	0.01789	3.38461	0.2809	0.26774	0.00428	0.09169	0.0073	1529	22	1461	159	104.7
7094-82.1	185.22	74.1	0.41	49	8	0.000196	5.02E-05	0.00339	0.11873	0.00319	3.18106	0.0575	0.25159	0.00312	0.0917	0.0011	1447	16	1461	22	99.0
7094-26A.1	429.57	205.7	0.49	117	4	3.89E-05	3.64E-05	0.00067	0.14413	0.01216	3.30566	0.0562	0.25509	0.00308	0.09399	0.0010	1465	16	1508	20	97.1
7094-93.1	78.89	34.1	0.45	22	1	6.13E-05	0.000383	0.00106	0.13469	0.01484	3.40607	0.2333	0.26042	0.00437	0.09486	0.0061	1492	22	1525	126	97.8
7094-37.1	87.51	35.8	0.42	24	6	0.000297	0.000116	0.00515	0.12799	0.00588	3.37204	0.0922	0.25577	0.0034	0.09562	0.0021	1468	17	1540	42	95.3

3.3. Sample CQA-00-314A: Hornblende and Biotite-bearing Quartz Monzodiorite Gneiss

The sample CQA-00-314A (GSC laboratory number z6718) is a hornblende and biotite-bearing quartz monzodiorite gneiss from D'Auteuil Lake. The outcrop is located at 625321mE and 5607529mN in NTS map sheet 12K11 (Fig. 3C). It is a member of the Marie-Claire Intrusive Suite of Lafrance et al. (2026) and of the unit mPagn5a2 of the former *Aguanish complex* (Fig. 3C; Appendix 1; Corriveau and Bonnet, 2005).

The monzodioritic gneiss is homogeneous in terms of mineral content, with about 10 vol.% mafic minerals, heterogranular but dominantly fine-grained, and pervasively recrystallized (Fig. 6). Millimetre clots of hornblende, biotite, magnetite and titanite occur among feldspar aggregates that locally preserve morphological relics of medium-grained (~3–8 mm) hypidiomorphic-granular igneous texture (Fig. 6A, B). The patina also displays whitish anastomosing zones that may reflect albitization. A weak lineation is defined by the mafic minerals.

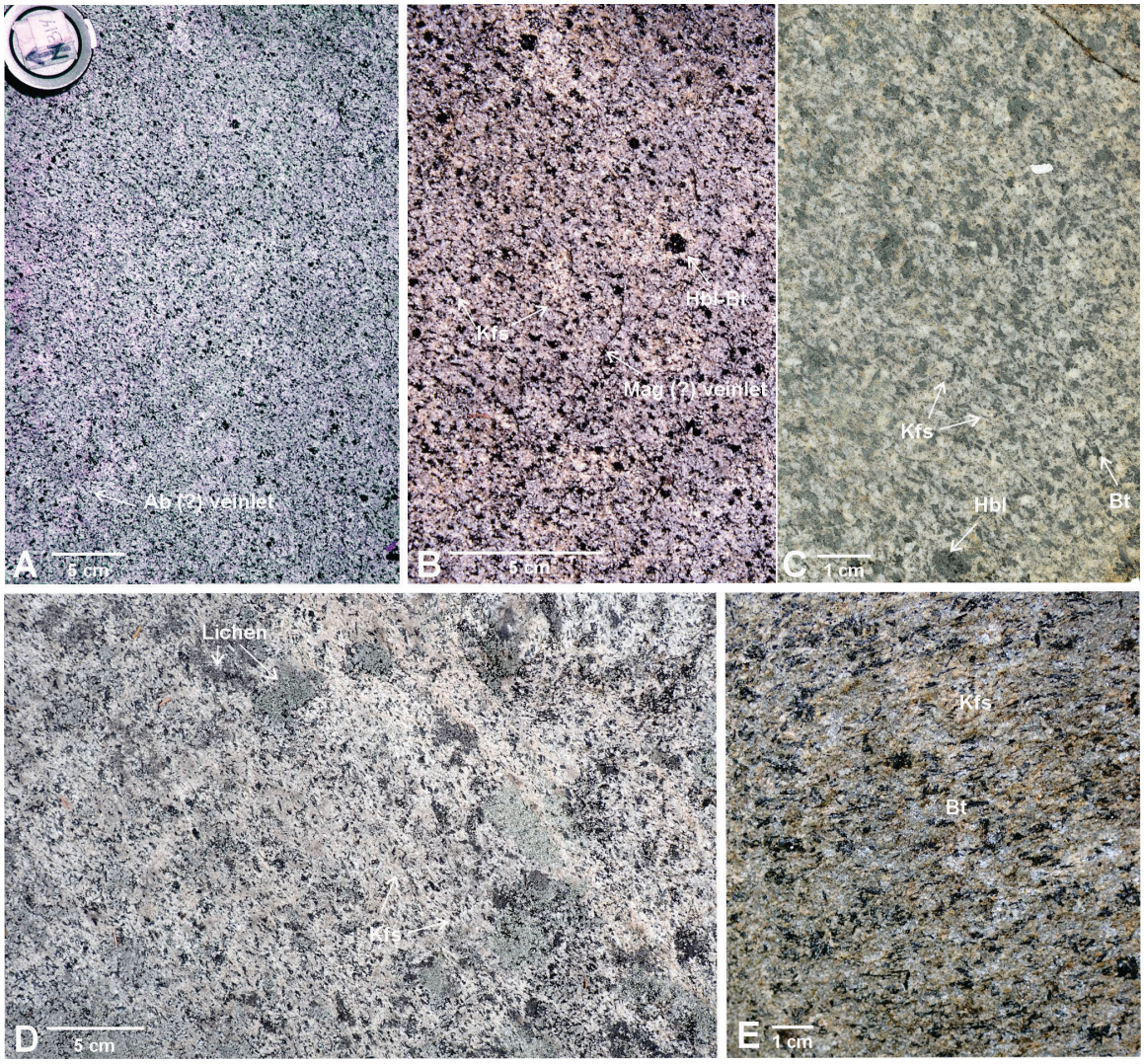


Figure 6. Field exposure of sample CQA-00-314A/25-SL-4219. **A, B.** Recrystallized monzodioritic gneiss (field estimate: 10 vol. % quartz, up to 60 vol. % K-feldspar, at least 20 vol.% plagioclase, and 10 vol. % biotite and hornblende), outcrop CQA-00-314. **C–E**. Outcrop 25-SL-4219 with morphological relics of a hypidiomorphic texture in C, a lath-shaped texture defined by feldspar with interstitial hornblende and biotite in D and in E morphological relics of a lath-shaped texture defined by recrystallized feldspar and outlined by biotite-and hornblende.

Adjacent to the sampled area, the protolith is locally better preserved and the quartz monzodiorite displays an igneous foliation defined by the preferred orientation of cm-long grey feldspar laths that are now recrystallized; biotite and hornblende form interstitial clots among the former laths (Fig. 6C–E). Possible weak albitization of the plagioclase laths is observed and appears to be most pronounced along irregular, crisscrossing, discontinuous light-coloured and locally mafic veinlets of multiple orientations.

Zircons are subhedral, prismatic with length to breadth (L:B) ratios ranging from 7 to equidimensional and 20 to 80 microns across. They have faint regular zoning that is characteristic of igneous zircons. The cores are surrounded by unzoned rims that are lighter in BSE images. Rims range from a few microns to 20 microns in width.

A cluster of seven, mostly concordant, U-Pb SHRIMP analyses from cores yields a weighted mean of 1505 ± 12 Ma (MSWD = 0.63; POF = 0.71) (Fig. 7A). This age is interpreted as the time of igneous crystallization. Four analyses yield $^{207}Pb/^{206}Pb$ ages that range from 1556 Ma to 1624 Ma and are interpreted as inherited zircon from older basement. Ages of 1012 ± 20 Ma and 1044 ± 44 Ma from rims with low Th/U are attributed to metamorphic zircon growth.

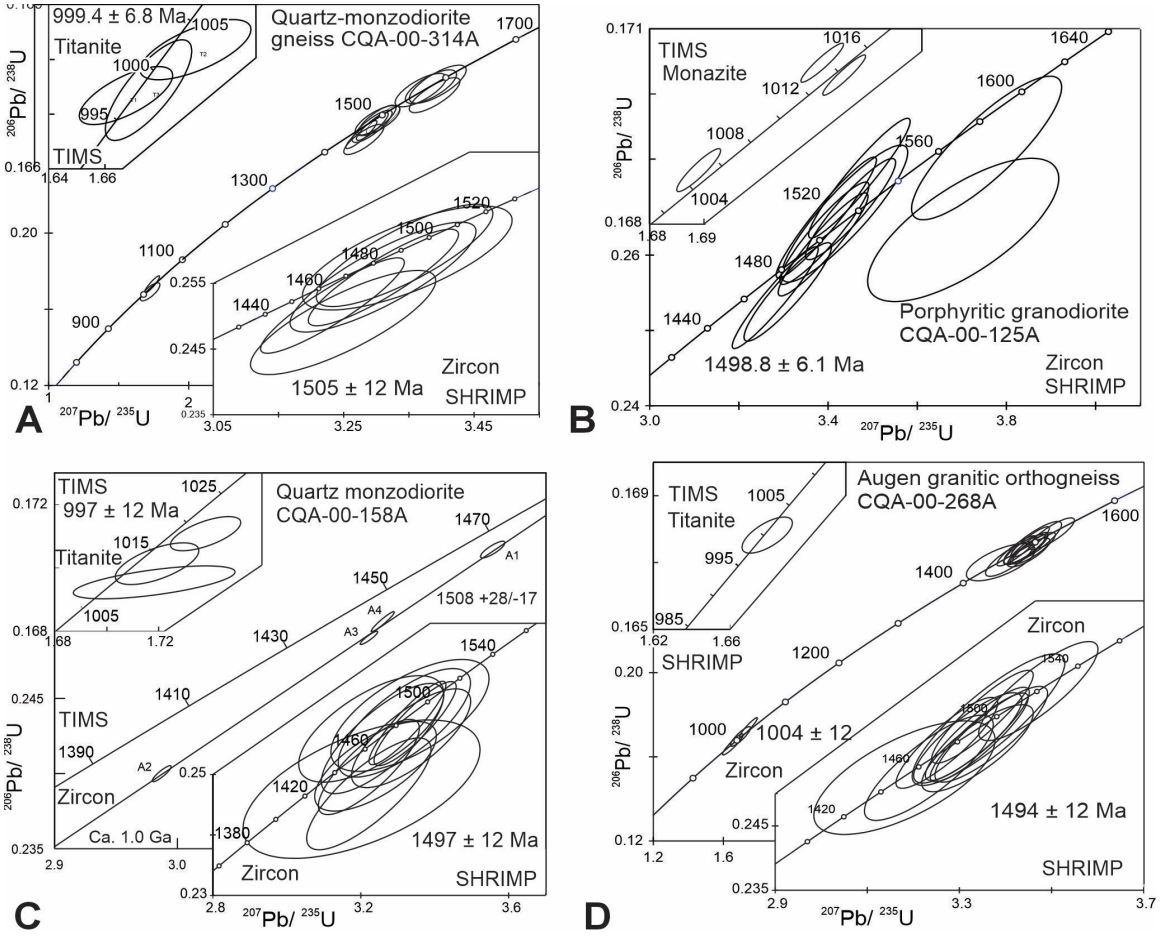


Figure 7. Concordia diagrams for U-Pb geochronology of granitoids from the *Aguanish complex*. **A.** Sample CQA-00-314A of a hornblende and biotite-bearing quartz monzodiorite gneiss has Wakamian zircon xenocrysts, Pinwarian igneous zircons and Rigolet age titanite. **B.** Sample CQA-00-125A of a hornblende and biotite-bearing granodiorite showing a SHRIMP zircon crystallization age and metamorphic monazite ages. **C.** Sample CQA-00-158A with zircon defining a crystallization age and titanite defining a metamorphic age. **D.** Sample CQA-00-268A with zircon defining a crystallization age and titanite defining a metamorphic age.

Three ID-TIMS concordant analyses on titanite yield a weighted mean $^{206}Pb/^{238}U$ age of 999.4 ± 6.8 Ma (MSWD = 2.7; POF = 0.066) (Fig. 7A). Titanite crystals are clear, pale orange, equidimensional, multi-faceted and 80 to 150 microns across. This morphology is interpreted in terms of metamorphic growth. The age is interpreted as a metamorphic age, although it could represent cooling through a temperature of ca. 650 °C (Cherniak, 1993).

3.4. Sample CQA-00-125A: Porphyritic Granodiorite

The sample CQA-00-125A (GSC laboratory number z6719) is a foliated and lineated porphyritic granodiorite metamorphosed under amphibolite-facies conditions from Musquaro Lake (Fig. 8). The outcrop is located at 641410mE and 5607216mN in NTS map sheet 12K11 (Fig. 3C). This unit was selected for geochronology for its homogeneous mineralogy and mineral content. It is a member of the Granodiorite de Grand-Portage of Lafrance et al. (2026) and of unit mPagn5a1 of the former *Aguanish complex* (Fig. 3C; Appendix 1; Corriveau and Bonnet, 2005).

The metagranodiorite is variably deformed and range from porphyritic (Fig. 8A, B) and weakly foliated to porphyroclastic and more gneissic (Fig. 8C). The outcrop also comprises foliated and lineated mafic dykes and mingled mafic-felsic dykes that are oriented parallel to, and share the gneissic foliation of, their host (Fig. 9A–D). The unit thus preserves evidence for early mafic magmatism prior to the Lillian Intrusive Suite amphibolite dykes. Local foliated granitic veinlets also occur parallel to the foliation of the granodiorite and within the dykes (Fig. 9B). The granodiorite, the mafic dykes and their gneissic fabric are cut by a hornblende lamprophyre dyke (Fig. 9C). A variety of granitic dykes cut the gneissic rocks, some are S-type granites containing biotite, muscovite and garnet.

Further south, this type of foliated granite contains enclaves of coticule and garnet-bearing hornblendite—either gneissic or foliated—that underwent deformation prior to, and record a higher metamorphic grade than, the granite. Dating this rock therefore helps constrain the minimum age of the metasedimentary rocks located south of the Musquaro arm (which are incorporated into the granite) and the maximum age of the deformation recorded by the granite.

The granodiorite has a pink to grey patina and is relatively homogeneous in terms of matrix biotite and K-feldspar phenocryst contents and distribution. It was sampled in a homogeneous part of the outcrop. The K-feldspar phenocrysts are idiomorphic to hypidiomorphic, rectangular to lenticular in shape, and partly to completely recrystallized. The tectonic foliation is defined by the orientation of biotite, K-feldspar augens and elongated polycrystalline lenses of quartz and feldspar. The primary rectangular phenocrysts are either aligned with the foliation or at an angle to the tectonic foliation and may have locally defined an igneous foliation. The foliated mafic dykes are either mesocratic and gabbroic, with hornblende and plagioclase, or dioritic, with hornblende and biotite.

Zircons from the granodiorite are subhedral to euhedral and prismatic with L:B ratios ranging from 2 to 4 and sizes of ca. 80 microns. Most grains have unzoned interiors and regularly zoned margins. Overgrowths are rare. A cluster of five concordant and three slightly discordant U-Pb SHRIMP analyses yields a weighted mean of $^{207}Pb/^{206}Pb$ age of 1499.8 ± 6.1 Ma (MSWD = 1.08; POF = 0.37) (Fig. 7B). This age is interpreted as the time of igneous crystallization. One 6%-discordant analysis is significantly younger, with a $^{207}Pb/^{206}Pb$ age of 1284 Ma and was obtained from what appeared to be an overgrowth. This age is likely a mixed igneous and metamorphic age. Two grains are likely inherited, as they yielded $^{207}Pb/^{206}Pb$ ages of 1611 Ma and 1660 Ma, while a third yields an Archean age of 2578 Ma.



Figure 8. Geology of the porphyritic intrusion sampled for geochronology at outcrop CQA-00-125 in **A, B, D, E, G, H** and more deformed facies 290 m NNW (outcrop 25-SL-4150) in **C** and **I,** and 825 m W (25-GS-1167) in **F** and **J** at Musquaro Lake. Fine-grained, granoblastic and foliated granitic veins occur locally (B, D and H).

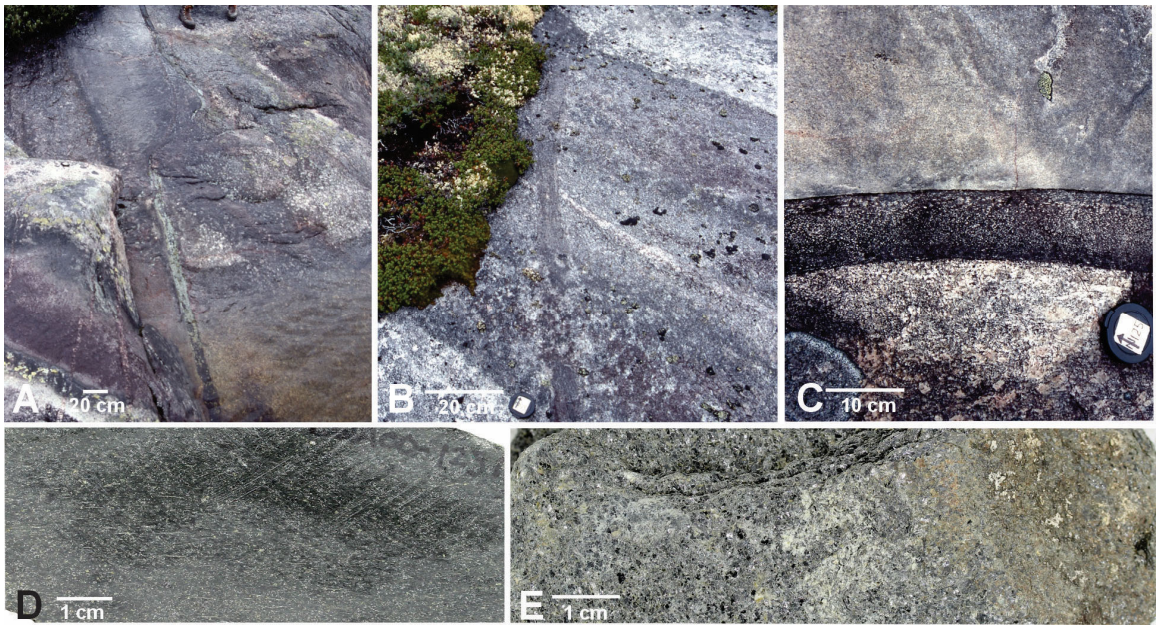


Figure 9. Mafic dykes with fine- to medium-grained textures are foliated parallel to the tectonic foliation of the host metagranodiorite. Younger generations of mafic dykes sharply cut the foliated mafic dykes (outcrop CQA-00-125).

Three U-Pb ID-TIMS monazite analyses are concordant to 0.6% negatively discordant (Fig. 7B). Assuming the negative discordance is the result of unsupported ^{206}Pb (Schärer, 1984), the $^{207}Pb/^{235}U$ ages are interpreted as most reliable and these range from 1014 ± 2 Ma to 1004 ± 2 Ma. The closure temperature of the U-Pb system in monazite is estimated around 900 °C (Cherniak et al., 2004), and the older two analyses yield a mean age of 1013.7 ± 1.1 Ma, interpreted as the time of metamorphic monazite growth.

3.5. Sample CQA-00-158A: Foliated Hornblende-biotite Quartz Monzodiorite

The sample CQA-00-158A (GSC laboratory number z6720) is a metamorphosed quartz monzodiorite from Musquaro Lake (Fig. 10). The outcrop is located at 641581mE and 5611659mN in NTS map sheet 12K10 (Fig. 3D). It is a member of the Marie-Claire Intrusive Suite of Lafrance et al. (2026) and of the unit mPagn5b1 of the former *Aguanish complex* (Fig. 3D; Appendix 1; Corriveau and Bonnet, 2005).

The metamorphosed monzodiorite is medium grained and leucocratic and comprises about 5 vol.% quartz, as well as less than 10 vol.% hornblende, biotite, magnetite and titanite. Its texture ranges from foliated to massive (i.e., isotropic). It is cut by granitic dykes, local syenite dykes and quartz veins, as well as by a parallel set of linear hematized bands (Fig. 10A).

Zircons range from euhedral to subhedral prismatic grains with L:B ratios of up to 5:1, to multifaceted equidimensional grains. A regression through four strongly discordant zircon U-Pb TIMS analyses yields upper and lower intercept ages of 1510 ± 4 Ma and 1008 ± 10 Ma (MSWD = 6.7), respectively (Fig. 7C). Fraction A4 consisted of multifaceted equidimensional crystals while the other three fractions consisted of elongate prismatic grains. The concordia plot shows no systematic difference in U-Pb isotopic composition between the different zircon morphologies.

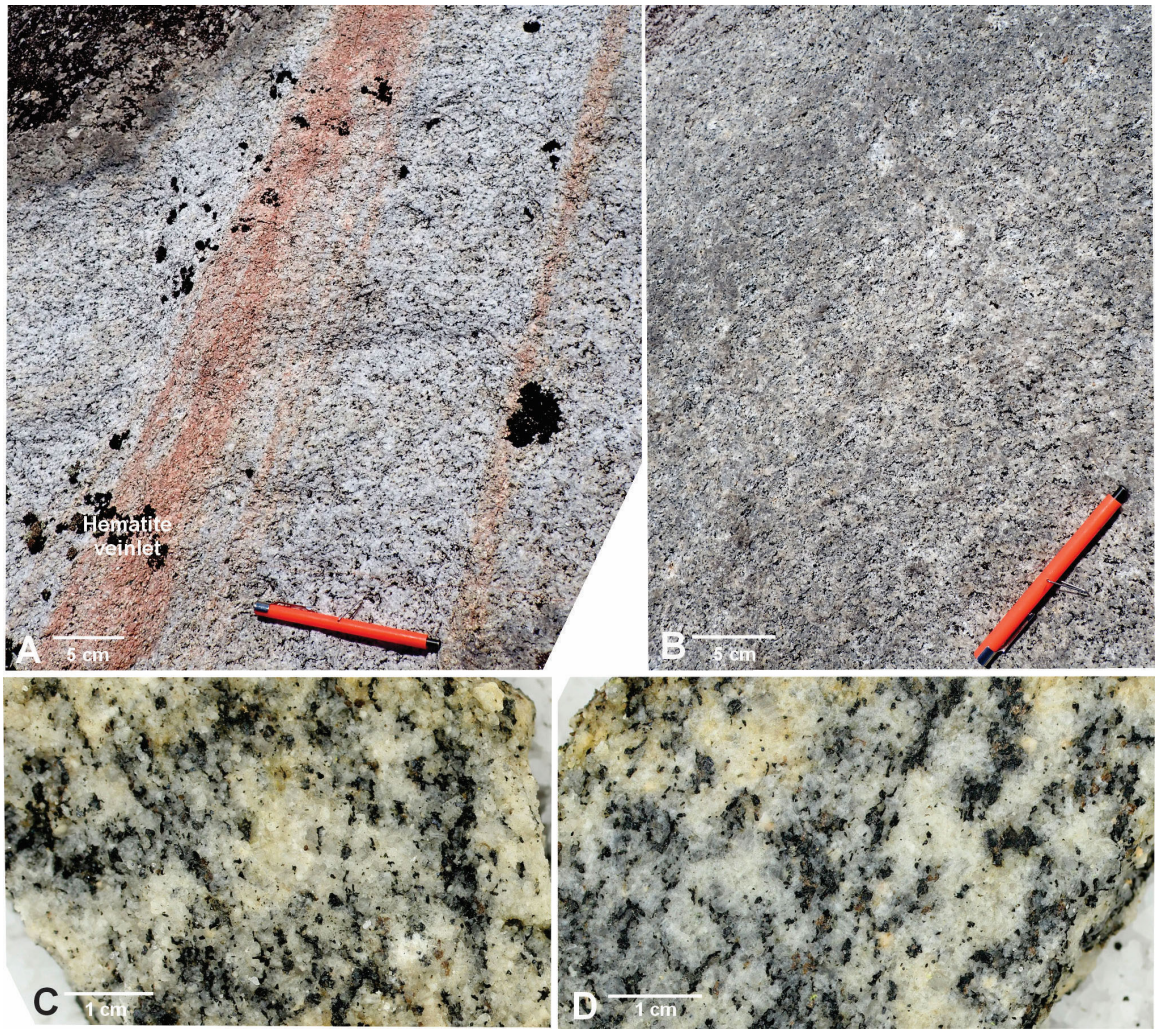


Figure 10. Field exposure and rock slabs of the foliated quartz monzodiorite at outcrop 25-IL-3151, representative of sample 3, CQA-00-158A. The mafic minerals consist of hornblende, biotite, magnetite and titanite. The monzodiorite is locally hematized at mild to moderate intensity along swarms of discrete parallel bands with diffuse contacts.

Zircon SEM secondary backscattered electron images show faint prismatic zoning and no overgrowths. A cluster of 10 concordant and one slightly discordant U-Pb SHRIMP zircon analyses yields a weighted mean of 1497 ± 12 Ma (MSWD = 0.57; POF = 0.84), in agreement with the U-Pb TIMS results. This age is the preferred age for the time of igneous crystallization. The range in morphologies is, therefore, of primary igneous origin, while the discordance of the U-Pb TIMS analyses is interpreted in terms of significant Pb loss.

Titanite was also separated from this sample and consisted of clear, orange, irregular fragments 300- to 400-microns across. Three multi-grain analyses are concordant to slightly reversely discordant (Fig. 7C). A regression through the three titanite analyses, assuming an upper intercept at 1.5 Ga, yields a lower intercept age of 997 ± 12 Ma (MSWD = 0.21; POF = 0.81). As the morphology is not distinctive, this age can be interpreted in terms of either titanite growth or closure of the U-Pb system during cooling following a thermal peak.

3.6. Sample CQA-00-268A: Augen Granitic Orthogneiss

The sample CQA-00-268A (GSC laboratory number z6721) is a granitic gneiss with an augen texture that is interpreted as having been coarse grained prior to deformation. It is located northeast of D'Auteuil Lake at 620120mE and 5615870mN in NTS map sheet 12K11 (Fig. 3C). Station 25-IL-3152 overlaps the GSC station. The host unit extends across D'Auteuil and Musquaro lakes (Fig. 3) and is a member of the D'Auteuil Intrusive Suite of Lafrance et al. (2026) and of unit mPagn5b1 of the former *Aguanish complex* (Fig. 3C; Appendix 1; Corriveau and Bonnet, 2005). The granite is leucocratic and medium-grained with minor biotite and magnetite (Fig. 11). It is locally overprinted by a network of faint anastomosing earthy hematite alteration that is likely associated with K-feldspar alteration.

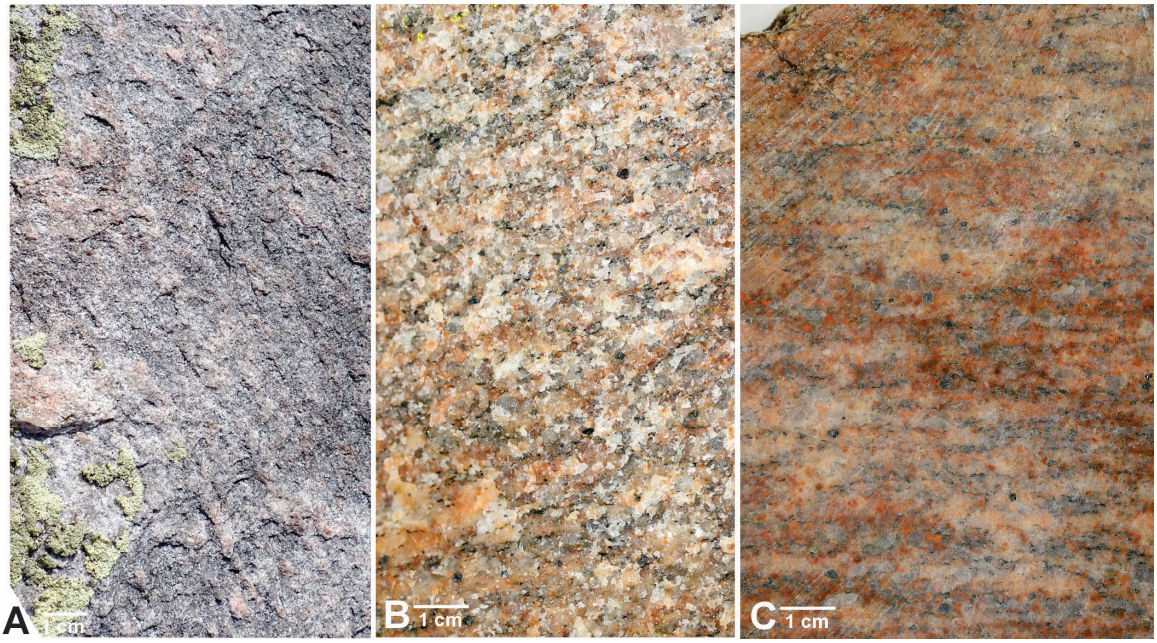


Figure 11. Field and rock slab photographs of sample CQA-00-268A. A weak anastomosing overprint by a K-feldspar alteration is observed in B and C.

Zircons are subhedral and prismatic, with L:B ratios of 2:1 to 4:1 and weak prismatic zoning. In SEM images, lighter-colored overgrowths occur at crystal tips or in embayment, but only rarely forms complete thin rims. A cluster of 11 concordant U-Pb SHRIMP analyses (Fig. 7D) yields a weighted mean of 1494 ± 12 Ma (MSWD = 1.4; POF = 0.18) and this age is assigned to the time of igneous crystallization. Three concordant analyses from overgrowths yield a weighted mean of $^{207}Pb/^{206}Pb$ age of 1004 ± 12 Ma (MSWD = 0.25; POF = 0.78). Low Th/U ratios (Table 2) are consistent with an interpretation of metamorphic zircon overgrowths. Titanite crystals are pale orange and are equidimensional with multiple facets, which suggests metamorphic growth. One titanite TIMS analysis yielded a $^{206}Pb/^{238}U$ age of 1000 ± 3 Ma.

3.7. Sample CQA-01-353A: Lapillistone, La Romaine Supracrustal Belt

The sample CQA-01-353A (GSC laboratory number z7090) is a lapillistone of the La Romaine supracrustal belt (unit mPcsr2a; Fig. 4C; Appendix 1; Corriveau and Bonnet, 2005). It is located west of La Romaine at 660189mE and 5563952mN in the NTS map sheet 12K02 (Figs. 4C, 5).

The lapillistone is grey, monomict and of intermediate composition, with ca. 50% felsic, elongate lapilli (Fig. 12). The sample comes from a 1 m thick bed within a series of lapillistone layers and

fine-grained, banded, biotite-bearing quartzofeldspathic gneisses. Primary textures are locally well preserved. They include accretionary lapilli and lapilli shattered in situ (Fig. 12A–C).

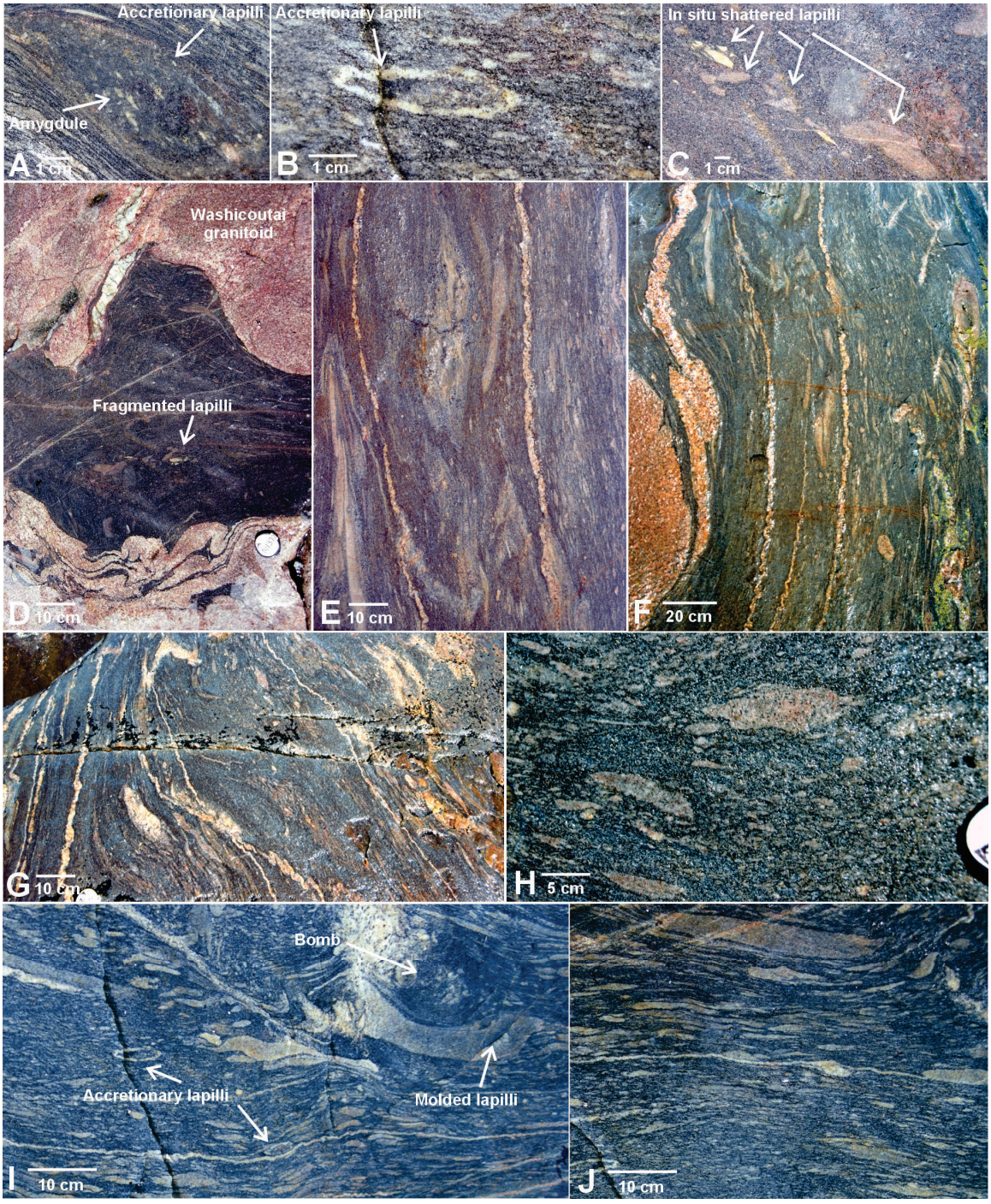


Figure 12. Field geology of the lapillistone at outcrop CQA-01-353, supplemented by photographs from the adjacent outcrop CQA-01-1370 in A–D, I, and J. Zones without veining were available for sampling the metamorphosed lapillistone alone. Note the presence of lapilli molded around bombs, accretionary lapilli and the fairly felsic nature of the lapilli. In D, the granitic veins are folded likely in a magmatic state and belong to the Washicoutai Intrusive Suite, a dyke of which was dated within the outcrop.

The sampled area was very homogeneous and had very few granitic veins which were avoided during sampling. In contrast, most photographs of the outcrop were taken where crosscutting relationships were best exposed, from zones of elongate but less tectonically deformed lapilli (Fig. 12D, H, I) to zones with strongly deformed lapilli (Fig. 12E, I, J) and zones cut by successive episodes of granitic veinlets (Fig. 12E–G, I, J) and dykes, the latter belonging to the Grenvillian Washicoutai Intrusive Suite dated herein (Fig. 12D–F).

The lapilli are elongate, flattened, centimetre wide and 2 cm to 2 dm long, with a high aspect ratio, buff-weathering surfaces and rounded margins. They are quartzofeldspathic, leucocratic, very fine grained and homogeneous. Biotite is minor. The matrix is very fine grained and has a more intermediate composition. The preservation of lapilli fragmented in situ during the volcaniclastic event in zones shielded from deformation by granitic dykes (Fig. 12C) indicates that at least part of the deformation is Grenvillian (Corriveau et al., 2026).

Zircons are rounded and range from equidimensional to prismatic grains with L:B ratios up to 3:1. Many grains consist of prismatic cores with vague prismatic zoning that are overgrown by unzoned rims that appear lighter in SEM back scattered electron images. Only two U-Pb SHRIMP analyses are concordant (Fig. 13A) and yield a mean $^{207}Pb/^{206}Pb$ age of 1502 ± 22 Ma (MSWD = 0.43; POF = 0.51). Despite the small number of concordant grains analyzed, the age is attributed to the time of zircon crystallization and extrusion of the lapillistone. Three other discordant zircon analyses are interpreted as inherited zircon, with $^{207}Pb/^{206}Pb$ ages of 1585 Ma, 1758 Ma and 2447 Ma.

3.8. Sample CQA-01-371A: Multiply Folded Tonalitic Gneiss

The sample CQA-01-371A (GSC laboratory number z7091) is a multiply folded tonalitic gneiss. It is located at 653929mE and 5562435mN in NTS map sheet 12K02 south of the La Romaine supracrustal belt (Fig. 4C). The tonalitic gneiss crops out preferentially on the coastal archipelagos of Fraser Harbour and Washicoutai Bay, west of La Romaine, as well as at Bluff Harbour further east (Fig. 4). It is a member of the Kegaska Intrusive Suite of Lafrance and Daoudene (2024) and of the unit mPagn4 of the former *Aguanish complex* (Fig. 4C; Appendix 1; Corriveau and Bonnet, 2005).

The tonalitic gneiss is heterogeneous, medium-grained, foliated, and banded, with a granoblastic texture. It consists of an assemblage of plagioclase, quartz, hornblende, biotite, and locally magnetite. Mafic minerals account for approximately 10% of the rock's modal composition in the more common layers. Decimetre-scale mafic layers—either hornblende-rich or dioritic in composition—define a banding parallel to the foliation. Granitic veins are abundant.

The gneiss is intensely folded, displaying dome-and-basin fold interference patterns that indicate a complex deformation history (Fig. 14; Corriveau et al., 2002; Bonnet and Corriveau, 2003; Corriveau et al., 2026). However, farther west towards Kegaska and on the southernmost islands, the tonalitic gneiss becomes homogeneous, medium grained, and porphyroclastic in texture. It locally contains dioritic enclaves and is cut by dykes ranging from decimetres to metres in thickness; these dykes locally exhibit apophyses of fine-grained, foliated black amphibolite typical of cogenetic emplacement with their host (Bonnet and Corriveau, 2003; Corriveau et al., 2026). The more homogeneous tonalite also contains medium-grained, foliated, porphyroclastic diorite and late-stage, foliated, fine- to medium-grained, leucocratic (3% biotite) pink granite in addition to the comagmatic mafic dykes as illustrated in Corriveau et al. (2026) and Bonnet and Corriveau (2003). Given these characteristics, this homogeneous gneiss was interpreted as the less-deformed equivalent of the folded tonalitic gneiss by Bonnet and Corriveau (2003). Recent mapping has shown that these tonalitic gneisses comprise components assigned to the Kegaska Intrusive Suite, as well as older components assigned to the L'Aigle Complex (Lafrance et al., 2026).

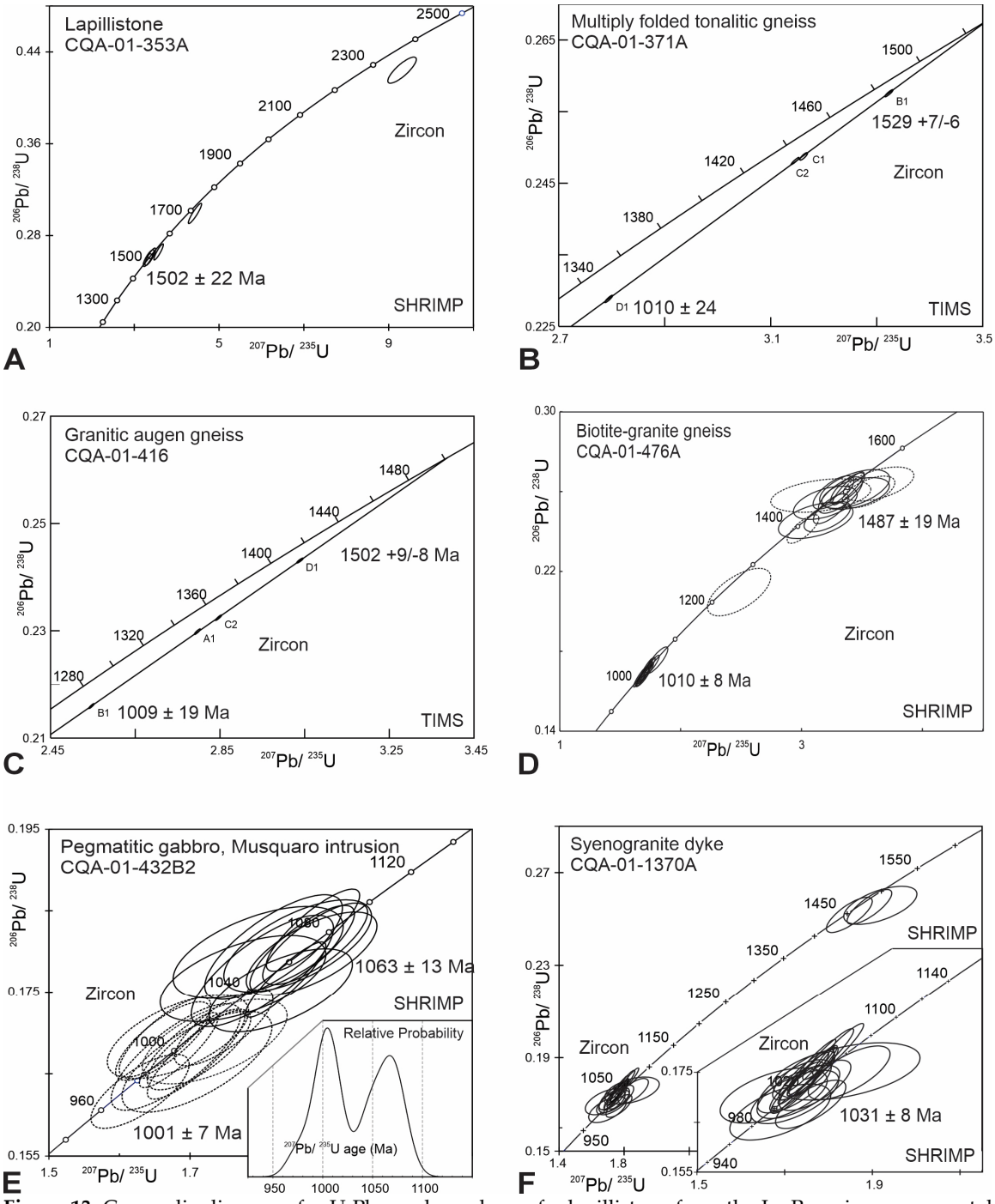


Figure 13. Concordia diagrams for U-Pb geochronology of a lapillistone from the La Romaine supracrustal belt, three granitoids from the *Aguanish complex* along the transect from Kegaska to Baie des Loups, a pegmatitic gabbro from the Musquaro ultramafic to mafic intrusion, and a late-stage syenogranitic dyke of the Washicoutai Intrusive Suite.

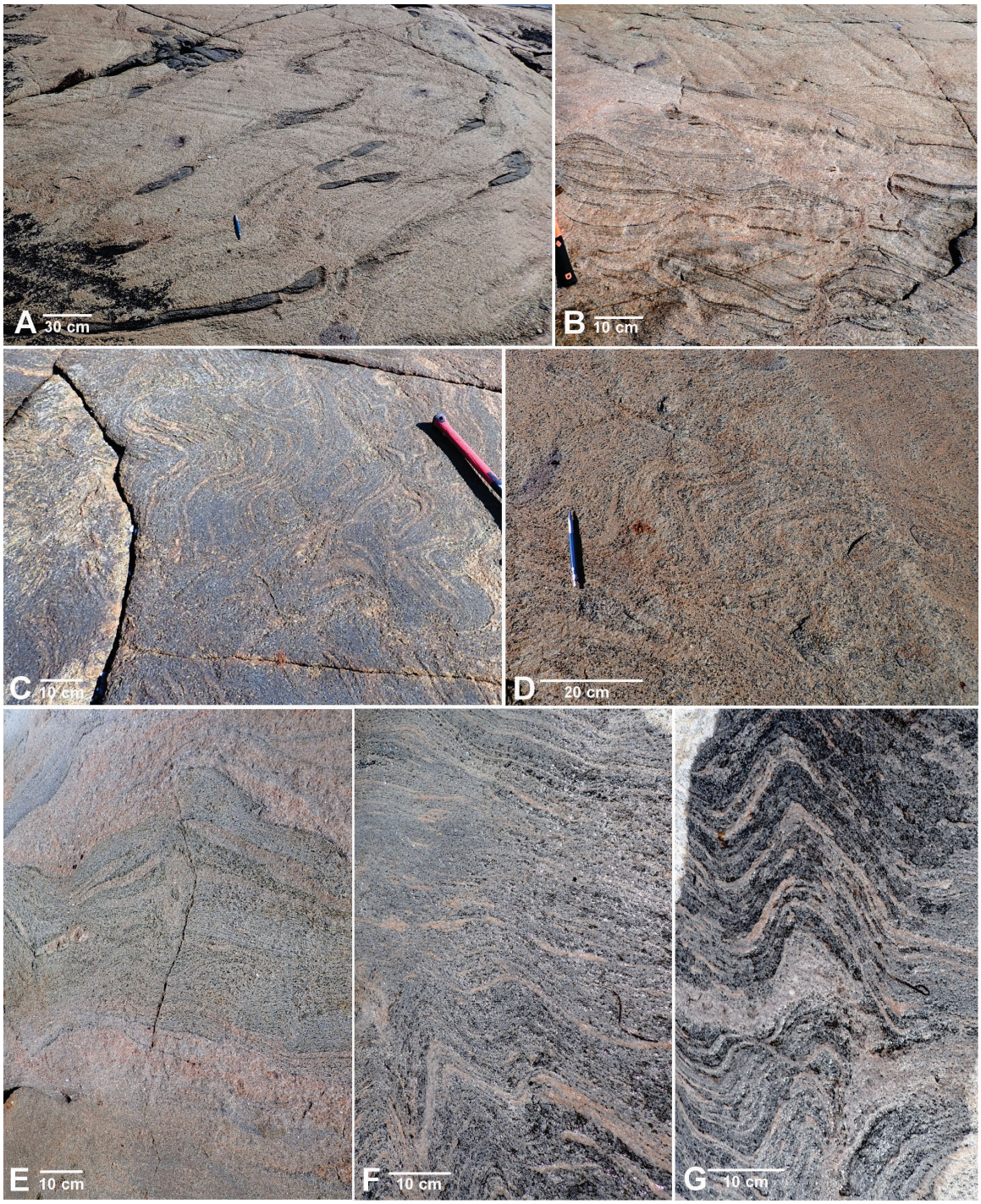


Figure 14. Field photographs of outcrop CQA-01-371. Additional photographs of this unit can be found in Corriveau et al. (2026) As shown in A, numerous mafic dykes were involved in the pervasive folding with well-developed interference patterns that characterizes the unit. They appear to preserve possible evidence of comagmatic emplacement. If so, magma mingling and mixing, together with multiphase injections of granitic dykes and veins variably affected by folding, may explain the extreme compositional heterogeneity observed in this unit.

Zircon morphology ranges from equidimensional to stubby prismatic grains and from irregularly shaped to multi-faceted crystals. Four fractions were selected with one, B1, consisting of irregularly

shaped crystals and the other three of multifaceted grains. U-Pb TIMS analyses yield four strongly discordant data points that are linearly aligned. Regression of the four aligned analyses yields an upper intercept age of 1529 +7/-6 Ma and a lower intercept age of 1010 ± 24 Ma (MSWD = 1.2; POF = 0.30). As the oldest analysis is from the irregular grains, the discordia is interpreted in terms of a mixing line between irregular igneous grains that grew at a late stage in the interstices of grains and metamorphic zircon as represented by the multifaceted types, forming either overgrowths or new zircon growth. The discordance may be partly attributable to Pb loss during the event that grew the younger zircon. The upper intercept age is, therefore, interpreted in terms of igneous crystallization and the lower intercept in terms of metamorphism.

3.9. Sample CQA-01-416: Granitic Augen Gneiss

The sample CQA-01-416 (GSC laboratory number z7092) is a granitic augen gneiss located west of Musquanousse River along the coast at 642791mE and 5563332mN in NTS map sheet 12K02 (Fig. 4C). The outcrop sampled was very homogeneous and represents the best megascopic equivalent of the granitic augen gneiss at Musquaro Lake (Fig. 15). It is part of the Grand Priant Intrusive Suite of Lafrance et al. (2026) and of unit mPagn5a2 of the former *Aguanish complex* (Fig. 4C; Appendix 1; Corriveau and Bonnet, 2005).

Zircons are euhedral to subhedral prisms with L:B ratios ranging from 2:1 to 5:1. Analyses of four fractions yield strongly discordant data points that are linearly aligned. Regression through the four analysis yields an upper intercept age of 1502 +9/-8 Ma and a lower intercept age of 1009 ±19 Ma (MSWD = 0.38; POF = 0.68) (Fig. 13C). The upper intercept age is interpreted in terms of igneous crystallization and the lower intercept in terms of lead loss during a subsequent event.



Figure 15. Field photographs of outcrop CQA-01-416 in A–D, sample CQA-01-416A in E, and a more deformed example in F.

3.10. Sample CQA-01-476A: Biotite-bearing Granitic Orthogneiss

The sample CQA-01-476A (GSC laboratory number z7093) is a biotite-bearing granitic orthogneiss located at 697459mE and 5565730mN in NTS map sheet 12K01 (Fig. 4D). It is a member of the Coacoachou Intrusive Suite of Daoudene and Lafrance (2025) and of unit mPagn5a2 of the former

Aguanish complex (Fig. 4D; Appendix 1; Corriveau and Bonnet, 2005). The granitic gneiss is slightly lenticular, penetratively recrystallized to a granoblastic texture, and leucocratic, with about 5 vol.% hornblende, 5 vol.% orthopyroxene, 1 vol.% biotite and no magnetite (Fig. 16).

Zircons are subhedral and vary from equidimensional grains to subhedral prisms. SEM images show prismatic cores with vague or absent zoning and light-colored rims. Fourteen SHRIMP analyses yield a cluster of ages around 1.5 Ga on the concordia (Fig. 13D), which correspond to a weighted mean of $^{207}Pb/^{206}Pb$ age of 1494 ± 25 Ma (MSWD = 2.2; POF = 0.008). A better fit is obtained by excluding the two youngest and two oldest, strongly discordant, analyses, yielding a weighted mean age of 1495 ± 17 Ma (MSWD = 0.64; POF = 0.77). Further improvement to this age can be obtained by filtering the data to less than 5 % discordance. Doing so 12 analyses are retained and the age is of 1487 ± 19 Ma (MSWD =1.2; POF = 0.27). This date is the preferred age and is attributed to the time of igneous crystallization. A younger cluster of 11 analyses from rims yields a weighted average $^{207}Pb/^{206}U$ age of 1002.6 ± 7.9 Ma (MSWD = 1.2; POF = 0.26). This age is attributed to zircon growth during metamorphism. Th/U ratios are not low; this can be explained by zircon growth during granulite-facies metamorphism.



Figure 16. Field photographs of outcrop CQA-01-476. **A.** Overview of the outcrop exposure. **B, D, E, G.** The granitic rock is cut by mafic dykes that belong to the Lillian Intrusive Suite and these mafic dykes are themselves cut by granitic veins that likely belong to the Washicoutai Intrusive Suite. The latter are cut by straight quartz veins. Close-up of the dated metaplutonic biotite granite. **F.** Multiple intrusive phases are

observed in the host granitoid. **H.** Close-up of the mafic dyke in G. **I.** Close-up of E. **J**. Close-up of the dated unit.

3.11. Sample CQA-01-432B2: Pegmatitic Gabbro of the Musquaro Ultramafic to Mafic Intrusion

The sample CQA-01-432B2 (GSC laboratory number z7089) comes from a series of four pegmatitic gabbro pockets in the layered ultramafic to mafic Musquaro intrusion located at 639058mE and 5563444mN in NTS map sheet 12K03 (Figs. 4B, 17). It is a member of unit mPmqo3 of the Musquaro layered intrusion (Fig. 17; Appendix 1; Corriveau et al., 2002) The Musquaro intrusion is described in Appendix 1, Corriveau et al. (2002), Corriveau et al. (2026), and as the Musquaro Gabbroic Intrusion in MRNF stratigraphic lexicon (MRNF d).

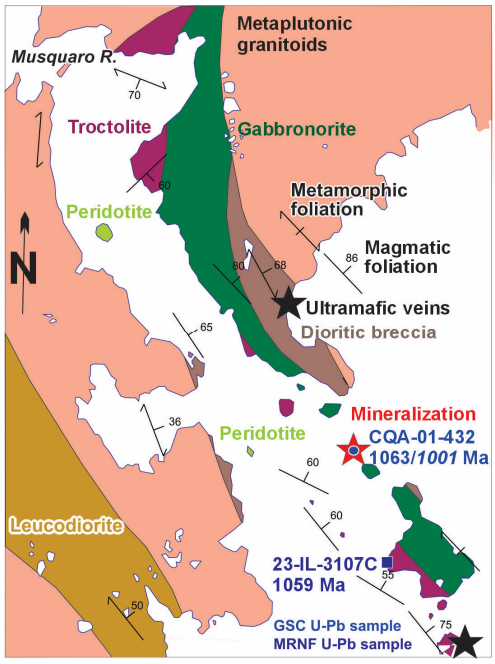


Figure 17. Map of the Musquaro ultramafic to mafic, subvertically layered intrusion (Corriveau et al., 2002). See the unit description in Appendix 1. The age obtained in this study (CQA-01-432) is shown in dark blue, whereas the age obtained by Rochín-Bañaga and Davis (in press) from another pegmatitic gabbro sample (23-IL-3107C) is shown in paler blue.

The pegmatitic pockets are dm in width and a few dm to 1 m in length. They are not interconnected at the surface (Fig. 18). They have a high aspect ratio, highly irregular shapes, and their contacts with the medium-grained gabbro are gradual over a few cm. The pockets grade inwardly from a pegmatitic gabbro component with interlocking coarse-grained plagioclase crystals and interstitial pyroxene to a more felsic component with medium-grained apatite, biotite, K-feldspar and quartz (Fig. 18). The irregular and gradual contacts with the host, the lack of interconnections among pockets and the inward transition from mafic to felsic compositions are typical of in situ crystallization and differentiation of a gabbroic fluid-rich magma. Fluid-enhanced grain coarsening occurs, and the gabbro differentiates in situ toward a more felsic composition, allowing the crystallization of datable zircon and apatite. Such pegmatitic gabbro pockets can therefore be used to directly date the crystallization age of the host gabbro, a method that has also been used to date a gabbro in the Central Metasedimentary Belt of Québec (Corriveau and van Breemen, 2000; Corriveau, 2013). The pockets and their host gabbro are cut by irregular granitic pegmatite dykes. These dykes were avoided during sampling for geochronology.

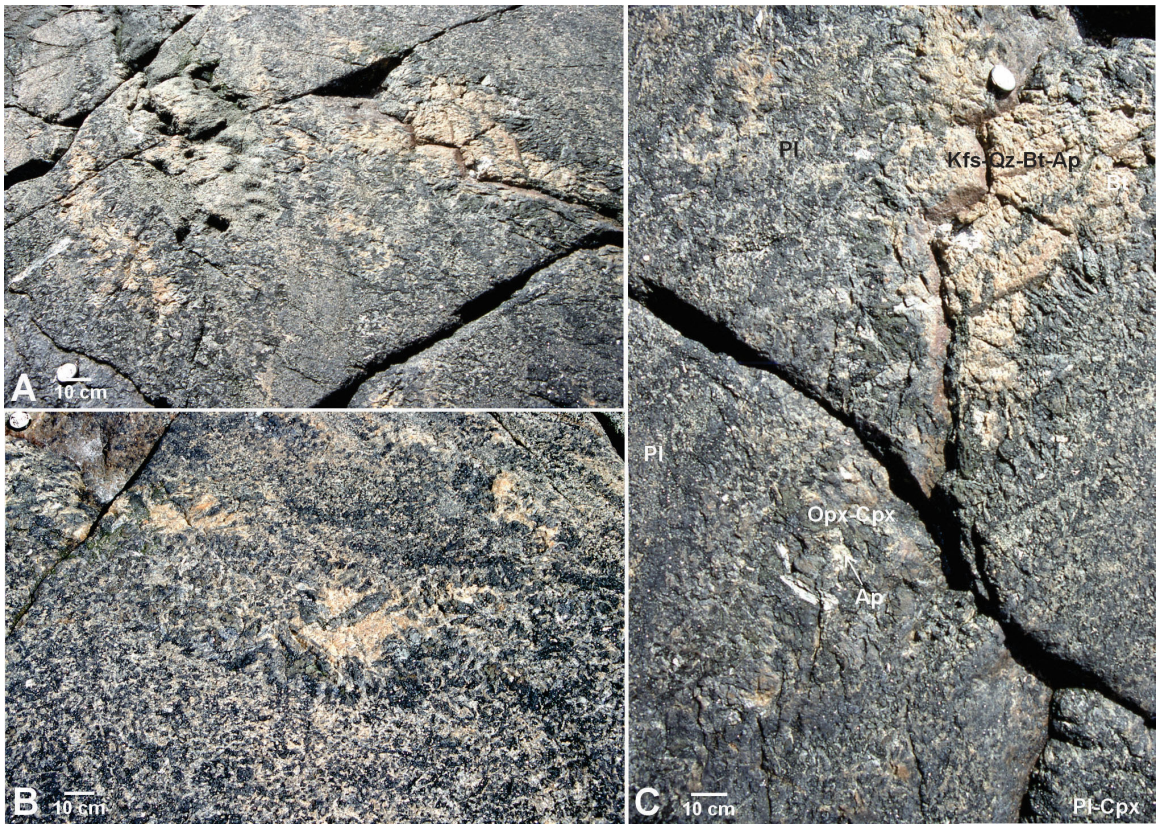


Figure 18. Field photographs of a pegmatitic gabbro with gradational contacts with the host gabbro of the Musquaro intrusion at outcrop CQA-01-432. The relationship of the pegmatitic gabbro sampled for geochronology is typical of in situ fluid-enhanced grain coarsening during the crystallization of the host and thus provides a direct age for crystallization of the host gabbro.

Within the pegmatitic gabbroic pockets, zircons vary from equidimensional to elongate, with L:B ratios of up to 2:1. Grains are subhedral to irregular in shape. SEM images suggest the existence of two generations, consisting of prismatic cores and overgrowths. Zoning is weak or absent from both cores and overgrowths, making it difficult to distinguish the two types in many grains. Twenty-two SHRIMP analyses yield a bimodal distribution (Fig. 13E) and a relative probability plot clearly distinguishes two age populations. The weighted mean $^{207}Pb/^{206}Pb$ age of the 11 older analyses, from what appear to be cores, is 1063 ± 13 Ma (MSWD = 1.08; POF = 0.38). The younger group of 11 analyses yields a weighted mean age of 1001 ± 7 Ma (MSWD = 1.17; POF = 0.3).

The style of magma emplacement and contact relationships with the host of the pegmatitic gabbro pockets dated herein are very different from those of a pegmatitic gabbro dyke dated at 1059 ± 15 Ma further south in the Musquaro intrusion by Rochín-Bañaga and Davis (in press) as illustrated in Figure 18 versus Figure 19. The dyke at outcrop 23-IL-3107 cuts sharply the host gabbro (Fig. 19). The age of this dyke informs on the timing of emplacement of the multiphase mafic magmatism within the Musquaro intrusion.

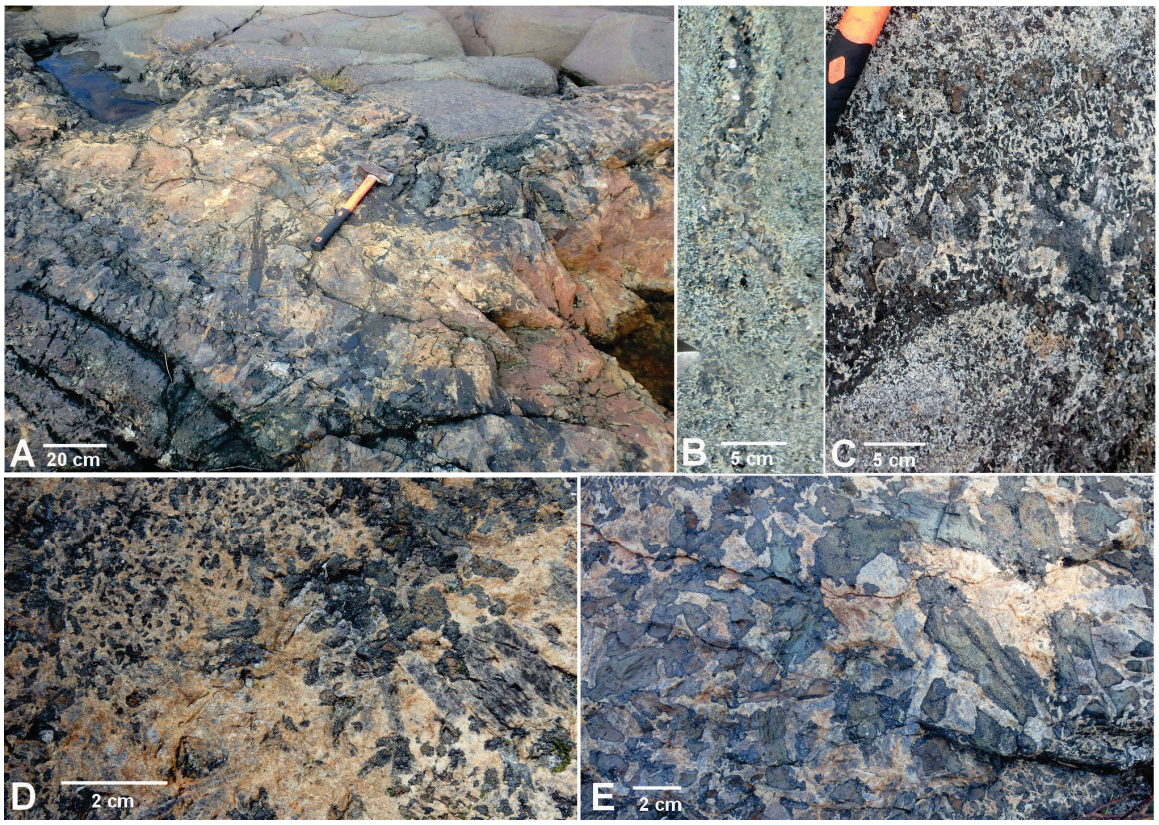


Figure 19. Field photographs pegmatitic gabbro with an interpreted crystallisation age of 1059 ± 15 Ma, in contact with a gabbronorite of the Musquaro intrusion at outcrop 23-IL-3107 (Rochín-Bañaga and Davis, in press).

3.12. Sample CQA-01-1370A: Syenogranite Dyke

The sample CQA-01-1370A (GSC laboratory number z7094) is a late-stage granitic dyke with igneous and local tectonic foliation fabrics, located at 660209mE and 5564344mN in NTS map sheet 12K02 (Figs. 4C, 5). The sample comes from a several-tens-of-metres-wide dyke of pink, leucocratic, medium-grained syenogranite with a hypidiomorphic-granular texture that cuts a lapillistone from unit mPcsr2a that was dated further south (Fig. 20). The preferred orientation of hypidiomorphic K-feldspar laths defines a weak igneous foliation largely parallel to the contacts of this and other dykes of this unit on the outcrop (Fig. 20B, C, G). The dykes have irregular shapes with synmagmatic boudinage (Fig. 20C–E). A weak tectonic foliation is superimposed on the igneous foliation (Fig. 20H). These fabrics suggest that the emplacement of these dykes was syntectonic and late in the development of the regional metamorphism and associated deformation. Some of dykes also host pegmatitic phases along their contacts (Fig. 20D). Subsequent pegmatitic dykes are linear and were emplaced orthogonally to the fabric of the syenogranite dykes (Fig. 20A). The sampled syenogranite dyke is representative of the mPwai1 unit of the Washicoutai Intrusive Suite of Lafrance and Daoudene (2024). The suite is the youngest intrusive suite observed and dated throughout the region (Daoudene and Lafrance, 2024; Lafrance and Daoudene, 2025; Lafrance et al., 2026).

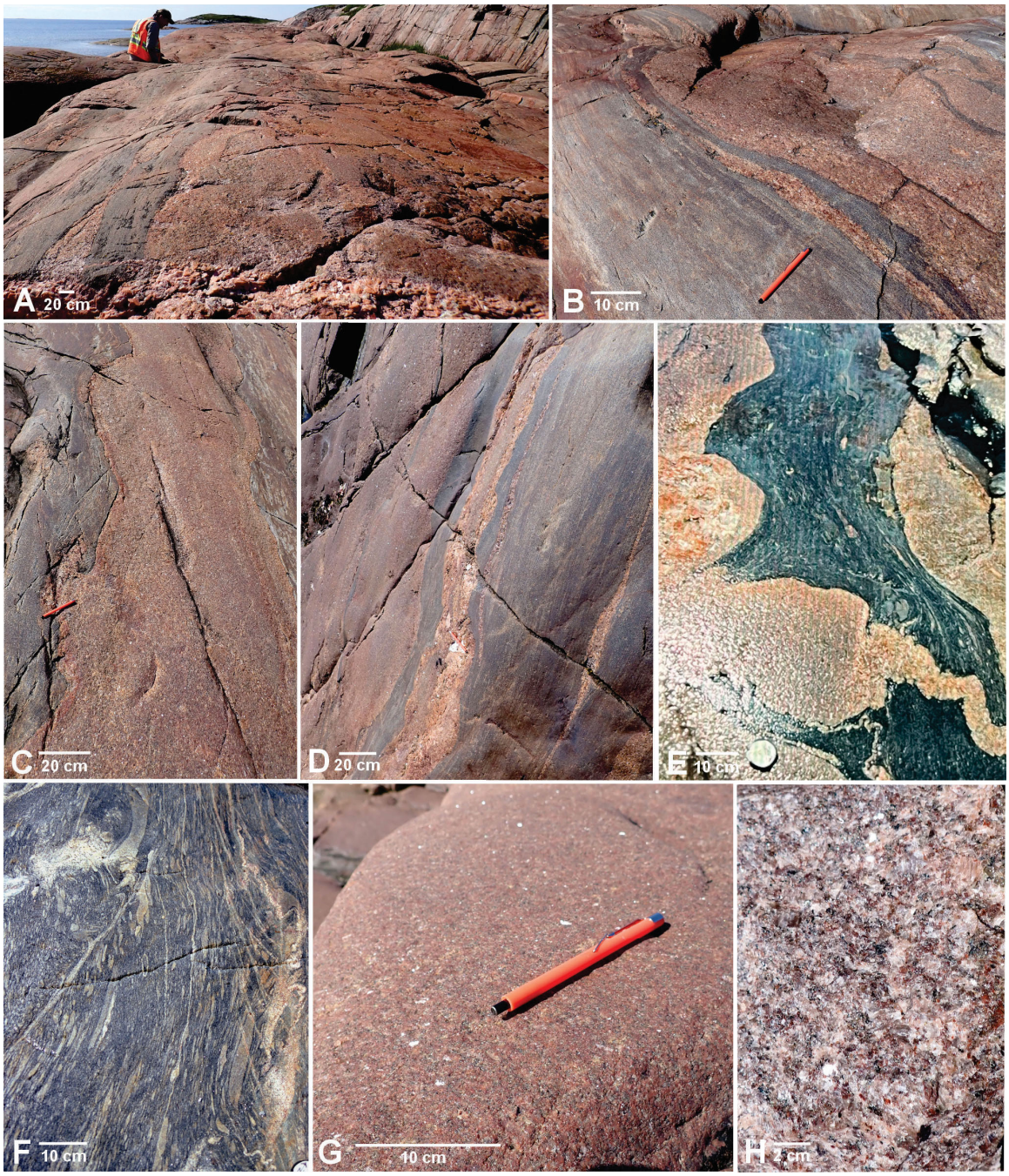


Figure 20. Field photographs of a medium-grained granitic dyke preserving cm-scale K-feldspar laths that define an igneous foliation at outcrop CQA-01-1370. The dyke is part of the Washicoutai Intrusive Suite of Lafrance et al. (2026). The granitic dyke cuts an earlier foliation in the host volcaniclastic rock that was dated farther south at outcrop CQA-01-353. Pegmatitic dykes cut the granitic dyke and its host. These pegmatites are also included within the Washicoutai Intrusive Suite by Lafrance et al. (2026).

Offshoots of this dyke intrude the lapillistone and are open to tightly folded while apparently in a magmatic state (Fig. 20E). They cut the gneissic fabric of their host lapillistone (Fig. 20E, F) which has been dated at CQA-01-353 farther south. The dyke also shields the lapillistone from extensive deformation in areas that were initially less deformed (Fig. 12D), illustrating the multiphase development of the foliation, including deformation of the volcaniclastic fragments (Fig. 12). As

such, the dyke post-dates peak granulite-facies metamorphism and the volcanic and gneissic fabrics of the supracrustal rocks. Its weak tectonic foliation indicates it is itself slightly deformed in the solid state.

Zircons are subhedral to rounded, equidimensional to prismatic grains with L:B ratios up to 3:1. Some grains contain cores that feature weak, prismatic zoning. In most cases, zoning is absent. U-Pb SHRIMP analyses show that most of the zircon is ca. 1.0 Ga as compared to a few ca. 1.5 Ga analyses (Fig. 13F). Back scattered electron images (not available) show that the young, light-colored zircon is intergrown with and hosted within the older, prismatic zircon. A tentative explanation is that much of the original prismatic zircon was rich in U, especially in the cores and developed extensive lattice damage, which was replaced by new zircon.

The two oldest $^{207}Pb/^{206}Pb$ ages have large uncertainties, while the remaining ca. 1.5 Ga ages show a spread and are interpreted as inherited zircons. Their age is close to 1.51 Ga based on the $^{207}Pb/^{206}Pb$ age of analysis 26A1. The weighted mean $^{206}Pb/^{238}U$ age of the younger 21 analyses is 1031 ± 8 Ma (MSWD = 2.1; POF = 0.0003) and is interpreted as the age of igneous crystallization. This interpretation is not straight forward as the dates fall in the range of metamorphic ages while the older near-concordant dates fall in the range of Pinwarian magmatism. As the U content of the host rock is low (8.8 ppm) and that the ages fall in tight clusters, it is unlikely that the older zircons have been all reset to a metamorphic age. In addition, a 1031 Ma crystallization age supports the field relationships. The dyke has well-preserved K-feldspar laths that are delicate and not the large megacrysts seen in the Pinwarian intrusions, hence the laths would have been prone to extensive recrystallization if the unit had been Pinwarian and pervasively recrystallized during the Grenvillian tectonometamorphic event. Pinwarian xenocrysts could be sourced in the host lapillistone dated at 1502 Ma further south at outcrop CQA-01-353.

3.13. Sample CQA-02-547A: Argillic-altered Lapillistone (Aluminous Gneiss)

The sample CQA-02-547A (GSC laboratory number 7537) is an aluminous gneiss interpreted as an argillic-altered lapillistone of the La Romaine supracrustal belt. The sample is located at UTM 661195mE and 5565111mN in NTS map sheet 12K02 (Figs. 4C, 5). It belongs to unit mPcsr4b as described in Appendix 1 (Figs. 4C, 5; Corriveau and Bonnet, 2005; see discussion of mPcsr units in Corriveau et al., 2026). The aluminous gneiss has a granulite-facies assemblage of biotite, sillimanite, cordierite, garnet, K-feldspar, plagioclase, Fe-sulphides (dominantly pyrite), titanite and quartz (Fig. 21). It contains coarse-grained amoeboid- or stromatitic-shaped garnet- and cordierite-bearing leucosomes in which the cordierite is locally retrogressed to sillimanite.

Primary felsic volcanic fragments (lapilli and bomb size) are locally well preserved and display similar size, morphology and composition to those found in the adjacent unaltered coarse felsic lapillistone (Corriveau and Bonnet, 2005). These fragments attest to a volcaniclastic origin for the aluminous gneisses. In thin section (Fig. 22A–F), the sample displays a fragmental texture with foliated feldspathic fragments surrounded by a fine-grained sillimanite- and biotite-rich matrix. The fragments are abundant and are composed of medium-grained K-feldspar with abundant inclusions of biotite, quartz, plagioclase and zircon (Fig. 22C, E, F). The fragments are rimmed by a recrystallized inclusion-free zone of K-feldspar (Fig. 22E, F). Zircon grains also occur within garnet-cordierite leucosomes. On an AFM diagram (Fig. 22G), the sample is more aluminous than the North American Shale Composite (i.e., it plots above its composition) of Gromet et al. (1984).

The aluminous gneiss yielded euhedral to subhedral zircon grains displaying fine-scale oscillatory zoned cores (Zircon 1 in Fig. 22H). Most of these grains average 100 to 200 μm in length and show

minor cracking (Fig. 23). Scanning electron imaging reveals the euhedral to irregular morphology of these cores (Fig. 23). The Th/U ratios of the cores range from 0.34 to 0.89, and their U and Th contents range from 111 to 395 ppm and from 52 to 339 ppm, respectively (Fig. 23; Table 4).

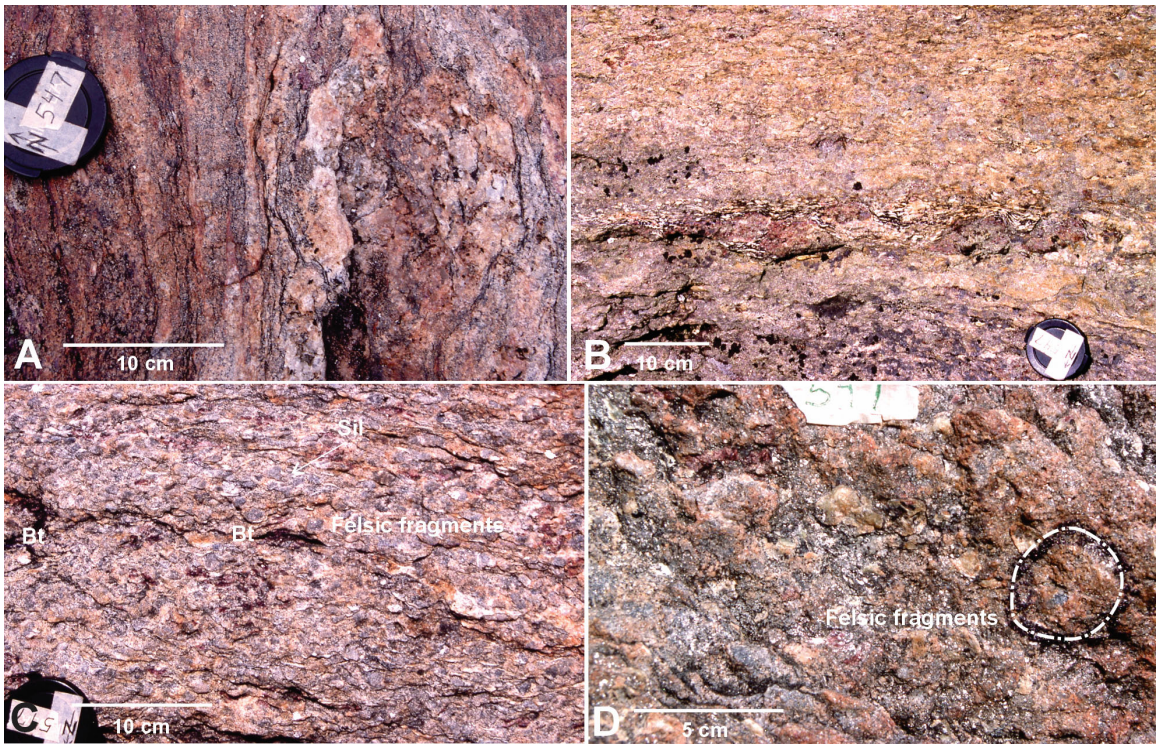


Figure 21. Field photographs of the aluminous gneiss, interpreted as an argillic-altered lapillistone (CQA-02-547A).

The subhedral prismatic morphology, weak oscillatory zoning and typically igneous Th/U ratios of these cores suggest that they are magmatic in origin. Zoned cores are overgrown by unzoned rims, which impart the rounded subhedral external morphology of the grains. Rims are generally a few μm wide; where their thickness increases, they may constitute up to 40% of the cross section in some of the grains. None of the rims were analyzed, because more precise metamorphic ages could be obtained from other samples. Many of the cores are embayed, which is typical of metasomatic dissolution (Figs. 22H, 23).

A total of eleven analyses were carried out on oscillatory zoned cores. Analyzed spots were located away from any visible cracks. Five additional analyses have been discarded (7537-71.1, 7537-142.1, 7537-20.1, 7537-89.1 and 7537-80.1) and not listed in Table 4. Data from zircon cores are dominated by a cluster of eight concordant analyses with a weighted mean $^{207}Pb/^{206}Pb$ age of 1508 ± 14 Ma (MSWD = 0.73; POF = 0.65) (Fig. 23B). However, three concordant analyses plot outside this cluster, while the main cluster shows a slight spread along the concordia. A regression line passing through all eleven analyses intersects concordia at 1532 ± 43 Ma (1σ) and 962 ± 230 Ma (1σ). The lower intercept age suggests that the cores experienced some Pb loss during Grenvillian metamorphism. The upper intercept age agrees with the mean $^{207}Pb/^{206}Pb$ age for the cluster of eight points, but this age is considered unreliable because recent Pb loss would pull the upper intercept towards an older age. Our best estimate of the crystallization age is therefore based on the three concordant analyses with the oldest $^{206}Pb/^{208}Pb$ ages (analyses 24.1, 40.1 and 143.1). A 'concordia' age calculated according to the method of Ludwig (2000) yields 1516.0 ± 6.9 Ma with 0.95% probability of

concordance, which is interpreted as the time of zircon crystallization just prior to eruption and deposition of the volcaniclastic material.

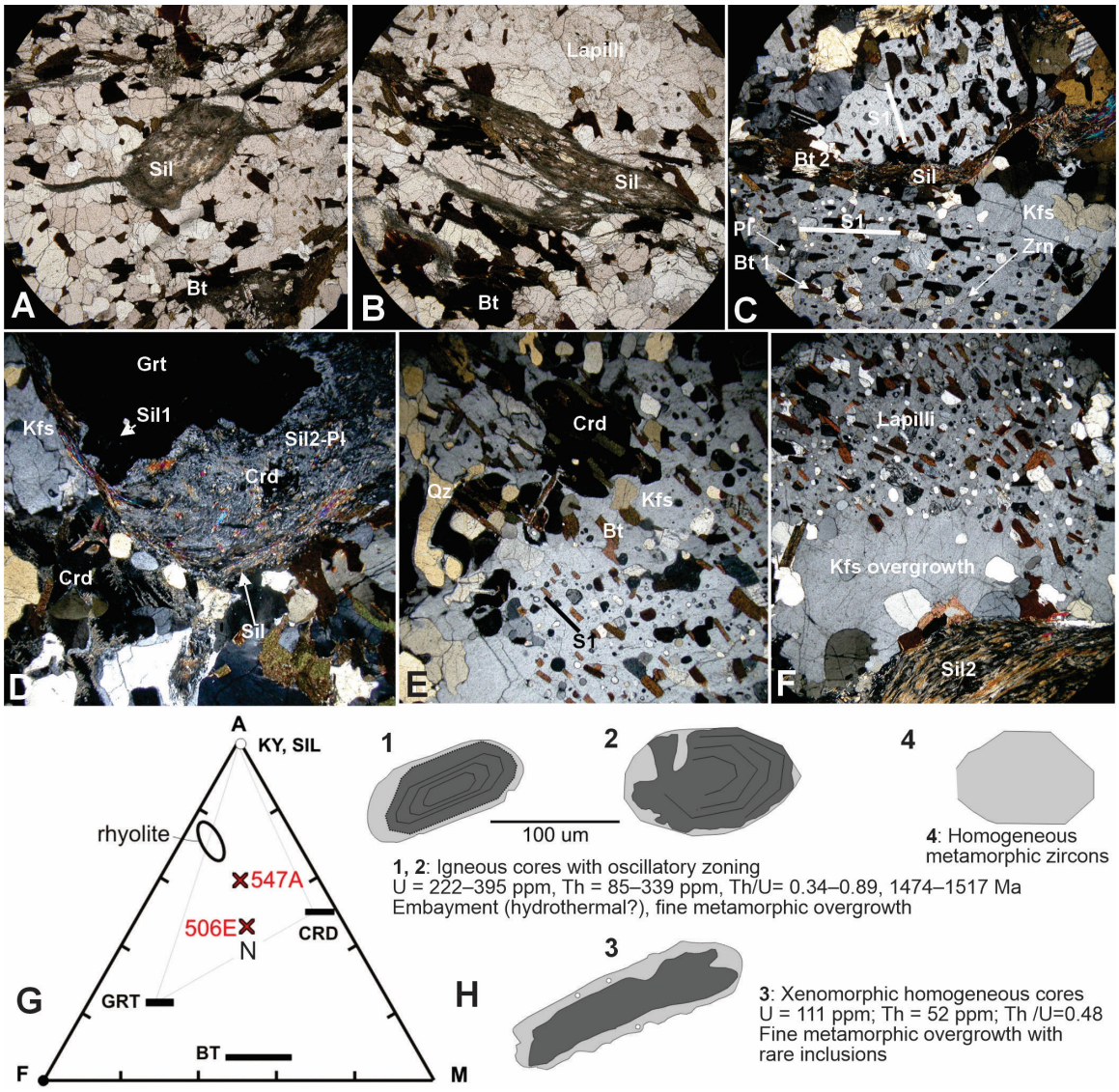


Figure 22. Microphotographs showing zircon types and an AFM diagram illustrating the composition of the aluminous gneiss, interpreted as an argillic-altered lapillistone (sample ALB1, CQA-02-547A). **A–C.** Lapilli composed of medium-grained K-feldspar rich in inclusions of biotite, quartz, plagioclase and zircon. The lapilli are surrounded by a matrix that is now rich in biotite and sillimanite, with accessory cordierite. **D–F.** Leucosome in D and E are cordierite-bearing, while in E and F, K-feldspar overgrowths occur along the margins of lapilli. **G.** AFM diagram showing the composition of samples CQA-02-547A and CQA-01-506E. **H.** Types of zircons observed in sample CQA-02-547A.

Table 4. SHRIMP isotopic data for zircon from the argillic-altered lapillistone at La Romaine (sample CQA-02-547A), the Ca-Fe- and K-Fe-altered amphibolite unit (sample CQA-01-1564E) and the metagabbro unit metamorphosed under granulite-facies conditions (sample CQA-02-1840A). IZ is igneous zircon, Mz is metamorphic zircon and IRZ is inclusion-rich zircon. Spreadsheet in the supplementary file.

Sample Spot # *	Type	Spot size	U (ppm)	Th (ppm)	Th/U	Pb (ppm)	^{204}Pb (ppb)	^{204}Pb/^{206}Pb	±1s	f206	^{208}Pb/^{206}Pb	±1s	^{207}Pb/^{235}U	±1s	^{206}Pb/^{238}U	±1s	^{207}Pb/^{206}Pb	±1s	age ^{206}Pb/^{238}U	±1s	age ^{207}Pb/^{206}Pb	±1s
CQA-02-547A, metamorphosed aluminous (argillic-																						
7537-100.1	IZ	120	160,95	55,11	0,354	38	10	0,00031	6,01E-05	0,0053	0,0937	0,0052	2,815	0,064	0,2326	0,0032	0,0878	0,0015	1348	17	~~1378~~	~~32~~
7537-4.1	IZ	120	202,71	73,42	0,374	49	0	0,00001	0,00001	0,0002	0,1147	0,0018	2,943	0,048	0,2346	0,0031	0,0910	0,0007	1359	16	~~1446~~	~~15~~
7537-59.1	IZ	120	272,74	95	0,360	66	5	#####	5,07E-05	0,0017	0,1081	0,0024	2,905	0,053	0,2348	0,0031	0,0897	0,0010	1360	16	~~1420~~	~~21~~
7537-13.1	IZ	120	222,15	85,18	0,396	59	2	4,25E-05	2,96E-05	0,0007	0,1192	0,0021	3,260	0,068	0,2538	0,0040	0,0932	0,0011	1458	21	1491	22
7537-39.1	IZ	120	111,8	52,12	0,482	30	4	1,58E-04	4,44E-05	0,0028	0,1430	0,0042	3,288	0,076	0,2545	0,0041	0,0937	0,0014	1462	21	1502	28
7537-9.1	IZ	120	336,44	202,2	0,621	95	6	8,47E-05	2,23E-05	0,0015	0,1784	0,0020	3,306	0,054	0,2570	0,0033	0,0933	0,0008	1474	17	1494	16
7537-48.1	IZ	120	303,35	110,9	0,378	81	4	5,91E-05	3,63E-05	0,0010	0,1112	0,0019	3,315	0,060	0,2577	0,0036	0,0933	0,0009	1478	19	1494	18
7537-97.1	IZ	120	337,59	188,7	0,577	96	0	3.03E-	3.B0E-05	0,0001	0,1710	0,0021	3,425	0,064	0,2596	0,0033	0,0957	0,0012	1488	17	1541	23
7537-24.1	IZ	120	307,67	196,62	0,660	90	5	6,96E-05	3.B4E-05	0,0012	0,1962	0,0031	3,472	0,079	0,2645	0,0044	0,0952	0,0013	1513	22	1532	26
7537-143.1	IZ	120	395,35	339,55	0,887	123	6	6,61E-05	1,94E-05	0,0012	0,2653	0,0046	3,443	0,059	0,2650	0,0039	0,0942	0,0006	1515	20	1513	13
7537-40.1	IZ	120	303,88	101,21	0,344	83	4	5,23E-05	9,76E-05	0,0009	0,1009	0,0039	3,448	0,080	0,2654	0,0035	0,0942	0,0016	1517	18	1513	33
CQA-01-1564E, metamorphosed Ca-Fe and K-Fe altered amphibolite																						
7535-104.1	IRZ	70	568	755	1,372	130	16	1,85E-04	4,85E-05	0,0032	0,4659	0,0059	1,798	0,062	0,1722	0,0035	0,0757	0,0019	1024	19	1087	52
7535-103.1	IRZ	70	530	169	0,329	95	10	1,19E-04	6,44E-05	0,0021	0,1093	0,0041	1,827	0,038	0,1766	0,0020	0,0750	0,0012	1048	11	1069	33
7535-128.1	IRZ	70	938	248	0,273	166	10	6,87E-05	6,20E-05	0,0012	0,0827	0,0027	1,853	0,044	0,1775	0,0026	0,0757	0,0013	1053	14	1088	35
7535-129.1	IRZ	70	1304	304	0,240	230	138	6,83E-04	6,12E-05	0,0118	0,077	0,0027	1,817	0,052	0,1784	0,0032	0,0739	0,0015	1058	17	1038	41
7535-32.1	IRZ	70	610	277	0,468	116	7	7,76E-05	9,77E-05	0,0013	0,1572	0,0042	1,883	0,105	0.178B	0,0020	0,0764	0,0041	1060	11	1105	111
7535-5.1	IRZ	70	567	160	0,292	103	16	1,87E-04	5,69E-05	0,0033	0,1004	0,0036	1,850	0,054	0,1789	0,0025	0,0750	0,0018	1061	14	1069	49
7535-99.1	IRZ	70	944	635	0,695	193	22	1,53E-04	8,44E-05	0,0027	0,2481	0,0084	1,860	0,044	0,1791	0,0021	0,0754	0,0015	1062	11	1078	39
7535-151.1	IRZ	70	971	298	0,317	177	24	1,58E-04	3,94E-05	0,0027	0,0988	0,0027	1,831	0,033	0,1805	0,0023	0,0736	0,0008	1070	13	1030	22
7535-7.1	IRZ	70	993	908	0,944	220	23	1,47E-04	3,63E-05	0,0026	0,3261	0,0066	1,978	0,044	0,1834	0,0024	0,0782	0,0013	1085	13	1153	33
7535-63.1	IRZ	70	1028	309	0,311	192	14	8,77E-05	4,00E-05	0,0015	0,1003	0,0027	1,934	0,044	0,1846	0,0031	0,0760	0,0010	1092	17	1094	28
7535-130.1	IRZ	70	423	319	0,780	98	17	2,24E-04	7,22E-05	0,0039	0,2506	0,0067	2,284	0,054	0,2028	0,0028	0,0817	0,0014	1191	15	1238	35
7535-98.1	IRZ	70	454	292	0,664	111	10	1,17E-04	6,70E-05	0,0020	0,196	0,0048	2,562	0,056	0,2227	0,0029	0,0834	0,0013	1296	15	1279	31
CQA-02-1840A, metamorphosed amphibolite (metagabbro)																						
7534-33.1	MZ	120	90	43	0,494	15	2	1,66E-04	1,25E-04	0,0029	0,1577	0,0075	1,658	0,062	0,1629	0,0028	0,0738	0,0023	973	15	1036	64
7534-36.1	MZ	120	322	90	0,288	54	2	4,59E-05	3,38E-05	0,0008	0,0870	0,0022	1,704	0,029	0,1676	0,0022	0,0737	0,0007	999	12	1034	20
7534-88.1	MZ	120	185	43	0,242	30	3	1,10E-04	4,66E-05	0,0019	0,0705	0,0026	1,634	0,032	0,1619	0,0022	0,0732	0,0010	967	12	1019	27
7534-35.1	MZ	120	320	182	0,586	55	2	4,99E-05	2,37E-05	0,0009	0,1794	0,0027	1,601	0,035	0,1595	0,0025	0,0728	0,0010	954	14	1009	28
7534-7.1	MZ	120	253	56	0,229	40	3	8.18E-	2,92E-05	0,0014	0,0692	0,0019	1,630	0,029	0,1610	0,0023	0,0734	0,0007	962	13	1026	20
7534-122.1	MZ	120	235	88	0,388	41	5	1,33E-04	1,40E-04	0,0023	0,1171	0,0065	1,699	0,060	0,1691	0,0023	0,0729	0,0023	1007	13	1010	64
7534-83.1	MZ	120	436	88	0,208	71	2	2,43E-05	3,66E-05	0,0004	0,0598	0,0025	1,707	0,030	0,1680	0,0022	0,0737	0,0007	1001	12	1034	20
7534-12.1	MZ	120	264	133	0,520	48	5	1,22E-04	9.B0E-05	0,0021	0,1578	0,0045	1,744	0,052	0,1697	0,0029	0,0746	0,0017	1010	16	1057	46
7534-53.1	MZ	120	224	49	0,224	37	3	1,05E-04	8,54E-05	0,0018	0,0665	0,0037	1,690	0,058	0,1665	0,0032	0,0736	0,0019	993	18	1031	54
7534-115.1	MZ	120	215	56	0,268	35	5	1,63E-04	8,71E-05	0,0028	0,0827	0,0038	1,664	0,045	0,1631	0,0023	0,0740	0,0016	974	13	1041	44
7534-97.1	MZ	120	292	133	0,470	50	9	#####	4,93E-05	0,0036	0,1395	0,0028	1,663	0,034	0,1650	0,0022	0,0731	0,0010	984	12	1017	29
7534-32.1	MZ	120	348	186	0,551	63	7	1,41E-04	4,82E-05	0,0025	0,1668	0,0028	1,724	0,034	0,1697	0,0024	0,0737	0,0009	1011	13	1033	26
7534-117.1	IRZ	70	686	1050	0,581	179	22	2,01E-04	9,37E-05	0,0035	0,5355	0,0071	2,004	0,059	0,1881	0,0034	0,0773	0,0016	1111	19	1128	42
7534-124.1	IRZ	70	507	1071	2,184	164	34	3,65E-04	6,75E-05	0,0063	0,6882	0,0057	2,485	0,051	0,2121	0,0026	0,0850	0,0013	1240	14	1315	30
7534-99.1	IRZ	70	407	581	1,477	120	12	1,55E-04	7,53E-05	0,0027	0,4201	0,0092	2,673	0,094	0,2269	0,0049	0,0854	0,0022	1318	26	1325	50
7534-73.1	IRZ	70	420	599	1,474	123	8	1,04E-04	5,56E-05	0,0018	0,4426	0,0053	2,611	0,067	0,2225	0,0028	0,0851	0,0018	1295	15	1318	41
7534-42.1	IRZ	70	977	712	0,753	223	34	2,05E-04	4.32E-05	0,0036	0,2496	0,0054	2,191	0,049	0,1997	0,0025	0,0796	0,0014	1174	13	1186	34

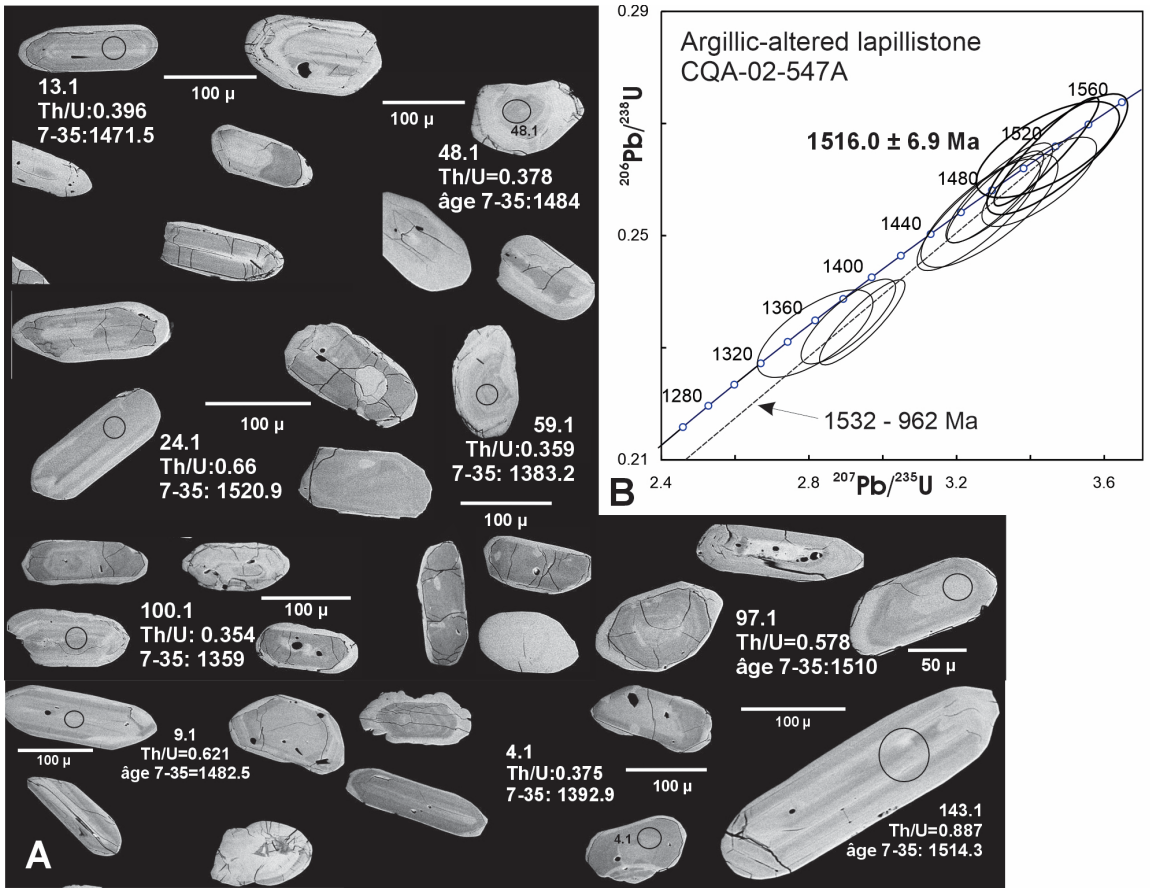


Figure 23. A. Backscattered electron images of zircon grains from the aluminous gneiss, interpreted as an argillic-altered lapillistone (sample ALB1, CQA-02-547A). **B.** Concordia diagram showing the distribution of SHRIMP data points for zircon.

3.14. Sample CQA-01-506A: Metapelite or Argillic Altered Volcanic Protolith

The sample CQA-01-506A (GSC laboratory number 7536) is a homogeneous sillimanite-garnet gneiss located within the La Romaine supracrustal belt at 665337mE and 5564631mN. The sample was taken from a narrow, metre-wide aluminous unit located near the contact between the composite amphibolite unit and the grey gneiss unit. It is representative of the aluminous gneisses of unit mPcsr4a that have uncertain protoliths (Figs. 4C, 5).

The sampled unit is homogeneous in terms of the distribution of garnet and sillimanite and of stromatitic cordierite and garnet-bearing leucosomes (Fig. 24A, B). Amoeboid leucosomes also occur (Fig. 24E). The mineral assemblage of the gneiss consists of biotite, cordierite, garnet, K-feldspar, plagioclase, quartz, sillimanite, and rare kyanite (one grain observed). Garnet is slightly purplish in hand specimen (Fig. 24D, E). The distribution of biotite, garnet and sillimanite in the melanosome and paleosome is regular but form atypical stringers (Fig. 24A–D). The gneiss yields abundant zircons, which appear as very fine, round to prismatic, grains commonly associated with the paleosome and the leucosome (Fig. 25). As the ferromagnesian and aluminous minerals account for 20 to 30 % of the rocks and have a fairly uniform distribution along layers, the rock resembles a metapelite. However, it is spatially associated with clinopyroxene-dominant calc-silicate rocks that are very heterogeneous and are interpreted as the result of metamorphosed carbonated alteration (see Corriveau et al., 2026). Hence a hydrothermal origin is also possible.

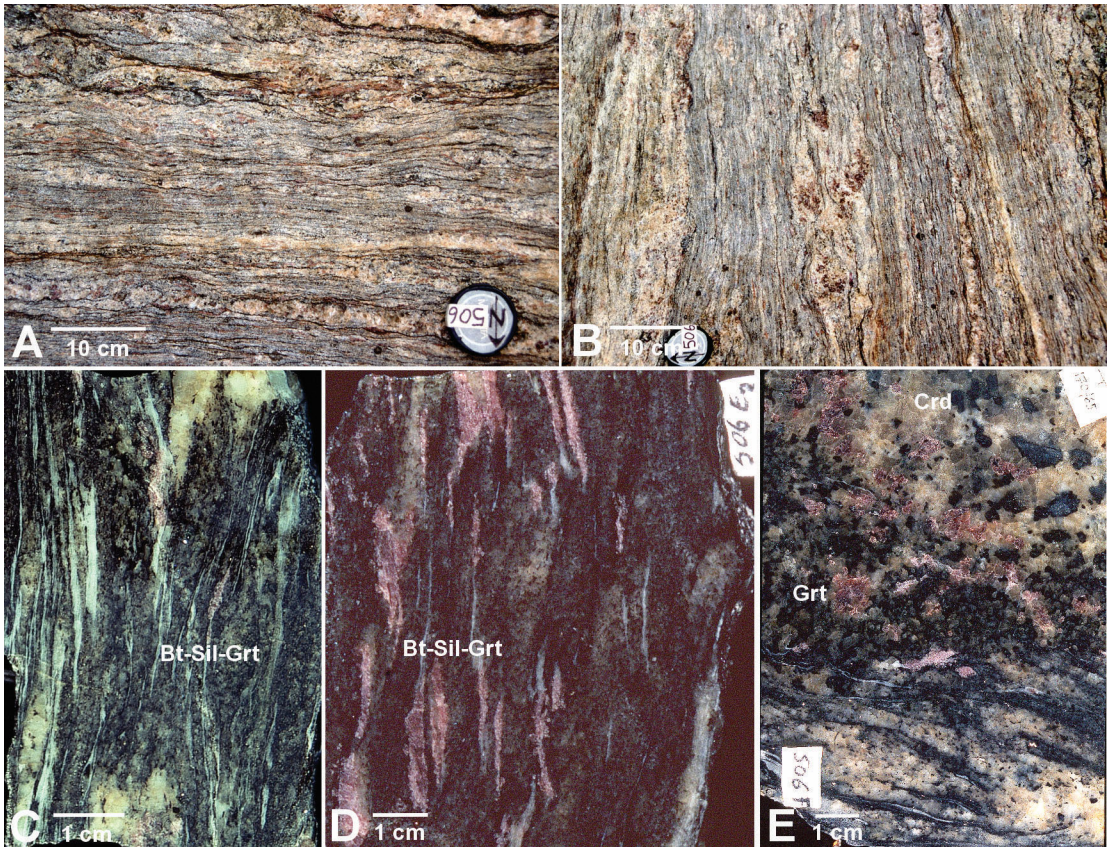


Figure 24. A, B. Field photographs of outcrop CQA-01-506. The aluminous gneiss is characterized by abundant garnet- and garnet-cordierite-bearing stromatitic leucosomes that are parallel to the foliation. The leucosomes do not display systematic melanosomes at their contact but comprises mafic stringers along part of the veins and among the veins. The gneiss is finely banded, leucocratic to mesocratic with abundant biotite-rich stringers and localized biotite-rich layers. **C.** Example of a biotite-rich zone with extensive stringers of sillimanite and localized leucosomes along part of which the gneiss is more biotite-rich and could represent melanosome material that provides permissive evidence that the rock may be a metapelite. However, the sillimanite stringers are numerous and slightly more abundant than in normal metapelite. **D.** Photograph of sample CQA-01-506E illustrating the biotite-rich component of the unit that can result from melt migration and the development of restites in a metapelite, or from metamorphism of an intense K-Fe alteration of a volcanic, volcaniclastic, or sedimentary protolith. The sample contains abundant stringers of either garnet or sillimanite. Not megascopically visible but in part shown in Figure 25, is the presence of cordierite, kyanite and muscovite. **E.** Photograph of sample CQA-01-506F illustrating a coarse-grained cordierite-bearing leucosome in contact with a paleosome of medium-grained sillimanite-biotite-garnet gneiss.

The presence of cordierite and garnet in the leucosomes indicates that they were generated in situ whereas their little connectivity with one another is typical of in situ melting without extensive transport, according to the criteria of Sawyer (1999). The cordierite is megascopically blue to green and as do the garnet, are not retrogressed. Later stage granitic veins cut the aluminous gneiss and were not present in the sample collected for geochronology. At the microscopic scale, there are inclusions of sillimanite, kyanite, cordierite or quartz in garnet (Fig. 25). Outside the garnet grains, cordierite occurs adjacent to garnet and lacks inclusions of sillimanite and quartz (Fig. 25). Zircon in leucosomes can be included in cordierite and K-feldspar (Fig. 25F–H).

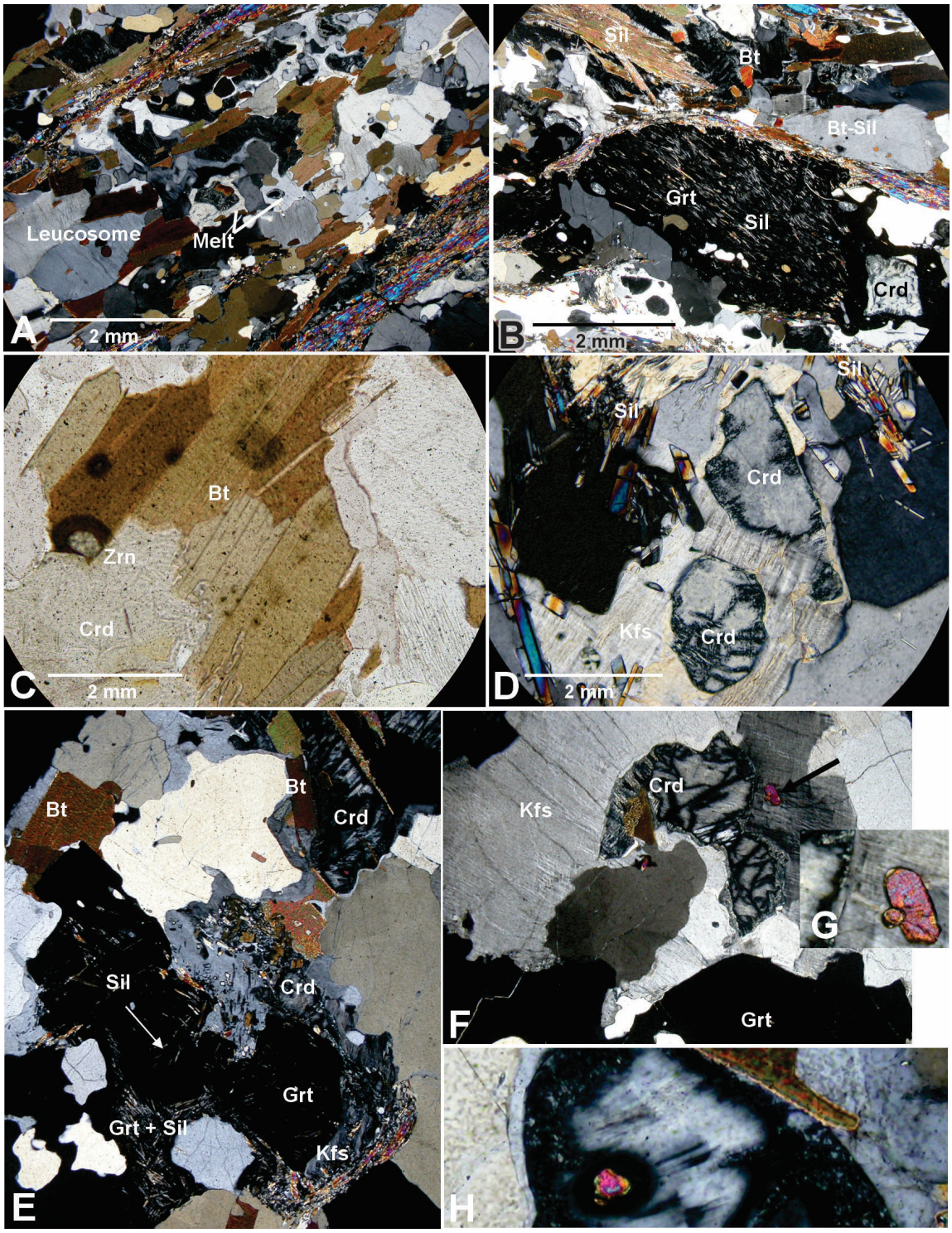


Figure 25. Microphotographs of units at outcrop CQA-01-506. **A–D.** In sample CQA-01-506E, B illustrates a first generation of garnet with oriented inclusions of an early generation of sillimanite needles, surrounded by a rim of clear garnet that encloses a pinnitized cordierite grain. Cordierite is not in contact with sillimanite. A second generation of sillimanite surrounds the garnet grains. Biotite growth occurs at the expense of cordierite. In C, details of the relationship between biotite, cordierite and sillimanite. **E.** A garnet-cordierite leucosome in sample CQA-01-506F. The garnet is euhedral, with rare sillimanite inclusions and rimmed by a garnet rich in sillimanite inclusions. **F–H.** Zircon inclusions in cordierite and K-feldspar.

The unit records the prograde metamorphic reaction:

sillimanite + biotite + quartz = garnet + cordierite + K-feldspar + melt

typical of granulite-facies metamorphism. On an AFM diagram (Fig. 22G), the sample falls adjacent to the composition of the North American Shale Composite of Gromet et al. (1984). This provides permissive evidence that the rock is a metapelite.

Minerals recovered from processing include red garnet, magnetite, hematite, abundant apatite, quartz, feldspar and potentially monazite. The presence of hematite is atypical of metasedimentary rocks; it may indicate that this aluminous gneiss is a pre-metamorphic hydrothermally altered unit, even though the composition appears typical of a metapelite.

Backscattered-electron images of zircon grains reveal greater complexity in their pre-metamorphic internal components (Fig. 26). The zircon grains are identical to those of the altered lapillistone, although cores are overgrown by a well-developed (10 - 20 μm) homogeneous metamorphic rims, which is characterized by a low back scattered electron response. Zircon grains average 100 to 200 μm in length.

Three populations of zircons were observed (Fig. 26A–I). The first is a small population of elongate and very clear zircon grains (some with fine and regular zoning typical of igneous zircon). The second is a small population of elongate zircons with inclusion-rich core surrounded by very fine and regular coronas (like those observed in igneous zircons). The third consists of rounded zircons with preserved rounded cores surrounded by one or more clear and irregular coronas interpreted as metamorphic.

Six analyses were carried out on oscillatory zoned cores. Analyses spots were sited away from any visible cracks. Data from zircon cores plot within two clusters (Fig. 26J). A cluster of four analyses yield ages from 1783 Ma to 1727 Ma while two others yield a $^{207}Pb/^{206}Pb$ ages of 1528 ± 44 Ma and 1364 ± 116 Ma (Fig. 26J). An additional analysis was discarded (7536-64.1) and not listed in Table 5 as it was strongly negatively discordant and considered unreliable. As the zircons cores are resorbed, it is likely that the host rock was hydrothermally altered. However, the variety of ages obtained, from Labradorian to Pinwarian, may reflect either a detrital zircon population or xenocrysts in a ca. 1.5 Ga volcanic protolith (Fig. 26J). A detrital origin for the cores is proposed, although in view of the small number of analyses, this inference is tentative. Accordingly, the rocks would be a sedimentary rock for which the aluminous nature could be primary or hydrothermal in origin, in line with the extensive hydrothermal alteration observed in the sedimentary sequence at Musquaro Lake (Corriveau et al., 2026). The unzoned rounded rims and rounded equidimensional grains have not been analyzed. It is inferred that they are of Grenvillian age as are the similar rims in sample CQA-02-457A.

Table 5. SHRIMP isotopic data for zircon from the aluminous gneiss (sample CQA-01-506A). See Table 2 for additional notes. Spreadsheet in the supplementary file.

																	Apparent ages			
Sample Spot #*	U (ppm)	Th (ppm)	Th/U	Pb (ppm)	^{204}Pb (ppb)	$^{204}Pb/^{206}Pb$	±1s	f206	$^{208}Pb/^{206}Pb$	±1s	$^{207}Pb/^{235}U$	±1s	$^{206}Pb/^{238}U$	±1s	$^{207}Pb/^{206}Pb$	±1s	$^{206}Pb/^{238}U$	±1s	$^{207}Pb/^{206}Pb$	±1s
7536-12.1	161	96	0.62	53	4	0.0000926	0.00003682	0.0016	0.18651	0.00328	4.34291	0.07	0.2979	0.0040	0.1057	0.0009	1681	20	1727	16
7536-28.1	246	147	0.62	86	0	5.87E-06	0.00002919	0.0001	0.17968	0.00191	4.62002	0.07	0.3169	0.0041	0.1057	0.0007	1775	20	1727	12
7536-71.1	217	131	0.62	76	10	0.000175	0.00002967	0.00303	0.17912	0.0039	4.60818	0.09	0.3153	0.0045	0.1060	0.0013	1767	22	1731	23
7536-76.1	110	46	0.43	29	2	8.714E-05	0.00010547	0.00151	0.12994	0.005	2.99843	0.1	0.2495	0.0044	0.0872	0.0021	1436	23	1364	48
7536-54.1	247	102	0.43	67	4	7.754E-05	0.00004843	0.00134	0.12359	0.00369	3.36974	0.07	0.2573	0.0036	0.0950	0.0011	1476	19	1528	22
7536-86.1	313	107	0.35	105	4	5.032E-05	0.00001908	0.00087	0.09936	0.0022	4.84907	0.16	0.3227	0.0044	0.1090	0.0030	1803	22	1783	51

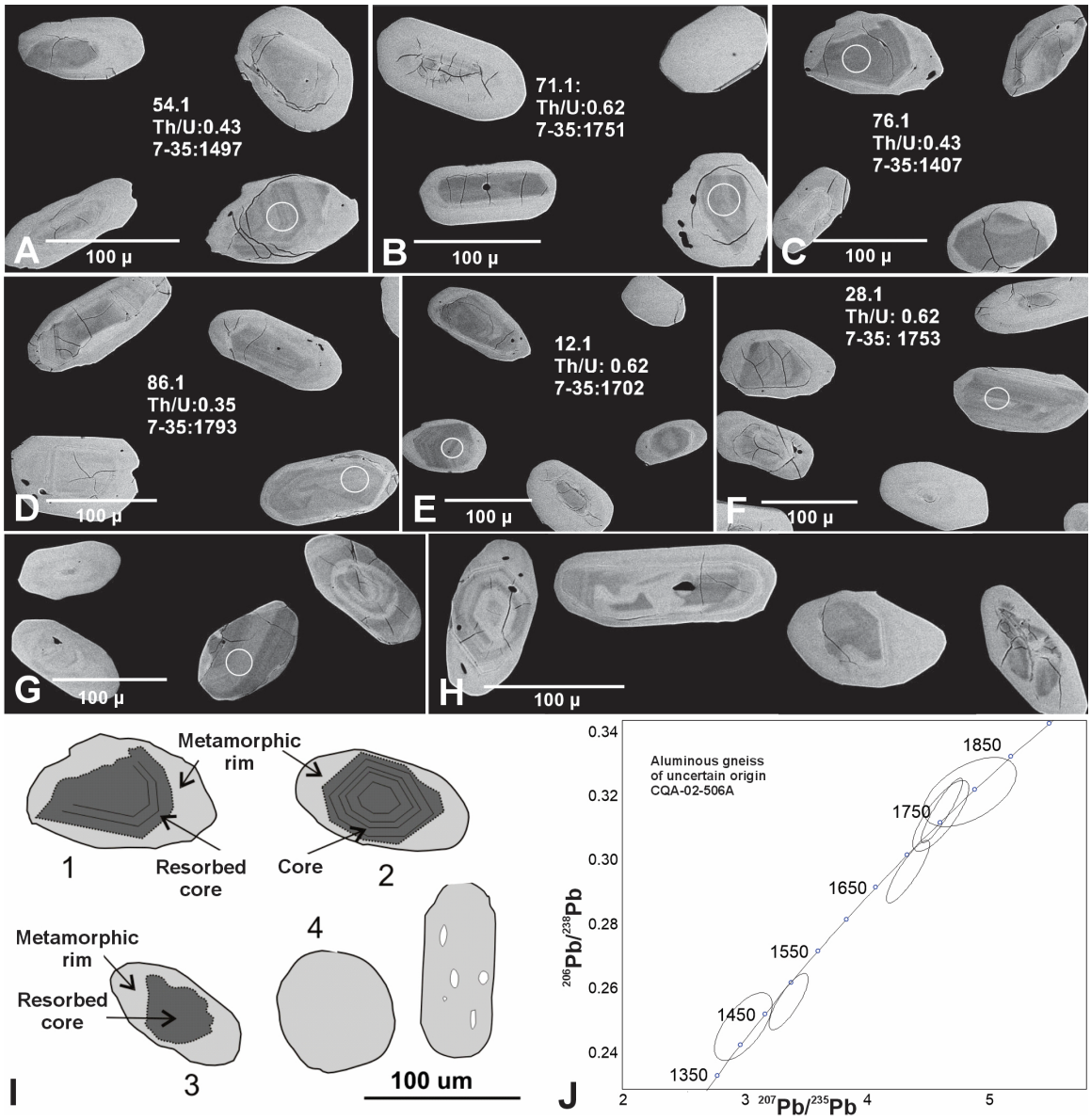


Figure 26. Sample CQA-01-506A and a concordia diagram. **A–H.** Backscattered electron images of zircon. **I.** Zircon populations observed. Populations 1 and 2 have cores with oscillatory zoning, are partly resorbed and have 110–313 ppm U, 46–131 ppm Th and Th/U ratios between 0.35 and 0.62. The third population has xenomorphic cores, homogenous in back scatted electron images. They have thin to thick metamorphic rims that are also homogeneous. The fourth population consists of metamorphic zircon with rare inclusions and are more common than the metamorphic zircons in sample CQA-02-547A. **J.** Concordia diagram.

3.15. Samples CQA-01-1564E: Ca-Fe- and K-Fe-altered Amphibolites

The sample CQA-01-1564E (GSC laboratory number 7535) is a Ca-Fe and K-Fe altered amphibolite layer that occur among aluminous gneisses resembling metapelites from the La Romaine supracrustal belt (Fig. 27A–F). It is located in NTS map sheet 12K02 at UTM 668155mE and 5565834mN (Figs. 4C, 5). The amphibolite layer is several metres wide and is interpreted as an extension of the hydrothermally altered amphibolite unit mPcsr3a of the composite amphibolite unit (Appendix 1; Bonnet et al., 2005).

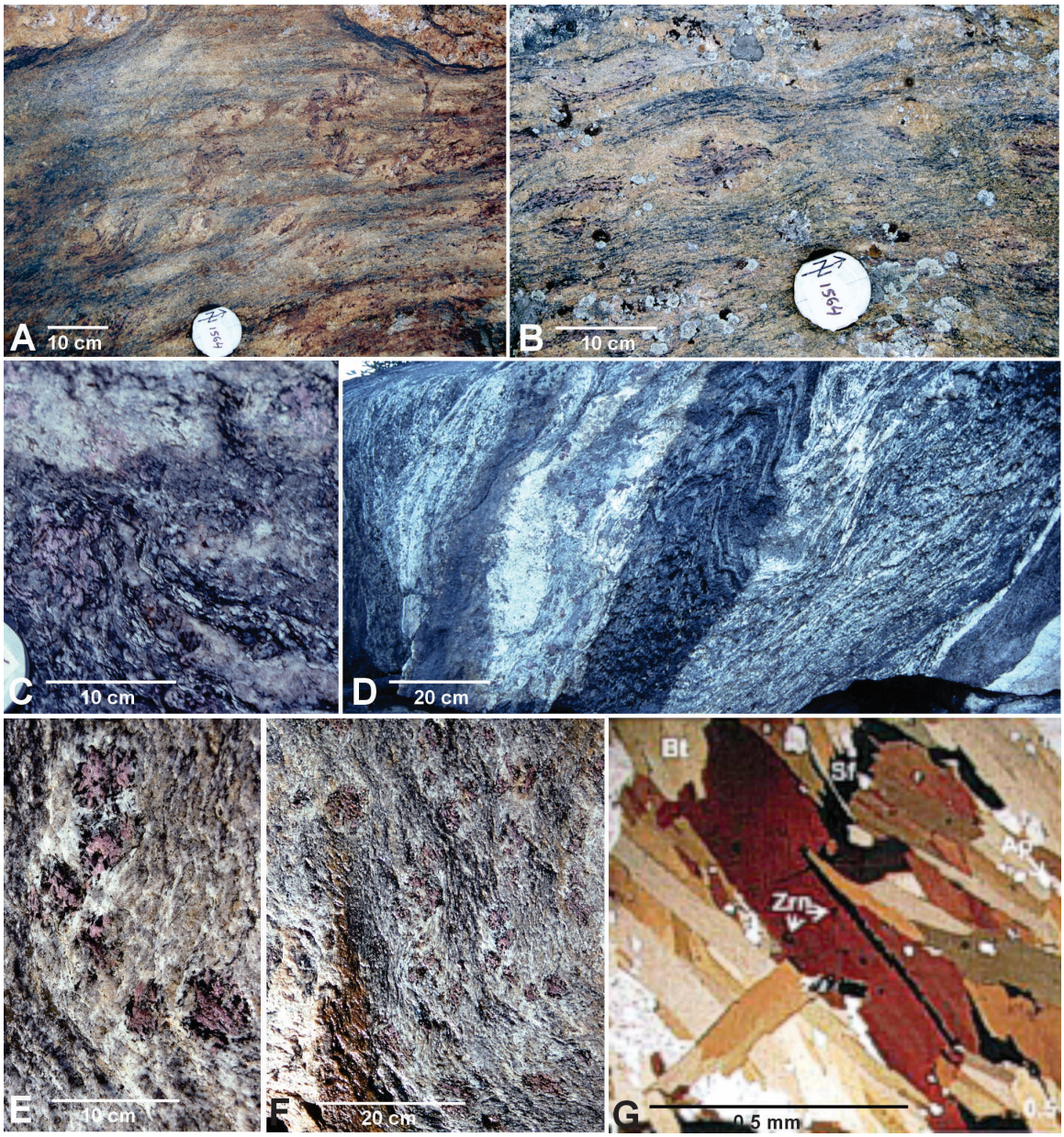


Figure 27. A–F. Field photographs of the aluminous gneiss that occurs next to the metamorphosed hydrothermally altered amphibolite at outcrop CQA-01-1564. No field photographs are available for the amphibolite itself. **G.** Microphotograph of the biotite (Bt)- and sulphide (Sf)-rich laminae within the metamorphosed K-Fe alteration zone of the hydrothermally altered amphibolite showing abundant inclusions of zircon (Zrn) and apatite (Ap).

The amphibolite is laminated with medium-grained clinopyroxene and epidote-rich laminae interlayered with coarser-grained biotite and sulphide-bearing laminae (Fig. 27G). The hydrothermally altered amphibolite is migmatized and displays a granulite-facies mineralogy consisting of plagioclase, clinopyroxene, hornblende, biotite, orthopyroxene, quartz, sulphides (pyrrhotite, pyrite) and accessory apatite, magnetite and zircon. Abundant magnetite and some epidote grains were also observed in the processed fractions for geochronology. The amphibolite contains orthopyroxene and clinopyroxene-bearing, stromatitic leucosomes parallel to the foliation

that account for about 5% of the rock. Zircon grains are preferentially distributed within biotite-pyrite-pyrrhotite-zircon-rich layers (Fig. 27G).

The altered amphibolite yielded zircon grains of two morphological types (Fig. 28A). One group, representing 60% of the zircon population, consists of subhedral grains, averaging 80 to 150 μm in length, with cores and rims that are clearly distinguishable as the cores contain numerous microscale inclusions (Fig. 28A, B). The cores are irregular or subhedral in shape, with an average length of ca. 100 μm (Fig. 28B). They display variable to high Th and U contents and a wide range of Th/U ratios (U = 423–1304 ppm; Th = 160–908 ppm; Th/U = 0.27–1.37; Table 4).

Inclusions are abundant, having rounded to irregular shapes. Based on SEM analyses, inclusions consist, in order of abundance, of quartz (37 grains), biotite (20 grains), K-feldspar (18 grains) and alkali feldspar (Na>K; 11 grains), chlorite (7 grains), hornblende (3 grains), albite (3 grains) and iron oxides (1 grain). Rims commonly have radial cracks, suggesting that the metamict cores underwent greater expansion because of their higher Th and U contents relative to the rims; this interpretation is corroborated by the lower birefringence and higher BSE response of the cores.

A second group of zircons consists of rounded equidimensional to subhedral elongate grains, generally smaller than 100 μm. They have a smooth, translucent appearance and display irregular but homogeneous zones with different U-Th compositions. Their morphology is consistent with growth during high-grade metamorphism.

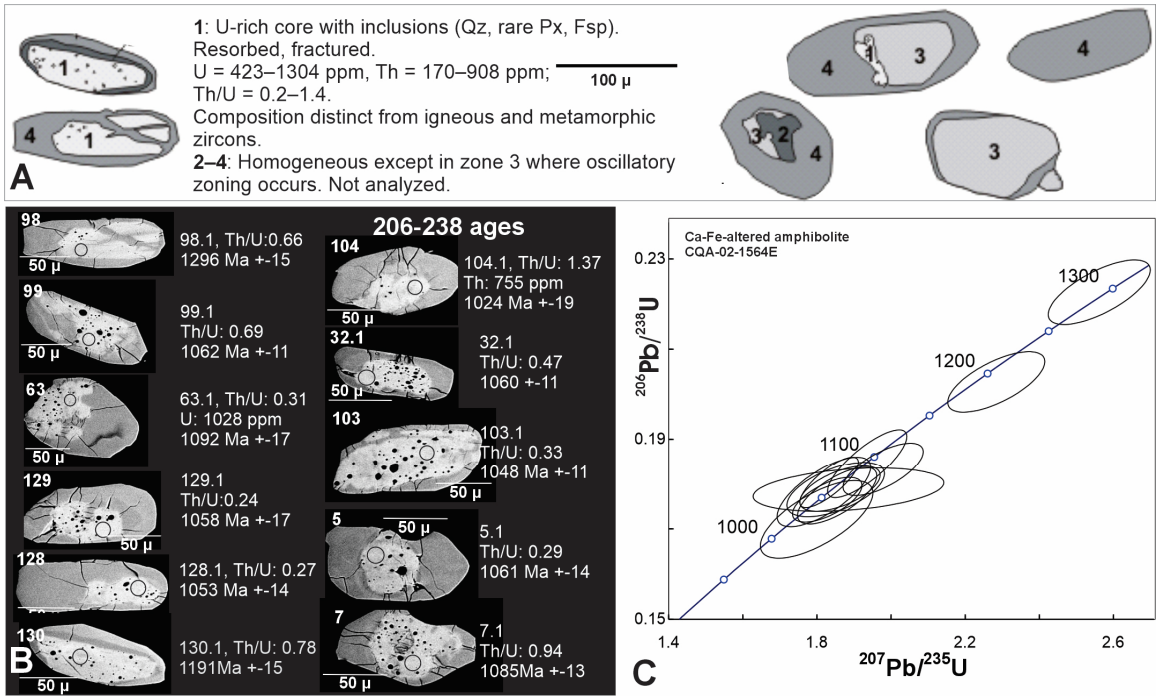


Figure 28. Hydrothermally altered zircon grains in sample CQA-01-1564E, and concordia diagram. **A.** Summary features of the four texturally distinct groups of zircon grains. **B.** Representative backscattered electron (BSE) images of hydrothermally altered zircon, their overgrowth and locations of individual spot analyses listed in Table 4. **C.** Distribution of SHRIMP data points from inclusion-rich zircon cores on a concordia diagram.

Only the inclusion-rich cores were analyzed in the metamorphosed hydrothermally altered amphibolite, because all rims analyzed in other samples were metamorphic in origin and Grenvillian in age. Data from zircon cores are dominated by a cluster of ten analyses with a

weighted mean $^{206}Pb/^{238}U$ age of 1062 ± 11 Ma (MSWD = 1.4; POF = 0.17) (Fig. 28C). Two concordant or near concordant analyses plot outside this cluster and display older $^{207}Pb/^{206}Pb$ ages of 1279 ± 31 Ma (1σ) and 1238 ± 35 Ma (1σ), whereas one discordant analysis yields a $^{207}Pb/^{206}Pb$ age of 1153 ± 33 Ma (1σ). These older ages are associated with zircon of lower U content (423–454 ppm).

3.16. Sample CQA-02-1840A: Metagabbroic Amphibolite at Granulite Facies

The sample CQA-02-1840A (GSC laboratory number 7534) is a metagabbroic amphibolite located within the composite amphibolite unit at UTM 662531mE and 5564088mN in NTS map sheet 12K02 (Figs. 4C, 5). The sample was selected from a homogeneous and medium-grained layer among a series of outcrops with metamorphosed hydrothermal alteration. A ghost texture of randomly oriented plagioclase laths indicates that the layer was a metagabbroic sill. It is interpreted as a least-altered facies because no unusual paragenesis, mineral color or abundance, or other visible indicators of alteration were observed in the field (Fig. 29A, B).

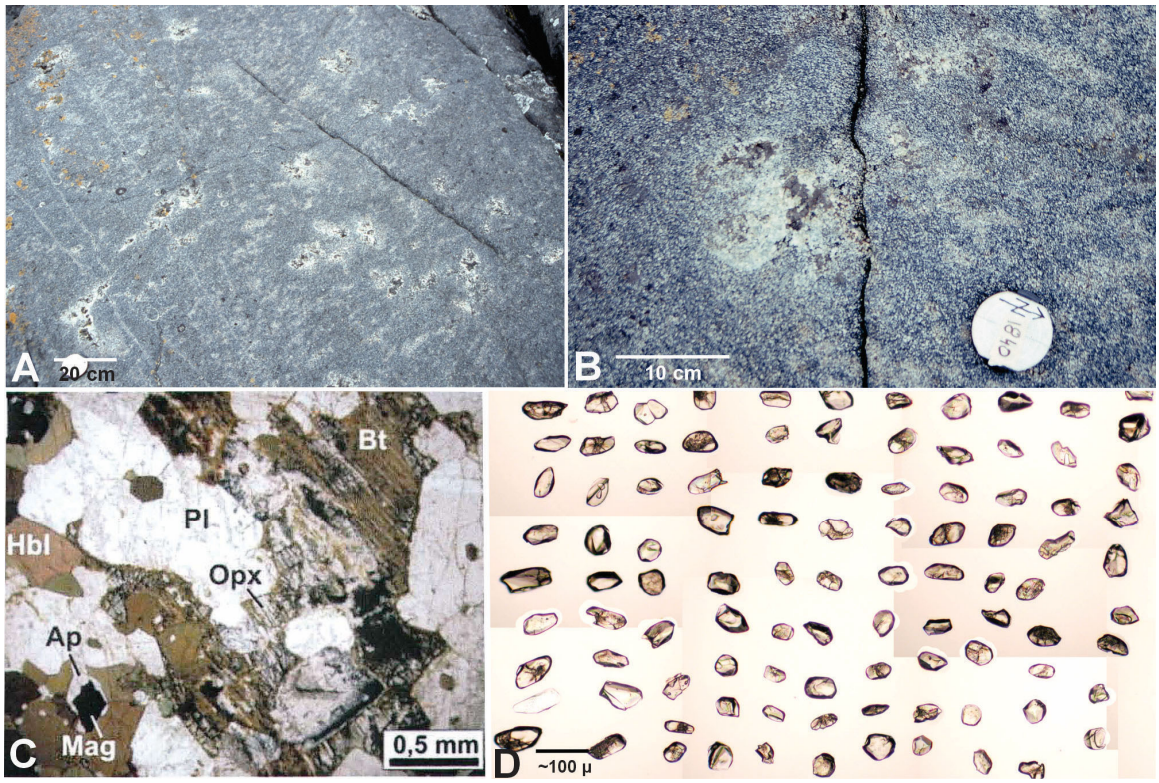


Figure 29. A, B. Field photographs of the metabasite and its amoeboid orthopyroxene-bearing leucosomes. The amoeboid character and the presence of orthopyroxene attest to in situ melting without significant melt migration. Note the presence of a ghost texture of randomly oriented plagioclase laths now recrystallized to a granoblastic texture in B. **C.** Microphotograph of an orthopyroxene-bearing leucosome in natural light. Orthopyroxene is replaced by retrograde hornblende (Hbl) and biotite (Bt). Apatite (Ap) and magnetite (Mag) also occur. **D.** Example of zircon grains observed under the microscope for sample CQA-02-1840A.

The metagabbro is medium grained and presents a granoblastic texture. Its mineralogy consists of hornblende (30%), biotite (20%), orthopyroxene (2%), plagioclase, quartz, and accessory apatite, magnetite, titanite and zircon (Fig. 29C). The orthopyroxene is partially replaced by retrograde biotite and amphibole (Fig. 29C). Accessory magnetite occurs as disseminated fine to medium grains, commonly in contact with orthopyroxene.

The rock is migmatized and contains amoeboid orthopyroxene-bearing, leucosomes about 5 by 10 cm in size that represent about 25% of the unit (Fig. 29A, B). The leucosomes are not interconnected megascopically. They are thus formed in situ, and they have not been penetratively deformed, likely due to their competent behaviour. Their orthopyroxene is megascopically pristine. The paleosome consists of plagioclase, hornblende and quartz, and is separated from the leucosome by a hornblende-rich melanosome. Zircon occurs as very fine rounded grains enclosed in hornblende or plagioclase closely associated with leucosomes or more rarely with the paleosome.

The leucosomes are interpreted as having formed through the following dehydration melting reaction:

Quartz + plagioclase + hornblende = orthopyroxene + magnetite + melt + zircon.

This metagabbro yielded similar zircon populations to those observed within the Ca-Fe- and K-Fe-altered amphibolite with elongate, prismatic and locally stubby zircon grains with xenomorphic to subhedral shapes that exhibit areas very rich in fluid or solid inclusions (Figs. 29D, 30).

Many grains are greater than 100 μm. The zircon grains, characterized by the presence of inclusion-rich, high U cores, are less abundant in the metagabbro (35%) than in the Ca-Fe-and K-Fe-altered amphibolite (60%). The inclusion-rich cores of zircon from the metagabbro are also smaller, less enriched in U (U= 407–977 ppm) and more enriched in Th (Th = 581–1071 ppm) than those observed in zircon from the Ca-Fe- and K-Fe-altered amphibolite. Their Th/U ratios vary between 0.75–2.18 (Table 4). Inclusions within U-rich cores were analyzed by SEM and are, in order of abundance: feldspars (32 grains of K-feldspar, 10 grains of alkali feldspar and 2 grains of albite), biotite (27 grains), chlorite (16 grains), quartz (13 grains) and traces of pyrite (2 grains).

The second group of homogeneous zircon grains consists of clear, sub-rounded to sub-angular, equant grains, in the 75–100 μm range (Fig. 30). Prismatic zircon grains also occur. Some zircon grains are attached to each other, as is typical of metamorphic zircon. This zircon population has U and Th concentrations (U= 90–436 ppm; Th = 43–186 ppm; Th/U = 0.2–0.6; Table 4) that are similar to those of the rims of the first group of zircon grains, and their morphology and composition are consistent with growth during high-grade metamorphism. Although the Th/U ratios of these grains are lower than those of the porous cores, metamorphic zircon grown during amphibolite facies metamorphism may have Th/U ratios below 0.07 (Rubatto, 2002). On the other hand, Vavra et al. (1999) point out that the Th/U ratio of metamorphic zircon increases with metamorphic grade, reaching higher values in the granulite facies.

Five analyses were carried out on the inclusion-rich cores and twelve on the metamorphic rims and equidimensional zircon grains. Data from zircon rims and homogeneous rounded equidimensional grains are dominated by a cluster of 12 analyses (Fig. 31). These analyses yield a weighted mean $^{207}Pb/^{206}Pb$ age of 1028 ± 16 Ma (MSWD = 0.12; POF = 1.00). There is no correlation between age and compositional variations in the metamorphic zircons. As it is unlikely that there was significant metamorphic Pb loss after this time, based on available geochronology from the region, the $^{207}Pb/^{206}Pb$ age of 1032 ± 16 Ma (MSWD = 0.12; POF = 1) obtained for all data is interpreted as the time of metamorphic zircon growth. The five zircon cores that have abundant inclusions yie1d concordant or near-concordant analyses with $^{207}Pb/^{206}Pb$ ages ranging from 1128 ± 42 Ma (at 1σ) to 1325 ± 50 Ma (at 1σ) (Fig. 31).

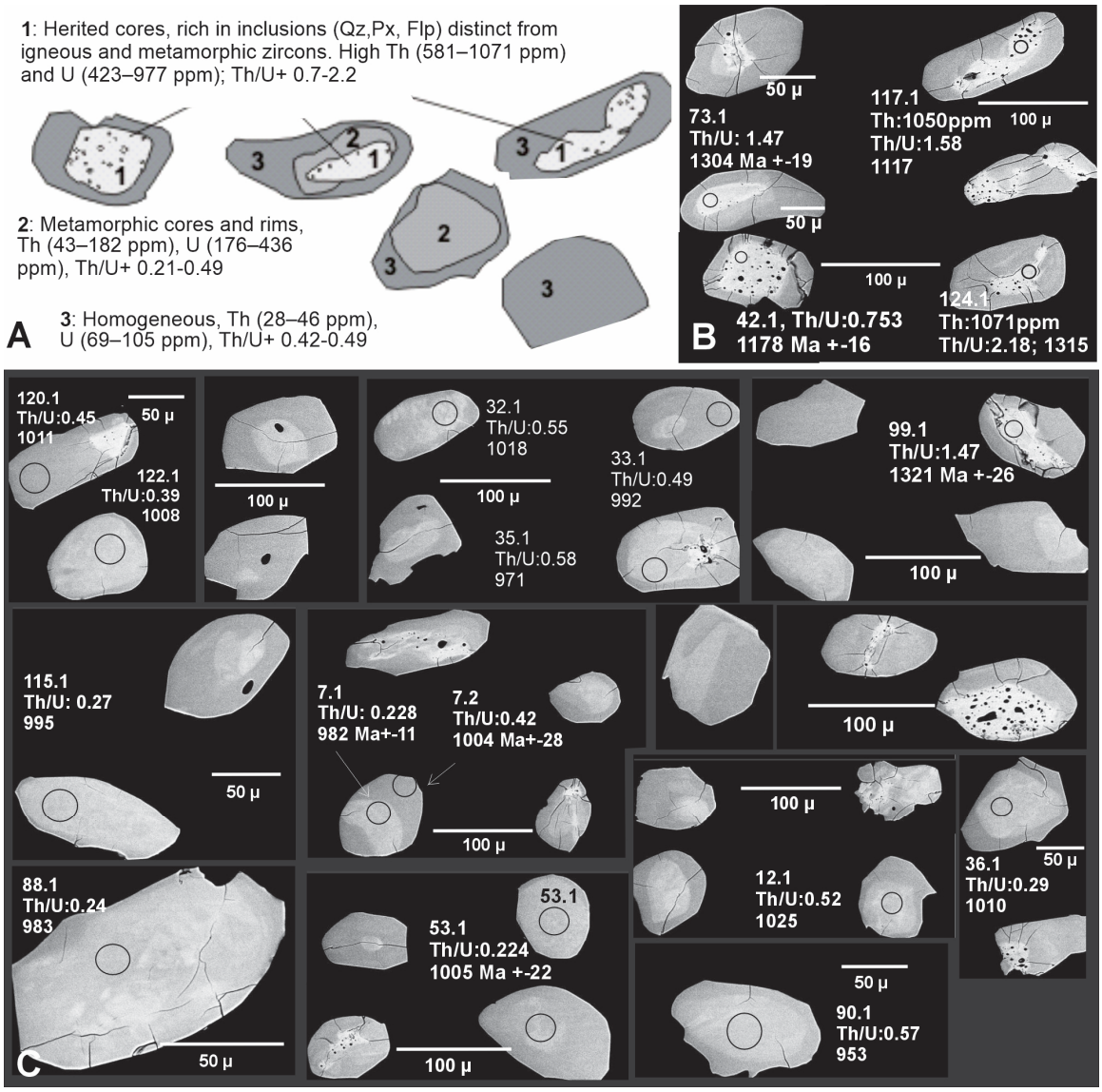


Figure 30. Representative backscattered electron (BSE) images of the hydrothermally altered zircon grains analyzed, as well as the locations of individual spot analyses. **A.** Summary features of the three texturally distinct populations of zircon grains. **B.** Representative backscattered electron (BSE) images of group 1 zircons and the locations of individual spot analyses marked by a circle with the analysis number (e.g., 117.1) listed in Table 4. **C.** Representative backscattered electron (BSE) images of group 2 and group 3 zircons and the locations of individual spot analyses listed in Table 4. Additional examples of zircons with pitted and inclusion-rich cores are also shown.

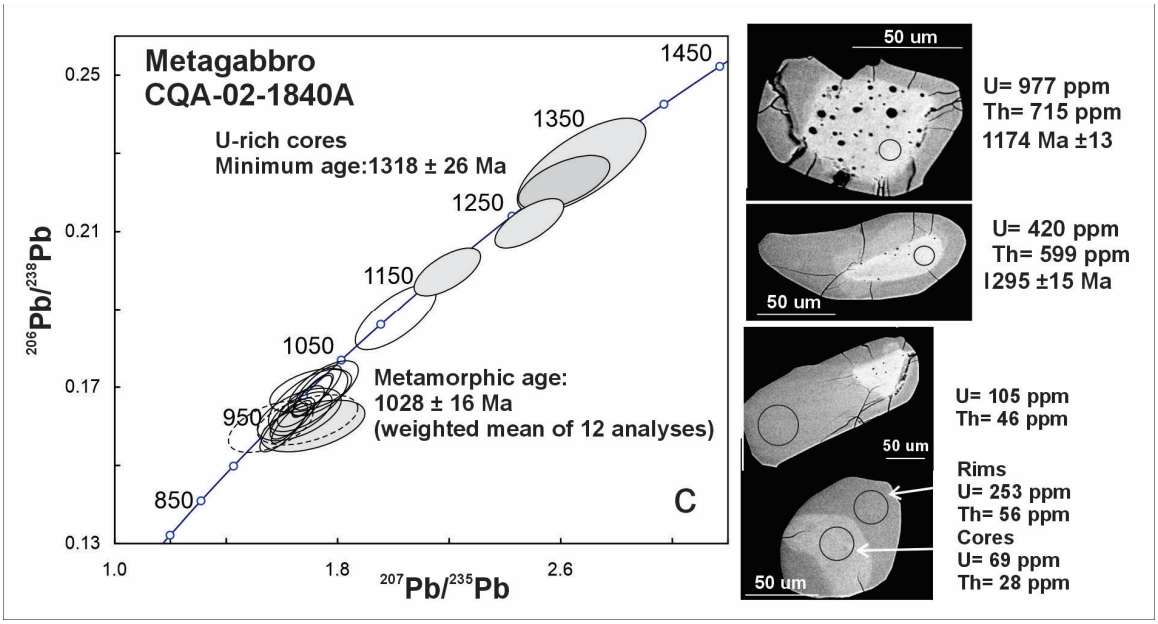


Figure 31. Distribution of SHRIMP data points for zircon from the metagabbro (CQA-02-1840A, GSC laboratory number 7534). Analyses on inclusion-rich zircons are shaded; two analyses not included in the weighted average $^{207}Pb/^{206}Pb$ age of metamorphic zircons are shown with dashed lines.

3.17. Sample CQA-00-330C: Garnet Porphyroblasts in a K-Fe-altered Amphibolite Dyke

The sample CQA-00-330C (GSC laboratory number z7538) comes from a garnet- and biotite-rich amphibolite dyke that is interpreted as a hydrothermally K-Fe altered mafic dyke metamorphosed at amphibolite facies (Corriveau et al., 2026). The outcrop is located in the SW section of Musquaro Lake at 50°31'12.2"N and 61°09'38.7"W in NTS map sheet 12K11 (Fig. 3C). The dyke is two-metres thick and occurs sub-parallel to the gneissic fabric of its host, an aluminous gneiss of unit mPwk7a (Appendix 1). The dyke is exceptionally rich in biotite (60%) and contains abundant red garnet porphyroblasts, several centimetres in diameter, with abundant inclusions (Fig. 32A, B).

The garnet porphyroblasts were sampled for geochronology and the amphibolite dyke matrix discarded. In thin section, inclusions in garnet consist of apatite, biotite, plagioclase, quartz, magnetite and other opaques (Fig. 32C). In addition, the mineral separate indicates that amphibole, apatite, epidote, feldspars, pyrite, quartz, zircon and rare monazite are present in the sample. The presence of allanite, chlorite, hematite and ilmenite is also suspected but not confirmed.

Two main populations of zircons were observed (Fig. 32D, E). One population consists of xenomorphic, rounded, clear zircons. The second population is like those interpreted as hydrothermal zircons in the amphibolites of the La Romaine composite amphibolite unit (samples CQA-01-1564E and CQA-02-1840A). These zircons feature similar irregular cores rich in inclusions and pits with clear rims (Fig. 32E).

Seven U-Pb SHRIMP analyses were carried out on the zircon population without pitted and inclusion-rich cores (Fig. 32D; Table 6). The cluster of four concordant analyses together with the two less concordant analyses on the concordia diagram have a weighted mean $^{206}Pb/^{238}U$ age of 1021 ± 11 Ma (MSWD = 0.51; POF = 0.73) (Fig. 32F). This age is interpreted as a metamorphic age.

An additional analysis (7538-69.1) was discarded from the weighted average because it yielded a very young age. It is not listed in Table 6 and is not shown in the concordia diagram of Figure 32F.

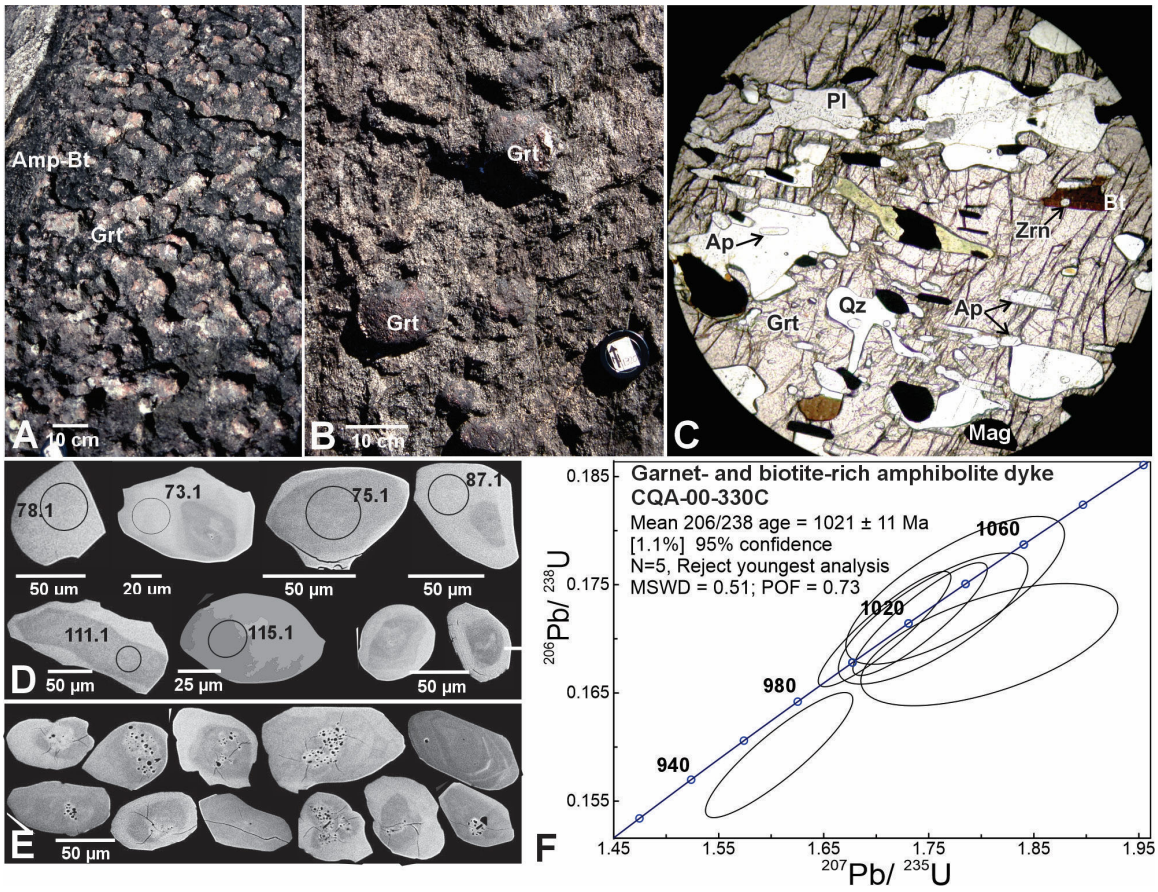


Figure 32. Sample CQA-00-330C (GSC laboratory number 7538). **A, B.** Field photographs of the garnet- and biotite-rich amphibolite dyke sampled for geochronology. **C.** Microphotograph of a garnet porphyroblast with inclusions of idiomorphic apatite with a preferred orientation, and of biotite, magnetite, plagioclase, quartz and zircon. **D, E.** Zircon grains extracted from the garnets sampled from the dyke. **F.** Distribution of SHRIMP data points on a concordia diagram. Only a metamorphic age was obtained as the zircon cores were not analyzed.

Table 6. U-Pb SHRIMP isotopic data for zircon from the garnet porphyroblasts in the K-Fe altered mafic dyke metamorphosed to amphibolite facies (sample CQA-00-330C). Spot size is K120. See Table 2 for additional notes. Spreadsheet in the supplementary file.

Sample Spot #*	U (ppm)	Th (ppm)	Th/U	Pb (ppm)	^{204}Pb (ppb)	^{204}Pb/^{206}Pb	±1s	f^{206}	^{208}Pb/^{206}Pb	±1s	^{207}Pb/^{235}U	±1s	^{206}Pb/^{238}U	±1s	^{207}Pb/^{206}Pb	±1s	Apparent ages ^{206}Pb/^{238}U	±1s	Apparent ages ^{207}Pb/^{206}Pb	±1s
7538-87.1	587.6	10.95	0.02	87	1	0.00001837	0.00001892	0.00032	0.00683	0.0008	1.60748	0.02862	0.15931	0.00236	0.07318	0.0006	953	13	1019	17
7538-73.1	599.1	11.98	0.02	96	3	0.00003444	0.00002473	0.0006	0.00645	0.00099	1.7421	0.02613	0.17186	0.00213	0.07352	0.00052	1022	12	1028	14
7538-75.1	170.6	2.59	0.02	28	2	0.00007965	0.00005762	0.00138	0.00525	0.00224	1.77539	0.04255	0.17453	0.0028	0.07378	0.00117	1037	15	1035	32
7538-111.1	195.9	2.61	0.01	31	0	0.00001	0.00001	0.00017	0.00802	0.00109	1.75433	0.03684	0.17192	0.00248	0.07401	0.00101	1023	14	1042	28
7538-115.1	152.2	4.98	0.03	24	2	0.00008005	0.00008825	0.00139	0.01328	0.00372	1.80799	0.05009	0.16951	0.0023	0.07736	0.00174	1009	13	1130	46
7538-78.1	579.3	7.82	0.01	92	1	0.00001	0.00001	0.00017	0.00502	0.00072	1.70825	0.02581	0.17097	0.00218	0.07247	0.00048	1017	12	999	14

4. Sm-Nd Isotopic Tracer Study

During the TGI project, Sm and Nd isotopes were analyzed by Dr. Otto van Breemen for six whole-rock samples from the Musquaro-D'Auteuil lakes area and four from the La Romaine area

(Table 7). Eleven of these analyses were done on the same rocks for which U-Pb zircon ages are reported in this study and in van Breemen and Corriveau (2005). Two analyses were done on samples for which no U-Pb ages are available.

Sm and Nd were separated using cation-exchange chromatography, after being spiked with ^{148}Nd-^{149}Sm tracers. Isotopic ratios were measured using the Nu Plasma multicollector ICP-MS at the GSC, with a fixed array of Faraday collectors in static multicollector mode. ^{143}Nd/^{144}Nd isotopic ratios are reported relative to the value of 0.51186 for the LaJolla Nd standard. Nine spiked and unspiked analyses of BCR-1 yielded the weighted mean ^{143}Nd/^{144}Nd value of 0.512636 ± 0.000009. The εNd is calculated at the igneous age, relative to the accepted Chondritic Uniform Reservoir (CHUR) with ^{143}Nd/^{144}Nd=0.512638 and ^{147}Sm/^{144}Nd=0.1967.

Sm-Nd whole-rock isotopic data are presented in Table 7 and the Nd isotopic evolution lines for individual samples are shown in Figure 33. For samples for which no U-Pb ages are available, **εNd** values are calculated assuming a crystallization age of 1.5 Ga. Figure 33 shows the depleted mantle growth curves according to the parameters of DePaolo (1981), Goldstein et al. (1984) and Nägler and Kramers (1998). The DePaolo (1981) model gives depleted mantle ages (T_{DM}; Table 7) that are ca. 150 Ma younger than those calculated according to the parameters of Goldstein et al. (1984) and is considered the most reliable model for the Nd-isotopic evolution of the mantle source of orogenic crustal terranes. It is, therefore, widely used in the Grenville Province (Dickin, 2005; Martin and Dickin, 2005).

Table 7. Sm-Nd whole-rock isotopic data. Spreadsheet in the supplementary file.

Sample#	Rock	Age (Ma)	Nd (ppm)	Sm (ppm)	^{147}Sm/^{144}Nd	2σ	^{143}Nd/^{144}Nd	ε^{143}Nd	TDM* (Ga)
Musquaro area									
CQA-00-268A	Augen granitic orthogneiss	1492	31.6	5.72	0.109377	0.0001	0.5118	0.53	1.8
CQA-00-111P	Polymict lapillistone	1511	30.2	5.4	0.10831	0.0001	0.5118	1.66	1.73
CQA-00-273A	Metarhyolite	1491	23.9	5.2	0.13106	0.0002	0.5121	1.81	1.76
CQA-00-105QFP	Quartz-feldspar porphyry	1493	31.5	6.42	0.123043	0.0002	0.5119	0.57	1.85
CAQ-00-135A	Augen orthogneiss	1500	13.5	2.2	0.098346	0.0001	0.5118	1.87	1.69
CQA-00-159A	Hornblende-biotite granite	1500	39.4	7.35	0.112645	0.0002	0.5118	0.61	1.81
CQA-00-159A	Duplicate	1500	43	7.9	0.110959	0.0002	0.5118	0.6	1.81
La Romaine area									
CQA-01-353A	Lapillistone	1502	33.1	6.16	0.112501	0.0002	0.5119	1.12	1.77
CQA-01-371A	Tonalitic orthogneiss	1529	15.2	1.85	0.073894	8E-05	0.5117	5.47	1.48
CQA-01-416	Granitic augen gneiss	1502	70.7	14.54	0.124292	0.0003	0.512	0.85	1.83
CQA-01-476A	Granitic orthogneiss	1490	41.4	7.69	0.11227	0.0002	0.512	3.09	1.61
*Mantle depletion age according to the model of DePaolo									

The εNd values vary from 0.53 to 5.47 and T_{DM} ages from 1.48 Ga to 1.85 Ga (Table 7). Crustal separation ages, which are generally mixed ages representing various proportions of mantle and crustal sources, range from the ca. 1.5 Ga igneous crystallization ages to 1.85 Ga. On average, there appears to be either an older and/or greater pre-existing crustal component in igneous rocks from the Musquaro-D'Auteuil lakes area (average εNd = 1.2) than in those from the La Romaine area (average εNd = 2.6). There is also a greater range in the inferred crustal contribution in the La Romaine area, as shown by the respective T_{DM} ranges (Fig. 33).

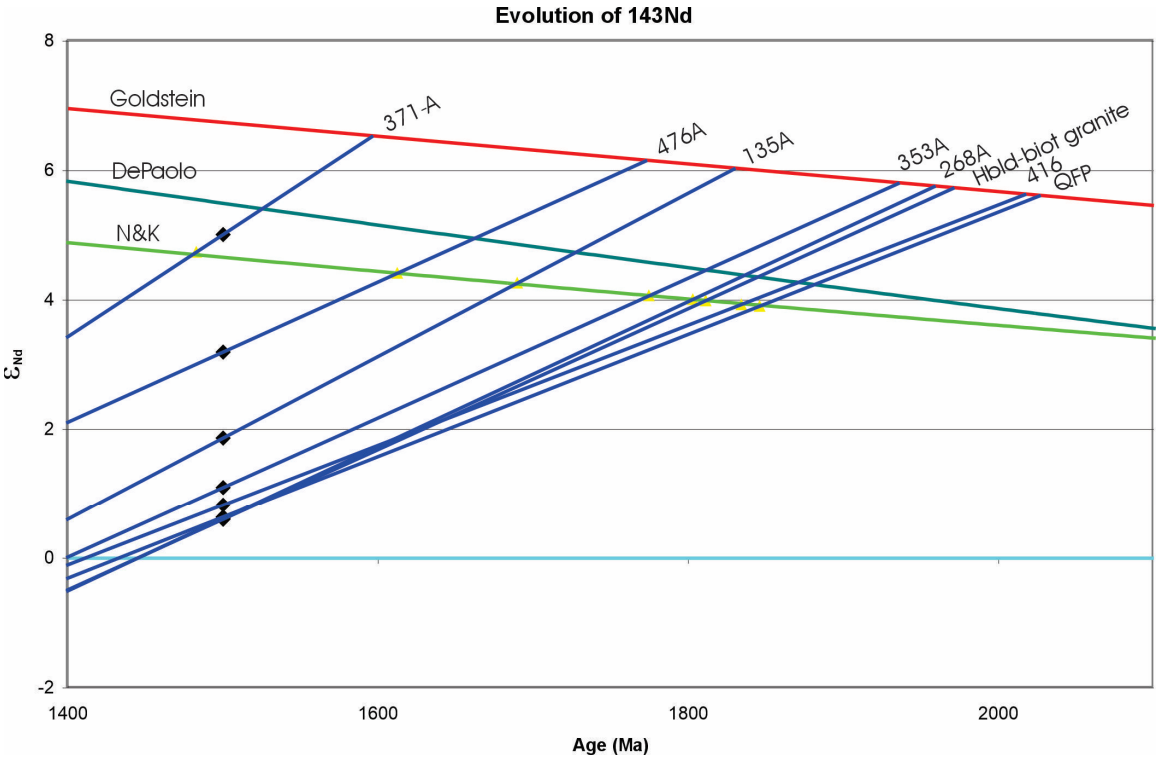


Figure 33. Nd isotopic evolution diagram for whole rock samples from the Musquaro-D'Auteuil lakes (solid lines) and La Romaine areas (dashed lines). Depleted mantle evolution curves are according to Goldstein et al. (1984), DePaolo (1981) and Nägler and Kramers (1998) (N&K).

5. Discussion

5.1. Extent of Pre-Pinwarian Crust

The SHRIMP xenocrystic data suggests that the Pinwarian continental magmatic arc in the study area was built on a Labradorian and Wakamian basement as a probability plot of U-Pb SHRIMP ages of 25 xenocrysts from igneous rocks shows a peak at 1592 Ma within a 1660–1554 Ma grouping of 15 grains (Fig. 34). There is no difference in the overall inheritance pattern between the Musquaro-D'Auteuil lakes and La Romaine areas. The peak is slightly younger than the Labradorian 1710–1600 Ma range and the ca. 1650 Ma Trans-Labrador batholith (Gower and Krogh, 2002). The age shift had initially been attributed to disturbance of the U-Pb zircon systems during Pinwarian magmatism. Considering the 1582 ± 5 Ma age of tonalitic gneisses from the L'Aigle Complex (Lafrance et al., 2026), the xenocrysts are best interpreted as indicating a potential extent of the L'Aigle Complex within the basement. This interpretation is also supported by the field observation of older components in the belt of tonalitic gneiss that is complexly folded (mPagn4 in Appendix 1; Kegaska Intrusive Suite, Lafrance and Daoudene, 2024).

Of particular interest are the 1546, 1586, and 1606 Ma ages of xenocrystic zircons in the polymictic lapillistone (CQA-00-1032M) at Musquaro Lake that was dated by van Breemen and Corriveau (2005). These ages may represent a Wakamian basement. In contrast, the 1755–1980 Ma age range in this sample falls within the main age range of the detrital zircon population in the underlying sedimentary unit (Fig. 35). in line with the interpretation that sedimentary rocks underlie the volcanic rocks. A xenocrystic zircon age of 1810 ± 42 Ma in the metarhyolite at D'Auteuil Lake does not fall within the detrital zircon population and may suggest a Paleoproterozoic crust at depth. A

xenocryst population like those of detrital zircons is found in a lapillistone in the La Romaine supracrustal belt (CQA-01-353A) where zircon xenocrysts have ages of 1585 Ma, 1758 Ma and 2447 Ma. This supports the field interpretation that sedimentary rocks underlie the volcanic rocks as well in the La Romaine supracrustal belt (Corriveau and Bonnet, 2005).

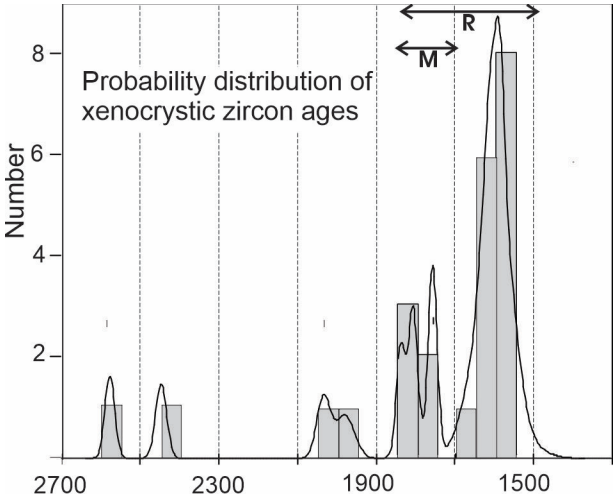


Figure 34. Probability density plot for combined SHRIMP $^{207}Pb/^{206}Pb$ ages of inherited zircon grains in igneous rocks from the study area. Lines with double arrows indicate the range of TDM for the Musquaro-D'Auteuil lakes area (M) and the Kegaska, through La Romaine, to Baie des Loups sector (R).

The Paleoproterozoic and Archean zircon xenocrysts (Fig. 34) help explain the older Nd model ages of up to 1.85 Ga (Table 7; Fig. 33). Unlike the U-Pb SHRIMP data from xenocrysts, there is a difference in the range of model ages between the Musquaro Lake and La Romaine areas, with the latter extending to as young as 1.48 Ga (Fig. 33).

No Labradorian granitoids and orthogneisses have been dated yet in the study area (this work; Lafrance and Daoudene, 2024; Daoudene and Lafrance, 2025; Lafrance et al., 2026). This apparent absence of Labradorian granitoids contrasts with what is observed in the eastern Pinware terrane, where both Pinwarian and Labradorian granitoids occur and display similar textures and mineral assemblages (Gower and Krogh, 2002; Heaman et al., 2004). For example, along the St Lawrence Gulf coast in the Blanc Sablon area (Fig. 1, transect H-G-P), the Pinware terrane comprises orthogneisses of Labradorian age (e.g., 1632 and 1650 Ma) among abundant Pinwarian metaplutonic granitoids (1467–1526 Ma) in addition to having younger syenites at 1.4 Ga, gabbros at 1248 Ma, and gabbros and anorthosites in the 979–974 Ma range (Heaman et al., 2004).

Sm-Nd isotopic mapping by Dickin (2004) extends the distribution of concealed Labradorian crust as far east as the Long Range inlier in the Appalachian orogen of Newfoundland, where it is in contact with a major juvenile crustal block with ca. 1575–1450 Ma Sm-Nd model ages. Such juvenile Pinwarian-age crust was also identified in central Québec (Dickin and Higgins, 1992; Dickin, 2000). Accordingly, the boundary could follow the north shore of the St Lawrence River (taking into account the post-Proterozoic jog in crustal architecture along the Appalachian front). If this interpretation is correct, then Labradorian crust should occur in the substrate of the Musquaro Lake and La Romaine areas, although the single T_DM age of 1.48 Ga obtained at La Romaine may indicate proximity to the boundary with a younger terrane or, alternatively, development on thinner continental crust. A thinner crust would be consistent with the interpretation that the La Romaine supracrustal belt is an intra-arc rift basin based on its lithogeochemical signature (Bonnet et al., 2005; Corriveau and Bonnet, 2005). While no Labradorian rocks have been found yet in the

study area, the systematic presence of Labradorian-age xenocrysts in igneous rocks and Labradorian intrusions east of the Natashquan domain (this work; Corriveau et al., 2002, 2003; Gower and Krogh, 2002) suggests that the Labradorian crust was extensive within the substrate.

5.2. Pinwarian Sedimentation and Provenance of Detrital Zircons

Detrital zircon ages were obtained on a clastic sedimentary rock of the southeastern extension of the Wakeham Group at Musquaro Lake (van Breemen and Corriveau, 2005). The age populations range from Archean to Labradorian (2935, 2861, 2744–2647, 2520–2280, 2100–2030, 1960–1750, 1864, and 1621 Ma; Fig. 35) and to a Pinwarian maximum deposition age of 1517 Ma. These authors interpreted the source (s) of the sedimentary rock dated at Musquaro Lake (sample CQA-00-006) to be in part related to the erosion of early Pinwarian volcanic rocks. Since then, two additional metasedimentary samples have been dated by David et al. (2026b) and Rochín-Bañaga and Davis (in press).

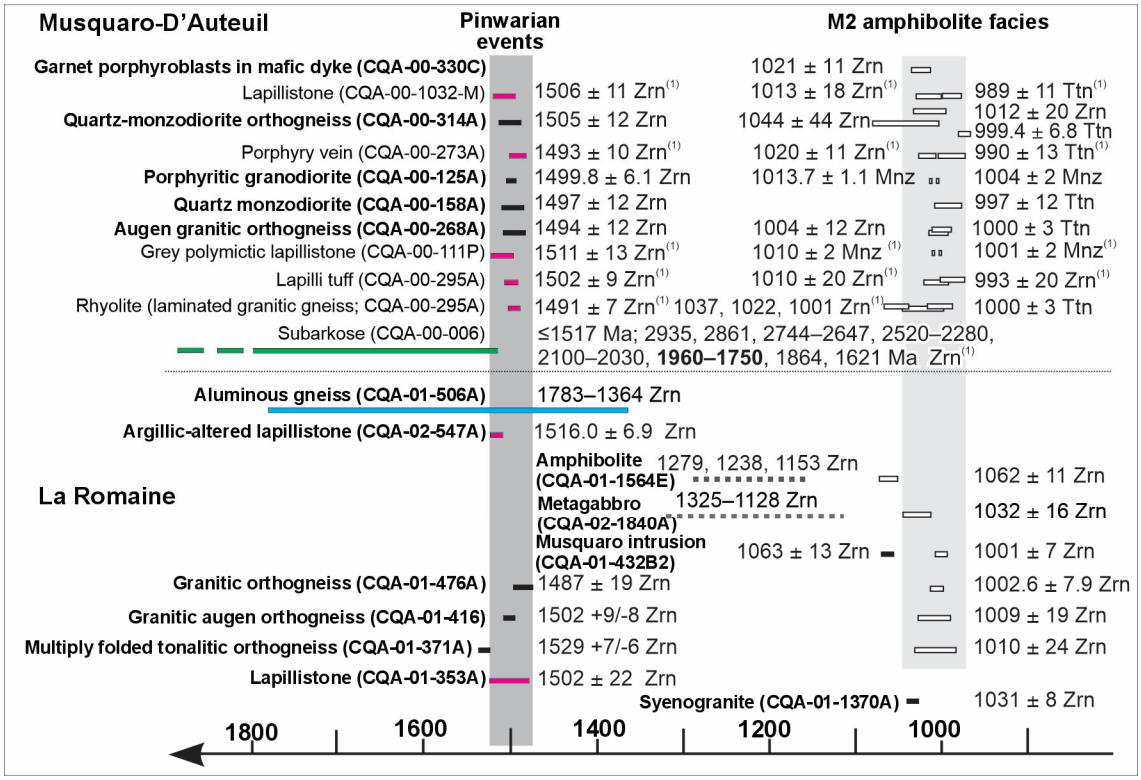


Figure 35. Summary table of geochronological data acquired during the TGI project (this work; van Breemen and Corriveau, 2005). Pink rectangles: volcanic and volcaniclastic rocks and associated porphyry vein stockwork; black: intrusive rocks; green: detrital zircon population; blue: uncertain origin of zircon grains; clear: metamorphic ages; Mnz: monazite; Ttn: titanite; Zrn: zircon. The length of the rectangles corresponds to uncertainties except for the green, blue and dash lines that represent the range of the data. In bold, is the main population of detrital zircons.

A sub-arkose (sample 25-SL-4116A) was dated by Rochín-Bañaga and Davis (in press). This sub-arkose occurs to the southwest of D'Auteuil Lake and yielded a maximum depositional age of 1509 Ma. It preserves exceptionally well primary cross stratification. The detrital zircon grains span ages up to 2 Ga, with many grains dated between 1.8 and 1.9 Ga, as in sample CQA-00-006. However, Neo- and Meso-Archean detrital zircon grains have not been recovered. Lafrance et al. (2026) interpret the sources as being in part distinct from those of the older metasedimentary rock.

The maximum depositional age indicates that this sub-arkose was deposited after at least some of the volcanic rocks in the region.

A paragneiss (sample 2024-IL-3179A) was dated from the La Romaine supracrustal belt, east of La Romaine in NTS sheet 12K01 and yielded a maximum age of deposition of 1557.6 Ma (David et al., 2026b). The detrital zircon grains are generally rounded to subrounded; this rounding may indicate relatively long transport and/or sedimentary recycling. Their morphology differs significantly from the post 1.7 Ga hypidiomorphic to nearly idiomorphic igneous detrital zircon population at Musquaro Lake, which showed minimal truncation of igneous oscillatory zoning and little evidence of abrasion during detrital transport. Accordingly, the 1557.6 Ma age either reflects an earlier sedimentation episode or a lack of easily erodible volcanic rocks contributing younger detrital zircon grains; both possibilities remain plausible, but the latter hypothesis is favoured here. Sediment sources may thus have varied significantly within the Pinwarian volcano-sedimentary basins of the study area.

Based on regional data and the established correlation —demonstrated by van Breemen and Corriveau (2005), Corriveau and Bonnet (2005), and Bonnet et al. (2005)— between the sedimentary and volcanic units north of Musquaro Lake and D'Auteuil Lake and those of the La Romaine supracrustal belt (in the La Romaine and Unamen Shipu areas), the discovery of quartzite units by Lafrance et al. (2026) and the maximum depositional age of 1509 Ma obtained southwest of D'Auteuil Lake indicate that sedimentation continued locally during volcanism and included episodes of sedimentary remobilization within a highly active tectonic setting.

The available data indicate that the correlations between the various undated supracrustal sequences in the study area and with the Wakeham Group remain to be clarified regarding the finer details of their age, sediment provenance, and depositional setting. However, some hypotheses regarding sediment sources and their spatial and temporal variations within the supracrustal sequences can be proposed.

Recent work by Lafrance and Godet (2024) indicates that the Archean component of the Baleine Domain of the New Québec Orogen may be a potential source even though provenance from the Labrador Trough and the New Québec Orogen had been considered less likely than the Torngat Orogen at the time by van Breemen and Corriveau (2005). The Meso- to Neoarchean basement of the Baleine Domain records metamorphic ages of 1873 and 1864 Ma. Older inherited zircon reaches 3154 Ma. Detrital zircon grains in the False Suite range from 3335 to 2678 Ma. The 1864 Ma metamorphism signature therefore is not unique to the Falcoz Domain, which includes part of the Torngat Orogen.

5.3. Pinwarian Plutonism, Volcanism and Sedimentation

The 1.5 Ga Pinwarian granitoids form a major sub-volcanic granitic to granodioritic batholith emplaced on older tonalitic basement (this work; Bonnet et al., 2005; Corriveau and Bonnet, 2005; van Breemen and Corriveau, 2005; Lafrance et al., 2026). Figure 35 summarizes the main age results for the Musquaro Lake and La Romaine areas from this study and van Breemen and Corriveau (2005). The dataset illustrates that both areas experienced broadly similar ca. 1.5 Ga magmatic histories. In the Musquaro Lake area, the volcanic rocks (lapillistone and laminated granitic gneiss interpreted as a flow-banded rhyolite) have been dated at 1511 ± 13 Ma, 1506 ± 11 Ma, 1502 ± 9 Ma and 1491 ± 7 Ma.

A porphyry vein was dated at 1493 ± 10 Ma by van Breemen and Corriveau (2005). It is part of a stockwork of irregular and anastomosing porphyry veins that cut a hydrothermally altered

rhyolite (Fig. 36). The style of magma emplacement of the veins is atypical of late-stage porphyry dykes but consistent with magma emplacement while the rhyolitic host was still not fully solidified. The age is interpreted as marking the end of volcanism in the D'Auteuil region (van Breemen and Corriveau, 2005). The 1493 ± 10 Ma age falls statistically within the range of a suite of younger volcanic rocks and ash tuffs —unassociated with sedimentary rocks and lacking lapillistone beds— dated at 1502 ± 9 and 1491 ± 7 Ma along the shores of Lake D'Auteuil (van Breemen and Corriveau, 2005). Consequently, volcanism as currently understood appears to have ceased around 1.49 Ga, at a time when the vast majority of the Pinware batholith in the region was being emplaced (Wodicka et al., 2003 and references therein; Corriveau et al., 2026; Lafrance et al., 2026), with emplacement continuing across the Pinware terrane until 1.46 Ga (Indares et al., 2022). Subsequent pegmatite veins cut the porphyry network and are themselves cut by a porphyritic granitoid with textures more typical of the Pinwarian intrusions (Fig. 36C, D).

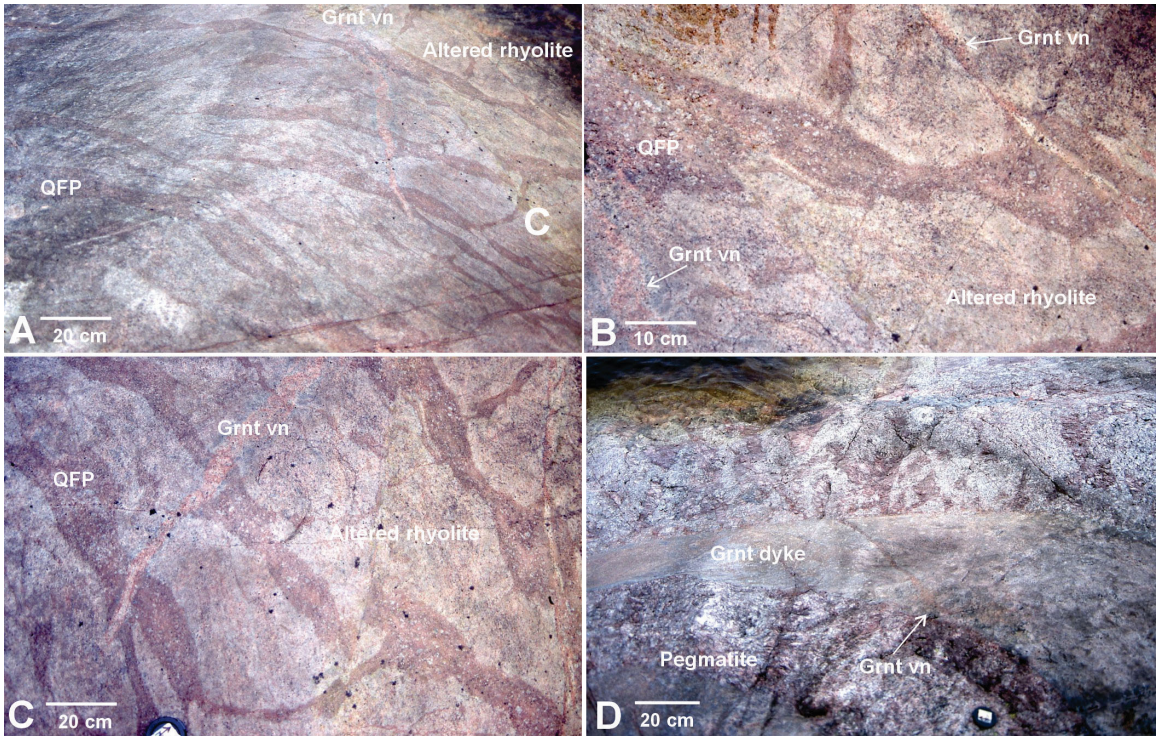


Figure 36. Stockwork of anastomosing, 1493 Ma, quartz and K-feldspar porphyry (QFP) veins cutting a hydrothermally altered rhyolite at Musquaro Lake (CQA-00-105). The stockwork and the rhyolite are also cut by a granitic dyke and a late-stage granitic vein. **A.** The QFP veins are discontinuous, anastomosing, interconnected, and of variable thicknesses. C locates Figure C in A. The subsequent granitic vein (Grnt vn) cuts sharply the porphyry veins and is continuous and linear. **B.** Close up on the phenocrysts of the porphyry veins. **C.** Close up of A illustrating the interconnection and locally arcuate shape of the QFP veins as well as the irregular apophyses. **D.** A granitoid (Grnt) dyke with an igneous foliation parallel to the dyke contact cuts a pegmatite and is itself cut by a granitic vein like the one in A to C.

The 1505 Ma to 1494 Ma igneous ages documented in this study on gneissic granitoids show that the plutonism was largely synchronous with the volcanism that post-dated deposition of the underlying sedimentary rocks in the Musquaro Lake area. In the La Romaine area, ages obtained from lapillistones of 1502 ± 22 Ma (sample CQA-01-353A) and 1516 ± 6.9 Ma (sample CQA-02-547A) show that volcanism was coeval with volcanism in the Musquaro-D'Auteuil lakes area, whereas the plutonic ages of 1502 +9/-8 Ma and 1487 ± 19 Ma show that there too plutonism was synvolcanic and continued for a few million years subsequently.

All igneous ages of the granitoid intrusions are consistent with being synchronous with or younger than the supracrustal rocks, except for the multiply folded tonalitic gneiss (sample 6, CQA-01-371A) from the La Romaine area, which yielded an older age of 1529 +7/-6 Ma. This tonalitic gneiss, and the tonalitic gneiss with a recently published age of 1582 Ma from the l'Aigle Complex south of Musquaro Lake (Fig. 3E) record Wakamian magmatism. These gneisses are interpreted as part of the older basement, whereas the Pinwarian felsic to minorly mafic magmatism that extends across the study area and southeast and in the northern part of the Wakeham Group (Fig. 2) represents the major magmatic event in the western Pinware terrane.

The extensive Makkovikian, Labradorian and Wakamian inheritance in the Pinwarian intrusions is consistent with a pre-Grenvillian Andean setting along the southeastern margin of the proto-Laurentia and with northward subduction during the Pinwarian orogeny (e.g., Gower and Krogh, 2002).

5.4. Pinwarian Hydrothermal System

5.4.1. Timing of the Volcanism and Hydrothermal Activity

The aluminous gneiss derived from an argillic-altered lapillistone (sample CQA-02-547A) has a zircon U-Pb crystallization age of 1516 ± 6.9 Ma. This age is consistent with zircon U-Pb crystallization ages obtained on least-altered metavolcaniclastic rocks in the Musquaro-D'Auteuil lakes extensions of the Wakeham Group (1511 ± 13 Ma, 1506 ± 11 Ma, 1502 ± 9 Ma; van Breemen and Corriveau, 2005). The strong influence of volcaniclastic rock permeability on focussing hydrothermal fluids suggests that the hydrothermal activity is coeval with the volcanic event and that the 1516.0 ± 6.9 Ma magmatic crystallization age, while strictly a maximum age, provide a reasonable estimate for the timing of the hydrothermal activity. Minimum ages are provided by the stockwork of 1493 ± 10 Ma quartz-feldspar porphyry veins that cuts the hydrothermal alteration of a rhyolite (Fig. 36) and the presence of rafts of hydrothermally altered rocks and potential meta-exhalite in a Pinwarian granitoid at Musquaro Lake (Corriveau et al., 2026).

5.4.2. Origin of Inclusion-rich Zircon in the Composite Amphibolite Unit at La Romaine

Hydrothermal zircon is commonly used to date hydrothermal alteration and mineralization (Claoué-Long et al., 1990; Kerrich and King, 1993; Barrie and Krogh, 1996; Yeats et al., 1996; Williams, 1998; Hartmann et al., 2000). The metagabbro and the Ca-Fe- and K-Fe-altered amphibolite of the La Romaine hydrothermal system yield an atypical population of zircon characterized by inclusion-rich cores with variable to high U and Th content and Th/U ratios. The spongy inclusion-filled texture and the U-rich chemistry of these zircon cores are consistent with zircons that crystallized from or were altered by an aqueous fluid (Corfu et al., 2003; Hoskin and Schaltegger, 2003).

The development of zircon during fluid-dominated processes involves the mobility of Zr and Si. Recent studies have shown that hydrothermal, magmatic and metamorphic fluids can mobilize Zr and can have a significant impact on zircon morphology and chemistry (Rubin et al., 1989; Claoué-Long et al., 1990; Kerrich and King, 1993; Williams et al., 1996; Tomaschek et al., 2003; Hoskin, 2005).

Inclusions in zircon cores from the Ca-Fe- and K-Fe-altered amphibolite and the least-altered metagabbro, are mainly quartz, potassic and alkali feldspar, biotite, chlorite, hornblende, plagioclase, and traces of iron oxide or pyrite. This suite of minerals does not include

orthopyroxene or clinopyroxene, which are diagnostic minerals of the granulite-facies paragenesis of the host metagabbro and amphibolite. It is unlikely, therefore, that the inclusion-rich zircons formed through metamorphic processes. Furthermore, as the inclusion-rich zircons did not preserve euhedral zoning, they are unlikely to be of magmatic origin (Nutman and Ehlers, 1998). The most likely alternative is that these zircon populations resulted from growth in a hydrothermal environment.

Rubin et al. (1993) showed that Zr mobility occurs during hydrothermal alteration processes involving F-rich hydrothermal fluids, as F complexing ions promote the preferential solubility of Zr. The presence of metamorphosed and deformed fluorite-bearing veins crosscutting a Ca-Fe alteration zone confirms the abundance of F during the hydrothermal activity. The unusually high zircon content in the biotite-sulphide-apatite-rich layer within the Ca-Fe- and K-Fe-altered amphibolite provides further evidence for hydrothermal zircon precipitation or recrystallization within the discharge zone. If the inclusion-rich zircons have a hydrothermal origin, then the inclusions may represent mainly minerals precipitated during the hydrothermal activity (Claoué-Long et al., 1990; Kerrich and King, 1993; Yeats et al., 1996; Williams, 1998; Hartmann et al., 2000; Corfu et al., 2003; Hoskin and Schaltegger, 2003).

The high-grade metamorphosed, zircon-rich alteration facies of the discharge zone contains a high modal abundance of K- and Fe-rich minerals, such as biotite, iron oxides and sulphides. Zircon inclusions consist mainly of K- and Fe-rich phases (biotite, potassic feldspar, chlorite, iron oxide). The abundance of K- and Fe-rich minerals in both zircon and zircon-rich altered rocks may support the hydrothermal origin of the inclusion-rich zircon population. In contrast to the Ca-Fe- and K-Fe-altered amphibolite, the metagabbro does not display field-evidence of strong chemical changes associated with hydrothermal alteration and thus is interpreted as a least-altered rock (Bonnet et al., 2005). However, some layers of metagabbro in other outcrops contain inclusions of ironstones and some of the inferred hydrothermal zircons may have come from the assimilation of such xenoliths.

The near-concordant U-Pb ages obtained from the inclusion-rich zircon occurring within the Ca-Fe- and K-Fe-altered amphibolite range from 1279 ± 62 Ma to 1030 ± 44 Ma *(1σ).* These ages are not distributed uniformly along the concordia as nine analyses form a cluster with a concordant $^{206}Pb/^{238}U$ age of 1062 ± 11 Ma, whereas two analyses display older $^{207}Pb/^{206}Pb$ ages of 1279 ± 62 Ma and 1238 ± 70 Ma, ca. 200 Myr younger than the volcanic activity. The large age spread suggests that the hydrothermal zircon U-Pb systems were reset. The disturbance of the U-Pb isotopic system of hydrothermal zircon is correlated with a decrease in Th/U ratio that points to a chemical control on Pb loss. The Pb loss could be related to the high-grade metamorphism that affected the La Romaine cupriferous hydrothermal system. The three oldest analyses of inclusion-rich zircon of the metagabbro yield a weighted mean $^{207}Pb/^{206}Pb$ age is 1325 ± 50 Ma (1σ). Given the evidence for resetting, this age is not interpreted as a direct crystallization age.

5.5. Elsonian Event

West of the Wakeham Group, the Matamec Complex and its crosscutting mafic dykes with Ni-Cu magmatic sulphides were respectively emplaced at 1.38 and 1.35 Ga (Gobeil et al., 1999; Nabil et al., 2003). They are interpreted as forming a large mafic-silicic layered intrusion (Saint-Germain and Corriveau, 2003).

In the study area, 1.3 Ga dates were obtained from the amphibolite unit interpreted as hydrothermally altered basalt and from a mafic sill of the composite amphibolite unit of the La Romaine supracrustal belt, as described above. As the host units were extensively hydrothermally altered and the zircon subsequently reset, these dates are not interpreted as meaningful ages. To date, no Elsonian magmatism has been documented in the study area (David et al., 2026a, b). The strong resetting of zircon U and Pb, however, suggest that fluid potentially circulated at high temperature during the Elsonian. Field evidence of such an event could include the late-stage fluorite-bearing veins that cut the composite amphibolite unit at La Romaine. At this time the age of F-rich fluid circulation remain uncertain as the deformation could be Grenvillian. In addition, renewed fluid circulation may have mobilized a primary endowment in F of the host hydrothermal system to form veins, a process that is common in MIAC and other mineral systems (e.g., Corriveau and Montreuil, 2025).

5.6. Grenvillian Magmatic Events

Within and along the western margin of the Pinware terrane extends the Buit Complex, composed mainly of foliated granite and granite gneisses (Gobeil et al., 2003), for which a 1079 ± 5 Ma zircon age was obtained (Loveridge, 1986). To the west, the Havre St. Pierre anorthosite complex formed in the 1.13–1.06 Ga age range, with the Rivière au Tonnerre and Lac Allard anorthosite being systematically dated at 1.06 Ga (van Breemen and Higgins, 1993; Wodicka et al., 2003; Morisset et al., 2009). In the study area, the Musquaro ultramafic to mafic, subvertically layered intrusion was emplaced along a major shear zone at 1063 Ma and cut a subsequent pegmatitic gabbro dyke at 1059 Ma. This mafic magmatism is statistically coeval with the emplacement of the Lac Allard and Rivière au Tonnerre anorthosite (Fig. 2).

In the study area, the Washicoutai Intrusive Suite with members dated herein at 1031 ± 8 Ma and at 1043.4 ± 12.7 Ma by David et al. (2026a) is the most widespread Grenvillian magmatism in the study area. In contrast, the La Galissonnière Plutonic Suite (MRNF e) with the emplacement of unfoliated granites within the Wakeham Group north and west of the study area at 993 ± 3 Ma (Loveridge, 1986) and 984 ± 2 Ma and 981 ± 2 Ma (Wodicka et al., 2003) marks the last stage of voluminous magmatism in the eastern Grenville Province (Fig. 2).

5.7. Timing of High-grade Metamorphism

The combined field and U-Pb geochronological data on intrusive suites in the eastern part of the study area by Daoudene and Lafrance (2025) and David et al. (2026a) constrain the Grenvillian regional pervasive deformation and associated metamorphism to be between 1088 Ma (age of the metamorphosed Mantuh Suite intrusion) and 1043 Ma (age of the non deformed Rocher Rouge Intrusion that is part of the Washicoutai Intrusive Suite). Further constraints are provided by the Musquaro ultramafic to mafic layered intrusion dated at 1063 ± 13 Ma which is only moderately metamorphosed to amphibolite facies and commonly preserves an igneous foliation even though the margin are deformed. The intrusion may have been emplaced syntectonically based on its style of magma emplacement (Corriveau et al., 2026) and its association with a major shear zone documented by Lafrance and Daoudene (2024). Such mafic intrusions are particularly competent

and may not be pervasively deformed during regional tectonothermal metamorphic events as was shown for the vertically layered ultramafic to mafic intrusions of the Central Metasedimentary Belt in the western Grenville Province (Corriveau, 2013). Accordingly, the intrusion may have preceded or been coeval with the regional Grenvillian tectonothermal metamorphism. In contrast, the large syenogranite dyke of sample CQA-01-1370A has an age of 1031 ± 8 Ma and is most likely late syntectonic, providing an upper constraint on the end of the pervasive deformation during the Grenvillian tectonothermal metamorphism. In this respect, the metamorphic ages of 1062 ± 11 (CQA-01-1564E) and 1032 ± 16 Ma (CQA-02-1840A) obtained on the hydrothermally altered amphibolite and the metagabbro of the composite amphibolite unit in the La Romaine supracrustal belt provide potentially the closest ages for the tectonothermal metamorphism. However, most of the U-Pb ages obtained on zircon, monazite, and titanite during the TGI research vary between 1044 ± 44 Ma and 989 ± 11 Ma (Figs. 35, 37) which would largely postdate the tectonothermal metamorphic event. Daoudene and Lafrance (2025) have illustrated that the tectonothermal Grenvillian metamorphism was followed by widespread static recrystallization and cooling.

Figure 37 plots metamorphic ages from the study area. For the Musquaro-D'Auteuil lakes area, U-Pb ages on monazite, titanite and zircon rims are available. Homogeneous metamorphic zircons included in garnet porphyroblasts of a hydrothermally altered amphibolite give an age of 1021 ± 11 Ma. Their rims were not analyzed. Metamorphic zircon rims were individually analyzed from other samples. As their number is insufficient, a composite age was obtained from five samples, two from this study (samples CQA-00-314A and CQA-00-268A) and three from van Breemen and Corriveau (2005). This weighted average of 17 analyses is 1015 ± 8 Ma. Because the probability of fit is 0.2 %, the uncertainty cannot be relied upon to cover the age range of metamorphism.

Two U-Pb monazite ages of 1014 ± 2 Ma (sample CQA-00-125A) and 1010 ± 2 Ma (van Breemen and Corriveau, 2005) are in close agreement with the metamorphic zircon age. As zircon and monazite have high Pb closure temperatures, these dates could have been interpreted as dating the regional metamorphism at 1015–1010 Ma if there had not been the major constraint provided by the style of emplacement and the lack of intense and pervasive deformation of the dykes and intrusion of the Washicoutai Intrusive Suite. Considering these constraints, they are best interpreted as part of the late static recrystallization and thermal re-equilibration observed by Daoudene and Lafrance (2025).

Five U-Pb titanite ages range from 1000 ± 3 Ma to 989 ± 11 Ma and are statistically younger than the metamorphic zircon ages. The late granite intrusions at 993 ± 3 Ma (Loveridge, 1986) and 984 ± 2 Ma and 982 ± 2 Ma (Wodicka et al., 2003) to the west and north of the study area are similar in age to the U-Pb titanite ages. Accordingly, these ages could be interpreted as recording subsequent cooling and late thermal re-equilibration.

No U-Pb monazite or titanite data are available for the La Romaine area. An older Grenvillian remobilization event is recorded by a paragneiss sample dated east of La Romaine, which yielded a zircon population at 1067 ± 13 Ma (David et al., 2026b). Two zircon TIMS lower intercept ages at ca. 1010 Ma are in agreement with the younger SHRIMP metamorphic ages. The metagabbro sample (1840A) contains a late Grenvillian zircon generation dated at 1028 ± 16 Ma that occurs either as unzoned zircon grains or as overgrowths, both with low Th/U ratios. The morphology and Th-U chemistry of these zircon grains and overgrowths are typical of zircon crystallized during high-grade metamorphism (Vavra et al., 1999). The Ca-Fe- and K-Fe-altered amphibolite (CQA-01-l564E) and the aluminous gneiss (CQA-01-506A) display similar metamorphic zircons and

overgrowths, although these were not analyzed. Interestingly, the 1028 Ma age is statistically similar to the 1021 Ma age of the zircon inclusions in garnets at Musquaro Lake.

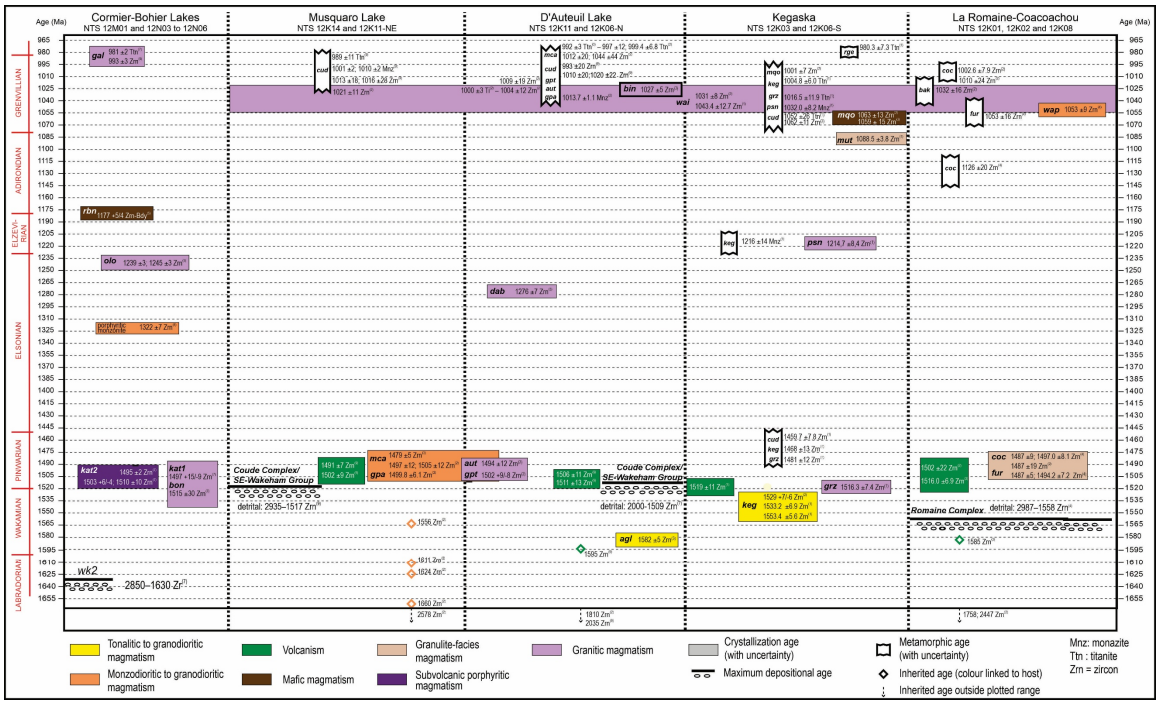


Figure 37. Regional compilation of U-Pb geochronological data from part of the southeastern Grenville Province. Numbers associated with individual ages refer to the following sources: (1) David et al. (2026a); (2) this study; (3) Rochín-Bañaga and Davis (in press); (4) David et al. (2026b); (5) Martignole et al. (1994); (6) Loveridge (1986); (7) Wodicka et al. (2003); (8) Martignole et al. (1992); and (9) van Breemen and Corriveau (2005). Abbreviations: **agl**, L'Aigle Complex; **aut**, D'Auteuil Intrusive Suite; **bak**, Blacklands Intrusive Suite; **bin**, Bouin Intrusive Suite; **bon**, Boulain Complex; **coc**, Coacoachou Intrusive Suite; **csr**, La Romaine Complex; **cud**, Coude Complex; **dab**, Dabin Intrusion; **fur**, Foucher Intrusive Suite; **gal**, La Galissonnière Plutonic Suite; **gpa**, Grand Portage Granodiorite; **gpt**, Grand Priant Intrusive Suite; **grz**, Grozieux Intrusion; **kat**, Kataht Felsic Suite; **keg**, Kegaska Intrusive Suite; **mca**, Marie-Claire Intrusive Suite; **mqo**, Musquaro Gabbroic Intrusion; **mut**, Mantuh Intrusive Suite; **olo**, Olomane Felsic Suite; **psn**, Parsons Intrusion; **wai**, Washicoutai Intrusive Suite; **wap**, Wapitagun Intrusive Suite.

It is noteworthy that U-Pb geochronology in the Grenville Province has commonly failed to date pre-Shawinigan metamorphism and associated gneissic fabrics, as emphasized by Corriveau and van Breemen (2000) and Wodicka et al. (2003). The identification of Pinwarian metamorphic ages by Lafrance et al. (2026) as shown in Figure 37 represents a major advance in constraining the tectonometamorphic evolution of the area and in reconciling the field relationships described in Part 1 (Corriveau et al., 2026) with the available geochronological record. In parallel, the timing of the main tectonothermal metamorphism that deformed the Pinwarian intrusions and the early Grenvillian intrusions, such as those of the Mantuh Intrusive Suite and the Musquaro layered intrusion, remained difficult to constrain despite the large number of rocks dated during this study and that of the MRNF. In summary, the ca. 1.01 Ga ages record a late Grenvillian thermal event, although they may in part reflect static recrystallization rather than a discrete metamorphic peak. Five U-Pb titanite ages range from 1000 ± 3 Ma to 989 ± 11 Ma and are statistically younger. These ages are interpreted as recording subsequent cooling and late thermal re-equilibration.

5.8. Integration with Recent Geological and Geochronological Work

Geological mapping and geochronological work conducted since the acquisition of the legacy U-Pb data presented in this report have substantially refined the geological framework of the region. Rocks formerly grouped within the broadly defined *Aguanish complex* have been reassigned to a series of lithodemic units based on field relationships, lithogeochemistry and new geochronological data (Lafrance and Daoudene, 2024; Daoudene and Lafrance, 2025; David et al., 2026a, b; Lafrance et al., 2026; Rochín-Bañaga and Davis, in press). The regional geochronological compilation presented in Figure 37 integrates the legacy ages reported herein with these recent results using the currently recognized unit names.

These data demonstrate that Wakamian magmatism constitutes a regionally extensive component of the crust. Tonalitic rocks of the L'Aigle Complex yielded an age of ca. 1582 Ma, whereas foliated to gneissic tonalitic to granodioritic rocks of the Kegaska Intrusive Suite yielded ages ranging from ca. 1553 to 1529 Ma. Inherited zircon ages recorded in younger magmatic rocks further indicate involvement of older crustal components, including Wakamian, Paleoproterozoic and locally Archean sources, consistent with recycling or assimilation of older crust during Pinwarian magmatism.

The Coude and La Romaine complexes, to which the supracrustal sequences of the Musquaro-D'Auteuil lakes area and the La Romaine supracrustal belt have been reassigned, respectively (Lafrance and Daoudene, 2024; Daoudene and Lafrance, 2025), record broadly coeval Pinwarian volcanism at ca. 1.52–1.49 Ga, but detrital zircon data reveal spatial variations in sedimentary provenance and depositional history. At Musquaro Lake, volcanic rocks stratigraphically overlie metasedimentary rocks with a maximum depositional age of ca. 1.52 Ga, whereas sedimentation locally continued during volcanism in the D'Auteuil Lake area. Farther east, the La Romaine Complex contains an older metasedimentary component with a maximum depositional age of ca. 1.56 Ga. Felsic porphyritic intrusions of the Kataht Felsic Suite (kat2; Fig. 2), dated at ca. 1.51–1.50 Ga, further document subvolcanic magmatism broadly coeval with the regional Pinwarian volcanic activity.

Pinwarian plutonism was widespread across the region and involved several compositionally distinct magmatic suites. Granitic magmatism is recorded between ca. 1516 and 1494 Ma, whereas granulite-facies granitic magmatism in the Coacoachou and Foucher intrusive suites ranges from ca. 1497 to 1487 Ma. In the Musquaro–D'Auteuil area, monzodioritic to granodioritic magmatism represented by the Marie-Claire Intrusive Suite and Grand Portage Granodiorite ranges from ca. 1505 to 1479 Ma (Fig. 37).

Together, these ages document compositionally diverse Pinwarian plutonism from ca. 1.52 to 1.48 Ga that broadly overlapped with, and outlasted, the associated volcanic and subvolcanic activity, highlighting the extent and protracted nature of Pinwarian magmatism. Pinwarian intrusive activity postdates regional high-grade metamorphism in the La Romaine area (based on field relationships; Corriveau et al., 2026), but may have locally overlapped with high-grade metamorphism, as suggested by metamorphic zircon ages of ca. 1.48–1.46 Ga recorded in the Kegaska area (Lafrance et al., 2026; Fig. 37).

Following the main Pinwarian tectonomagmatic episode, younger Mesoproterozoic activity is more sporadically recorded across the region. Elsonian magmatism includes a porphyritic monzonite dated at ca. 1.32 Ga in the Cormier–Bohier lakes area (north of Musquaro Lake; Fig. 2), the Dabin Intrusion at ca. 1.28 Ga in the D'Auteuil Lake area, and the Olomane Felsic Suite at ca.

1.24 Ga (Fig. 2). In the Kegaska area, a monazite age of ca. 1216 Ma coincides with the crystallization age of the Parsons Intrusion (ca. 1215 Ma). Considering that weak late-stage albitization, K-feldspar alteration and hematization are locally observed within the Pinwarian intrusions, this 1216 Ma age could be documenting Elzevirian metamorphism if the monazite is metamorphic or, alternatively and most likely, metasomatism induced by fluid circulation associated with magma emplacement.

After a substantial temporal gap (potentially only apparent considering that the amphibolite dykes of the Lillian Intrusive Suite have not been dated in the study area), renewed magmatic activity at ca. 1.09 Ga coincided with the onset of the Ottawan phase of the Grenvillian Orogeny. The Mantuh Intrusive Suite (ca. 1088 Ma), characterized by granulite-facies magmatic rocks, represents an early manifestation of this Grenvillian tectonothermal episode in the region. Grenvillian magmatism continued with emplacement of the mafic Musquaro Intrusion at ca. 1.06 Ga, the Wapitagun Intrusive Suite (ca. 1.05 Ga) and the Washicoutai Intrusive Suite (ca. 1.04–1.03 Ga), followed by anatectic granitic magmatism represented by the Bouin Intrusive Suite (1.03 Ga). Thermal input from late Grenvillian intrusions, particularly the Washicoutai and Bouin suites, may also have contributed locally to the widespread static recrystallization recognized during regional mapping. Late, weakly deformed to undeformed granitic intrusions of the La Galissonnière Plutonic Suite at ca. 0.99–0.98 Ga, occurring within and adjacent to the Wakeham Group, record the final magmatic stages preserved in the western Pinware terrane.

6. Conclusion

The supracrustal sequences in the southeastern extension of the Wakeham Group and the Pinwarian batholith from Musquaro and D'Auteuil lakes easterly to the La Romaine supracrustal belt and the Baie des Loups area display a protracted history of Pinwarian and Grenvillian events. This includes Pinwarian sedimentation, volcanism, hydrothermal activity, mineralization, and batholith emplacement, Pinwarian and Grenvillian metamorphism and deformation, and Grenvillian ultramafic to felsic magmatism. The Part 1 report describes the geological and geochemical footprint of these events whereas this Part 2 constrains the timing of these events based on legacy U-Pb geochronology acquired during a project of the Targeted Geoscience Initiative of the Geological Survey of Canada in the early 2000s. The information is augmented through extensive linkages to the recent geological and geochronological information obtained by the ministère des Ressources et des Forêts du Québec in the study area.

In the La Romaine supracrustal belt, the new zircon U-Pb crystallization age of 1516.0 ± 6.9 Ma obtained from an aluminous gneiss with igneous zircon populations further supports the field and geochemical interpretation of an argillic-altered lapillistone. This age and the 1502 ± 22 Ma age of a least-altered lapillistone in this same belt confirm the broadly coeval nature of the volcanic activity in the La Romaine supracrustal belt and the Musquaro-D'Auteuil lakes area.

In the amphibolite hydrothermally altered prior to metamorphism and spatially associated metagabbro sill of the composite amphibolite unit, inclusion-rich zircon cores yielded near-concordant U-Pb ages from 1325 Ma to 1030 Ma. These cores, interpreted to be of hydrothermal origin, were likely strongly reset during thermal events postdating the hydrothermal activity and, therefore, a direct age of the hydrothermal activity has not been obtained from hydrothermal zircon. Nevertheless, the 1516.0 ± 6.9 Ma crystallization age from the argillic-altered lapillistone (aluminous gneiss) provides a reasonable age estimate for the hydrothermal activity in line with the presence of rafts of hydrothermally derived rocks in 1.5 Ga granites, and intrusion of a 1493 Ma quartz-K-feldspar porphyry into hydrothermally altered 1.50 Ga rhyolite. The discovery of

albitized 1502 Ma metaplutonic rocks (Lafrance et al., 2026), together with the presence of the meta-exhalite rafts within granitoids, provides key evidence for the presence of sub-volcanic intrusions.

In the Lac Musquaro area, at the southeastern margin of the Wakeham Group, four plutonic units yielded ages of 1505 ± 12 Ma, 1499.8 ± 6.1 Ma, 1497 ± 12 Ma and 1494 ± 12 Ma. These ages overlap the previously obtained 1511 Ma to 1491 Ma ages from metavolcanic rocks and associated porphyry in the Musquaro-D'Auteuil area and are slightly younger than the two ages obtained for the metasedimentary rocks in the same area. To the east, in the La Romaine to Baie des Loups area, igneous zircon ages of 1502 +9/-8 Ma and 1487 ± 19 Ma from granitic gneisses are consistent with field and geochemical data that show plutonism to have been synchronous between the two areas.

A belt of tonalitic to granodioritic gneisses dated at 1529 +7/-6 Ma displays pervasive interference fold patterns that are significantly distinct from most of the Pinwarian gneisses in the region. The 1529 Ma age therefore records late Wakamian rather than Pinwarian magmatism. Together with the ca. 1582 Ma tonalitic rocks now assigned to the L'Aigle Complex (Lafrance and Daoudene, 2024; Lafrance et al., 2026), the belt of 1529 Ma tonalitic gneiss documents the presence of an extensive Wakamian basement and a significant Wakamian magmatic history in the region.

The legacy U-Pb ages provided herein for nine plutonic rocks formerly grouped within the *Aguanish complex* indicate that ca. 1530–1490 Ma Wakamian to Pinwarian continental-arc magmatism was a major crust-forming event that extends the main outcrop of the Pinware terrane into the Natashquan domain of Gobeil et al. (2003) as far as the Wakeham Group in the eastern Grenville Province. The metamorphosed extension of the Wakeham Group at Musquaro and D'Auteuil lakes and the La Romaine supracrustal belt are interpreted as Pinwarian intra-arc basins developed within a continental magmatic arc, with the main volcanic activity occurring at ca. 1520–1487 Ma. The presence of mafic to intermediate facies within the granitoids indicates that the arc was thermally active and capable of sustaining magmatic differentiation and a high geothermal gradient.

The data also provides an age constraint on Grenvillian mafic to ultramafic magmatism in the region and complement recent work distinguishing Pinwarian from Grenvillian intrusive rocks (Lafrance and Daoudene, 2024; Daoudene and Lafrance, 2025; Lafrance et al., 2026) among the former *Aguanish complex* that had been extended into the study area (Corriveau and Bonnet, 2005). Overall, the data contribute to the understanding of the geological evolution of the Wakeham Group and its extension toward the La Romaine supracrustal belt within the broader framework of the Grenville Province at ca. 1.52–1.46 Ga Pinwarian orogeny and its continental magmatic arc (Gower and Krogh, 2002; Tollo et al., 2004; Corriveau and Clark, 2005; Indares et al., 2022; Indares, 2024)

The older ages obtained for the Grenvillian regional metamorphism is 1062 ± 11 Ma and 1032 ± 16 Ma in the La Romaine area and 1044 ± 44 Ma in the Musquaro-D'Auteuil lakes area. However, most other zircon metamorphic ages fall in a ca. 1015–1000 Ma range. Crosscutting relationships of intrusive suites and their pervasive deformation fabric or lack thereof indicate that the pervasive moderate to intense Grenvillian deformation fabrics postdate 1.08 Ga and predate 1.04 Ga. Accordingly, the data illustrates that Ottawan metamorphism largely obliterated the earlier Pinwarian metamorphic geochronological record but that it is the static thermal event that followed the earlier Grenvillian tectonothermal event that is the metamorphic event most commonly registered by the currently dated minerals throughout the region (Ottawan Orogeny: 1090–1020 Ma; Rivers et al., 2012). A Rigolet phase is also locally registered by the titanite dated (Rigolet Orogeny: 1005–980 Ma; Rivers et al., 2012).

The nature of the substrate is further clarified through U-Pb dating of zircon xenocrysts and Nd isotopic data from the metaplutonic rocks. The results document a Wakamian basement component and are consistent with older Labradorian crust to the pre-Pinwarian substrate. The Wakamian component is now directly represented by tonalitic rocks dated at ca. 1.58–1.53 Ga, whereas Labradorian crust is inferred mainly from inherited zircon and isotopic data. This Wakamian magmatism therefore begins to fill the apparent gap in magmatic activity between the Labradorian and Pinwarian orogenies. Labradorian rocks have not been recognized at the present crustal level in the study area, although they occur farther north and east near the Labrador border among largely Pinwarian crust (e.g., area of HGP transect in Fig. 1; Wasteneys et al., 1997; Heaman et al., 2004) as well as farther east and northeast in Labrador (Gower and Krogh, 2002; Gower et al., 2008). Zircon xenocrysts reaching ca. 1.8 Ga in several intrusions also suggest the involvement of an older Paleoproterozoic crustal component. Part 1 (Corriveau et al., 2026) explores the possibility that such a basement component may provide further insights into the development of potential metasomatic iron and alkali-calcic (MIAC) systems in the study area.

Legacy Data Availability

The source of the legacy data that served to write this manuscript consists of files of preliminary versions of the manuscript by Otto van Breemen and Louise Corriveau and of preliminary and final versions of Chapter 5 of Bonnet (2009), as well as files of presentations of Anne-Laure Bonnet and Louise Corriveau, files of various geochronological proposals submitted to Dr. Otto van Breemen with descriptions of the rocks sampled and rationale for dating them, as well as spreadsheets of geochronological data and files with the concordia diagrams and interpretations prepared by Otto van Breemen and shared with Louise Corriveau. All these files have been kept by Louise Corriveau. Dr. Otto van Breemen (GSC) acquired the U-Pb geochronological and Nd isotopic data and interpreted some of the best ages and model ages provided herein. During his review of the manuscript, Dr. Bill Davis (GSC) recalculated some of the ages using the data in the spreadsheets in the Supplementary file and the data kept at the GSC geochronology lab.

The original Kodachrome slides of CQA outcrops are stored at the GSC and were taken by Louise Corriveau and Anne-Laure Bonnet and, for some, by the remaining members of the GSC field teams (see list in the acknowledgment). No documentation exists identifying the photographer of individual photographs. The slides were scanned by the MRNF except for some CQA-00 slides, which were scanned by Normand Tassé. Photographs for all other outcrops were taken digitally by the MRNF field teams (see list in the acknowledgment). The photographs were cropped on their sides to remove the sky, hammers, other objects used as scales, excessive lichens and dirt to best focus on the key attributes presented. Some photographs were slightly adjusted—equally for the entire image for contrast, brightness, intensity, and sharpness—to best illustrate the relationships among the various components of the rock types illustrated. Some scans required additional adjustments such as reducing colour saturation to restore the natural colour of the rocks.

Author Contributions, Legacy Contributions and Reviewer Contributions

Conceptualization, formal analysis, investigation, methodology: L.C., A.-L.B., O.V.B. and I.L. Funding acquisition: L.C., OVB, and I.L. Data curation: L.C. and I.L. Project administration: L.C. and I.L. Resources: L.C., O.V.B. and I.L. Validation during review: B.D. Writing – review and editing: L.C., A.-L.B., O.V.B. and I.L. Dr. Otto van Breemen (O.V.B.) is acknowledged below rather than listed as the main author, in accordance with his request that publications using his legacy

data after his retirement from the GSC do so. Dr. Bill Davis (B.D.) is acknowledged below. All authors have read and agreed to the published version of the manuscript.

Acknowledgements

The legacy geochronological and Nd isotopic data presented in this report were acquired through the Eastern Grenville Transect Project (TGI000019) of the Targeted Geoscience Initiative program of the Geological Survey of Canada (GSC), Natural Resources Canada, and through Anne-Laure Bonnet's PhD thesis at the Institut national de la Recherche scientifique. The GSC project took place in partnership with the Ministère des Ressources naturelles et de la Faune (MRNF), Québec and the Geological Survey of Newfoundland and Labrador. Research funding was also provided by the DIVEX research network and the Institut national de la Recherche scientifique – Eau-Terre-Environnement (INRS-ETE).

Dr. Otto van Breemen (GSC) is greatly acknowledge for acquiring the U-Pb geochronological and Nd isotopic data presented herein and co-writing with the first and second author early versions of manuscript. Dr. Bill Davis (GSC) is acknowledged for his thorough verification of the geochronological data and ages presented herein. Nicole Rayner, Julie Peressini, Diane Bellerive, and Carole Lafontaine are thanked for helping Dr. Otto van Breemen generate the analytical data.

Sampling of representative rock types, as well as geological observations and interpretations, was carried out by the first and second authors with field assistance from Guy Scherrer, Jérémie Lehmann, Yan Lavallée, Christian Stein, Ahmed Laamrani, Roxanne Gratton, Alphée Lalo and Philippe Normandeau and contributions from Pierre Pilote (MRNF). We express our thanks to Léopold Nadeau for managing the umbrella project, to Pierre Verpaelst, Pierre Pilote and Serge Perreault for scientific support, to Pierre Brouillette for GIS and database management, to the administrative team of the Québec division of the GSC and to M.R. LaFlèche (INRS-ETE) and A. Tremblay (UQAM), co-directors of A.-L. Bonnet Ph.D. thesis. Normand Tassé is thanked for scanning some CQA-00 photographs.

Recent field, geochronological and geochemical data were acquired by the MRNF mapping teams during projects in the Kegaska, Coacoachou and D'Auteuil areas. In addition to the third author, geological observations were carried out and photographs taken by Yannick Daoudene, Gaëlle St-Louis, Eve Gosselin, Sacha Lafrance, Anne-Laure Bonnet, Julie Vallières and Adina Bogatu. Field assistance was provided by Samantha Legrand, Benjamin Leclerc, Brahim Mali, Vincent Keenan, Thomas Schulz-Ratelle, Isabelle Izquierdo-Bernier, Natasha Sauvé, Rayan Alam, Hernan Mauricio Perez Burgos, Mathilde Vachon, Bettina Bourque, Samuel Adam, Félix Hamel, Lucas L'Espérance, Jérôme Langlois, Rémy Canuel, Simon Cottineau and Naïda Guérette-Lang. Jean David is thanked for his major contribution to the U-Pb geochronology associated with these mapping projects. The third author particularly thanks Yannick Daoudene and Gaëlle St-Louis for their major contributions to geological mapping, interpretation and preparation of the *Bulletin géologique* for these projects.

References

Artemieva, I.A., Thybo, H., Jakobsen, K., Sorensen, N.K., and Nielsen, L.S.K., 2017, Heat production in granitic rocks: Global analysis based on a new data compilations GRANITE2017: Earth-Science Reviews, v. 172, p. 1–26.

Barrie, C.T., and Krogh, T.E., 1996, U-Pb zircon geochronology of the Selbaie Cu-Zn-Ag-Au mine, Abitibi subprovince, Canada: Economic Geology, v. 91, p. 563–575.

Belousova, E.A., Griffin, W.L., O'Reilly, S.Y., and Fisher, N.I., 2002, Igneous zircon: Trace element composition as an indicator of source rock type: Contributions to Mineralogy and Petrology, v. 143, p. 602–622.

Bonnet, A., 2009, Les zones d'altération comme vecteur d'exploration des ceintures volcano-plutoniques felsiques métamorphisées à haut grade: Concepts et exemple du système hydrothermal de la Romaine dans la Province de Grenville: Unpublished PhD thesis, Université du Québec, INRS-Eau-Terre-Environnement, 289 p. https://espace.inrs.ca/id/eprint/472/

Bonnet, A.-L., and Corriveau, L., 2003, Caractérisation structurale et métamorphique de la marge sud-est du Groupe de Wakeham, régions du lac Musquaro et de La Romaine, Province de Grenville (Québec, Canada): Geological Survey of Canada, Current Research Paper 2003-C17, 11 p., https://doi.org/10.4095/222970.

Bonnet, A.-L., and Corriveau, L., 2007a, Alteration vectors to metamorphosed hydrothermal systems in gneiss terranes, *in* Goodfellow, W., ed., Mineral resources of Canada: A synthesis of major deposit-types, district metallogeny, the evolution of geological provinces, and exploration methods: Geological Association of Canada, Special Volume 5, pp. 1035–1050.

Bonnet, A.-L., and Corriveau, L., 2007b, Atlas et outils de reconnaissance de systèmes hydrothermaux métamorphisés dans les terranes gneissiques, *in* Goodfellow, W.D., ed., Mineral deposits of Canada: A synthesis of major deposit-types, district metallogeny, the evolution of geological provinces, and exploration methods: Geological Association of Canada, Mineral Deposits Division, Special Publication 5, DVD, 95 p.

Bonnet, A.-L., and Corriveau, L., 2009, Kegaska-SNRC 12K03, *in* Bonnet, A., ed., Les zones d'altération comme vecteur d'exploration des ceintures volcano-plutoniques felsiques métamorphisées à haut grade: Concepts et exemple du système hydrothermal de la Romaine dans la Province de Grenville: Unpublished PhD thesis, Université du Québec, INRS-Eau-Terre-Environnement, Annex II. https://espace.inrs.ca/id/eprint/472/

Bonnet, A.-L., Corriveau, L., and LaFlèche, M.R., 2005, Chemical imprint of high sulphidation volcanic-hosted hydrothermal alterations in the granulite-facies La Romaine Supracrustal Belt, eastern Grenville Province, Quebec, *in* Corriveau, L. and Clark, T., eds., The Grenville Province: A geological and mineral resources perspective derived from government and academic research initiatives: Canadian Journal of Earth Sciences, v. 42, p. 1783–1814.

Bonnet, A.-L., van Breemen, O., and Corriveau, L., 2009, Age constraints on a metamorphosed volcanic hosted cupriferous hydrothermal system in the La Romaine Supracrustal Belt, Eastern Grenville Province, Québec, *in* Bonnet, A.-L., ed., Les zones d'altération comme vecteur d'exploration des ceintures volcano-plutoniques felsiques métamorphisées à haut grade: Concepts et exemple du système hydrothermal de La Romaine dans la Province de Grenville: Unpublished PhD thesis, Université du Québec, INRS-Eau-Terre-Environnement, Chapter 5, pp. 217-241. https://espace.inrs.ca/id/eprint/472/

Bourne, J.H., Ashton, K., Goulet, N., Helmstead, H., Lalonde A., and Newman, P., 1978, Portions of the Natashquan, Musquaro and Harrington Harbour map-sheets, Eastern Grenville Province, Quebec - A preliminary report: Geological Survey of Canada, Current Research Paper 78-1A, p. 413–418.

Brisebois, D., and Clark, T., 2003, Géologie et ressources minérales de la partie est de la Province de Grenville: Ministère des Ressources naturelles et des Forêts, DV 2002-03, 421 p.

Cherniak, D.J., 1993, Lead diffusion in titanite and preliminary results on the effects of radiation damage on Pb transport: Chemical Geology, v. 110, p. 177–194.

Cherniak, D.J., Watson, E.B., Grove, M., and Harrison, T.M., 2004, Pb diffusion in monazite: A combined RBS/SIMS study: Geochimica et Cosmochimica Acta, v. 68, p. 829–840.

Chevé, S., Gobeil, A., Clark, T., Corriveau, L., Perreault, S., Dion, D.J., and Daigneault, R., 1999, Géologie de la région du lac Manitou (SNRC 221/14): Ministère des Ressources naturelles, Québec, RG 99-02.

Chevé, S., Gobeil, A., Clark, T., and Togola, N., 2001, Géologie de la rivière Baune (22P/02) et des lacs à l'Aigle (22P/03) et Canatiche (22P/04): Ministère des Ressources naturelles, Québec; RG 2001-03, 60 p.

Claoué-Long, J.C., King, R.W., and Kerrich, R., 1990, Archean hydrothermal zircon in the Abitibi greenstone belt: Constraints on the timing of gold mineralisation: Earth Planet Science Letters, v. 89, p. 109–128.

Clark, T., and Machado, N., 1995, New V-Pb dates from the Wakeham Terrane and its basement: Preliminary results, *in* Lithoprobe, Abitibi-Grenville project, results from a combined meeting on the Grenville province with the ECSOOT transect, Report 49, p. 29–35.

Corfu, F., Hanchar, J.M., Hoskin, P.W.O., and Kinny, P., 2003, Atlas of zircon textures, *in* Hanchar, J.M. and Hoskin, P.W.O., eds., Zircon: Reviews in Mineralogy and Geochemistry, v. 53, pp. 468–500.

Corriveau, L., 2013, Architecture de la ceinture métasédimentaire centrale au Québec, Province de Grenville: Un exemple de l'analyse de terrains de métamorphisme élevé: Geological Survey of Canada, Bulletin 586, 264 p., doi:10.4095/226449.

Corriveau, L., and Bonnet, A.L., 2001, Volcanisme pyroclastique protérozoïque dans le groupe de Wakeham, région des lacs Musquaro et D'Auteuil: Geological Survey of Canada, Current Research Paper 01D-18, 11 p. doi.org/10.4095/212172.

Corriveau, L., and Bonnet A., 2005, Pinwarian (1.50 Ga) volcanism and hydrothermal activity at the eastern margin of the Wakeham Group, Grenville Province, Quebec, *in* Corriveau, L. and Clark, T., eds., The Grenville Province: A geological and mineral resources perspective derived from government and academic research initiatives: Canadian Journal of Earth Sciences, v. 42, p. 1749–1782.

Corriveau, L., and Bonnet, A.-L. 2009a. Baie des Loups - SNRC 12K01, *in* Bonnet, A., ed., Les zones d'altération comme vecteur d'exploration des ceintures volcano-plutoniques felsiques métamorphisées à haut grade: Concepts et exemple du système hydrothermal de la Romaine dans la Province de Grenville: Unpublished PhD thesis, Université du Québec, INRS-Eau-Terre-Environnement, Annex II.

Corriveau, L., and Bonnet, A.-L., 2009b. La Romaine - SNRC 12K02, *in* Bonnet, A., ed., Les zones d'altération comme vecteur d'exploration des ceintures volcano-plutoniques felsiques métamorphisées à haut grade: Concepts et exemple du système hydrothermal de la Romaine dans la Province de Grenville: Unpublished PhD thesis, Université du Québec, INRS-Eau-Terre-Environnement, Annex II.

Corriveau, L., and Bonnet, A.-L. 2009c. Musquaro - SNRC 12Kl1, *in* Bonnet, A., ed., Les zones d'altération comme vecteur d'exploration des ceintures volcano-plutoniques felsiques

métamorphisées à haut grade: Concepts et exemple du système hydrothermal de la Romaine dans la Province de Grenville: Unpublished PhD thesis, Université du Québec, INRS-Eau-Terre-Environnement, Annex II.

Corriveau, L., and Clark, T., 2005, The Grenville Province: A geological and mineral resources perspective derived from government and academic research initiatives, *in* Corriveau, L. and Clark, T., eds., The Grenville Province: A geological and mineral resources perspective derived from government and academic research initiatives: Canadian Journal of Earth Sciences, v. 42, p. 1637–1642.

Corriveau, L., and Montreuil, J.-F., 2025, Metasomatic mineral systems with IOA, IOCG and affiliated critical and precious metal deposits: A review from a field geology perspective: Minerals, v. 15, 365. https://doi.org/10.3390/min15040365.

Corriveau, L., and Spry, P., 2014, Metamorphosed hydrothermal ore deposits, *in* Holland, H.D. and Turekian, K.K., eds., Treatise on geochemistry, second edition: Elsevier, v. 13, pp. 175–194.

Corriveau, L., and van Breemen, O., 2000, Docking of the Central Metasedimentary Belt to Laurentia in geon 12: Evidence from the 1.17-1.16 Ga Chevreuil intrusive suite and host gneisses, Québec: Canadian Journal of Earth Sciences, v. 37, p. 253–269.

Corriveau, L., Brouillette, P., Scherrer, G., and Bonnet, A.L., 2002, Extension orientale des roches volcaniques du Groupe de Wakeham et l'intrusion litée troctolitique de Musquaro, Province de Grenville, Basse-Côte-Nord, Québec: Geological Survey of Canada, Current Research Paper 02-C29, 11 p., doi.org/10.4095/213207.

Corriveau, L., Bonnet, A.-L., van Breemen, O., and Pilote, P., 2003, Tracking the Wakeham Group volcanics and associated Cu-Fe-oxydes hydrothermal activity from La Romaine eastward, Eastern Grenville Province, Québec: Geological Survey of Canada, Current Research Paper 2003-C12, 11 p., doi.org/10.4095/214194.

Corriveau, L., Bonnet, A.-L., Lafrance, I., Blein, O., and Soltanmohammadi, A., 2026. Volcanic-hosted mineral systems and Pinwarian–Grenvillian magmatism in the western Pinware terrane, Grenville Province, Québec: Part 1, geological and geochemical footprints: Ministère des Ressources naturelles et des Forêts (MRNF), MB 2026-16.

Daoudene, Y., and Lafrance, I., 2025, Géologie de la région du lac Coacoachou, Province de Grenville, région de la Côte-Nord, Québec, Canada: Ministère des Ressources naturelles et des Forêts (MRNF), BG 2024-06, 14 p., 1 map.

David, J., Bogatu, A., and Talla Takam, F., 2026a**,** Datations U-Pb dans la province de Grenville effectuées au GEOTOP en 2023-2024: Ministère des Ressources naturelles et des Forêts (MRNF), MB 2026-09, 38 p.

David, J., Bogatu, A., and Talla Takam, F., 2026b, Datations U-Pb dans la province de Grenville effectuées au GEOTOP en 2024-2025: Ministère des Ressources naturelles et des Forêts (MRNF), MB 2026-10, 22 p.

Davis, W., Corriveau, L., van Breemen, O., Bleeker, W., Montreuil, J.-F., Potter, E., and Pelleter, E., 2011, Timing of IOCG mineralizing and alteration events within the Great Bear Magmatic zone, *in* Fischer, B.J. and Watson, D.M. (compilers), 39th Annual Yellowknife Geoscience Forum Abstracts: Northwest Territories Geoscience Office, Yellowknife, NT, YKGSF Abstracts Volume 2011, p. 97.

DePaolo, D.J., 1981, Neodymium isotopes in the Colorado Front Range and crust-mantle evolution in the Proterozoic: Nature, v. 291, p. 193–196.

Dickin, A.P., 2000, Crustal formation in the Grenville Province: Nd isotope evidence: Canadian Journal of Earth Sciences, v. 37, p. 165–181.

Dickin, A.P., 2004, Mesoproterozoic and Paleoproterozoic crustal growth in the eastern Grenville Province: Nd isotope evidence from the Long Range inlier of the Appalachian orogen, *in* Tollo, R.P., Corriveau, L., McLelland, J., and Bartholomew, M.J., eds., Proterozoic tectonic evolution of the Grenville Orogen in North America: The Geological Society of America, Memoir 197, pp. 495–503.

Dickin, A.P., 2005, Radiogenic isotope geology: Cambridge University Press, 492 p.

Dickin, A.P., and Higgins, M.H., 1992, Sm/Nd evidence for a major 1.5 Ga crust-forming event in the central Grenville Province: Geology, v. 20, p. 137–140.

Emslie, R.F., and Hunt, P.A., 1990, Ages and petrogenetic significance of igneous-charnockite suites associated with massif anorthosites, Grenville Province: Journal of Geology, v. 98, p. 213–231.

Forshaw, J.B., and Pattison, D.R.M., 2023, Major-element geochemistry of pelites: Geology, v. 51, p. 39–43, https://doi.org/10.1130/G50542.1

Fowler, A.D., and Doig, R., 1983, The significance of europium anomalies in the REE spectra of granites and pegmatites, Mont Laurier, Quebec: Geochimica et Cosmochimica Acta, v. 47, p. 1131–1137.

Giles, D., and Nutman, A.P., 2003, SHRIMP U/Pb zircon dating of the host rocks of the Cannington Ag-Pb-Zn deposit, southeastern Mt Isa, Australia: Australian Journal of Earth Sciences, v. 50, p. 295–309.

Gobeil, A., Chevé, C., Clark, T., Corriveau, L., Perreault, S., Dion, D.-J., and Nabil, H., 1999, Géologie de la région du lac Nipisso (22I13): Ministère des Ressources naturelles, de la Faune et des Parcs, Québec, RG98-19, 60 p.

Gobeil, A., Brisebois, D., Clark, T., Verpaelst, P., Wodicka, N., and Chevé, S., 2003, Géologie de la Moyenne Côte-Nord, *in* Brisebois, D. and Clark, T., eds., Synthèse géologique et métallogénique de la partie est de la Province de Grenville: Ministère des Ressources naturelles, de la Faune et des Parcs, Québec, DV 2002-03, pp. 59–118.

Goldstein, S.L., O'Nions, R.K., and Hamilton, P.J., 1984, A Sm-Nd isotopic study of atmospheric dusts and particulates from major river systems: Earth and Planetary Science Letters, v. 70, 221–236.

Gower, C.F., and Krogh, T.E., 2002, A U-Pb geochronological review of the Proterozoic history of the eastern Grenville Province: Canadian Journal of Earth Sciences, v. 39, p. 795–829.

Gower, C.F., Kamo, S., Kwok, K., and Krogh, T.E., 2008, Proterozoic southward accretion and Grenvillian orogenesis in the interior Grenville Province in eastern Labrador: Evidence from U–Pb geochronological investigations: Precambrian Research, v. 165, p. 61–95.

Gromet, L.P., Dymek, R.F., Haskin, L.A., and Korotev, R.L., 1984, The North American shale composite: Its compilation, major and trace element characteristics: Geochimica et Cosmochimica Acta, v. 48, p. 2469–2482.

Hartmann, L.A., Leite, J.A.D., Da Silva, L.C., Remus, M.V.D., McNaughton, N.J., Groves, D.I., Fletcher, I.R., Santos, J.O.S., and Vasconcellos, M.A.Z., 2000, Advances in SHRIMP geochronology and their impact on understanding the tectonic and metallogenic evolution of southern Brazil: Australian Journal of Earth Sciences, v. 47, p. 829–844.

Heaman, L.M., Gower, C.F., and Perreault, S., 2004, The timing of Proterozoic magmatism in the Pinware terrane of southeast Labrador, easternmost Quebec and northwest Newfoundland: Canadian Journal of Earth Sciences, v. 41, p. 127–150.

Hoskin, P.W.O., 2005, Trace-element composition of hydrothermal zircon and the alteration of Hadean zircon from the Jack Hills, Australia: Geochimica et Cosmochimica Acta, v. 69, p. 637–648.

Hoskin, P.W.O., and Schaltegger, V., 2003, The composition of zircon and igneous and metamorphic petrogenesis, *in* Hanchar, J.M. and Hoskin, P.W.O., eds., Zircon: Reviews in Mineralogy and Geochemistry, v. 53, pp. 27–62.

Indares, A., 2024, The Grenville Province: Revisiting the orogenic framework and integrating recent findings: Canadian Journal of Earth Sciences, v. 62, p. 99–118. dx.doi.org/10.1139/cjes-2023-0143.

Indares, A., and Martignole, J., 1993, Étude régionale du Supergroupe de Wakeham, Moyenne Côte-Nord: Ministère de l'Énergie et des Ressources, Québec, MB 91-21.

Indares, A., Moukhsil, A., and Groulier, P.-A., 2022, Geon 14 to early Geon 13 granitoid magmatism in the Grenville Province of Canada, northeastern Laurentia: Distribution, geochemical patterns, and links with an active-margin setting, *in* Whitmeyer, S.J., Williams, M.L., Kellett, D.A., and Tikoff, B., eds., Laurentia: Turning points in the evolution of a continent: Geological Society of America, Memoir 220, doi:10.1130/2022.1220(17).

Kerrich, R., and King, R., 1993, Hydrothermal zircon and baddeleyite in Val-d'Or Archean mesothermal gold deposits: Characteristics, compositions, and fluid-inclusion properties, with implications for timing of primary gold mineralization: Canadian Journal of Earth Sciences, v. 30, p. 2334–2351.

Krogh, T.E., 1973, A low-contamination method for hydrothermal decomposition of zircon and extraction of U and Pb for isotopic age determinations: Geochimica et Cosmochimica Acta, v. 37, p. 485–494.

Krogh, T.E., 1982, Improved accuracy of U–Pb ages by the creation of more concordant systems using an air abrasion technique: Geochimica et Cosmochimica Acta, v. 46, p. 637–649.

Lafrance, I., and Daoudene, Y., 2024, Géologie de la région de Kegaska, Côte-Nord-du-Golfe-du-Saint-Laurent, Province de Grenville, Québec, Canada: Ministère des Ressources naturelles et des Forêts (MRNF), BG 2023-12, 1 map.

Lafrance, I., and Godet, A., 2024, Géologie simplifiée du Sud-Est de la Province de Churchill, Nunavik, Québec, Canada: Ministère des Ressources naturelles et des Forêts (MRNF), BG 2024-01, 1 map.

Lafrance, I., Daoudene, Y., and St-Louis, G., 2026, Géologie de la région du lac D'Auteuil, Province de Grenville, région de la Côte-Nord, Québec, Canada: Ministère des Ressources naturelles et des Forêts (MRNF), BG 2025-03, 1 map.

Lawrie, K.C., Mernagh, T.P., Ryan, C.G., van Achterbergh, E., and Black, L.P., 2007, Chemical fingerprinting of hydrothermal zircons: An example from the Gidginbung high sulphidation Au-Ag-(Cu) deposit, New South Wales, Australia: Proceedings of the Geologists' Association, v. 118, p. 37–46.

Loveridge, W.D., 1986, U-Pb ages on zircon from rocks of the Lac de Morhiban map area, Quebec: Geological Survey of Canada, Paper 86-1A, p. 523–530.

Ludwig, K.R., 2000, Isoplot/Ex, version 2.2, A geochronological toolkit for Microsoft Excel: Berkely Geochronology Center, Special Publication No. 1a, 53 p.

Madore, L., Verpaelst, P., Dion, D.-J., Choinière, J., Hocq, M., Marquis, R., Lefebvre, D., and David, J., 1997a, Géologie de la région du lac Briend (12N/05): Ministère des Ressources naturelles, Québec, RG 96-05, 30 p.

Madore, L., Verpaelst, P., Brisebois, D., Choinière, J., Dion, D.-J., and David, J., 1997b, Géologie de la région du lac Cormier (12N/04): Ministère des Ressources naturelles, Québec, RG 97-08, 32 p.

Martignole, J., Indares A., and Desjardins, D., 1992, Géologie de la région des lacs Arthur et Ruffin, Moyenne-Côte-Nord: Ministère de l'Énergie et des Ressources, Québec, MB 91-20, 74 p.

Martignole, J., Machado, N., and Indares, A., 1994, The Wakeham Terrane: A Mesoproterozoic terrestrial rift in the eastern part of the Grenville Province: Precambrian Research, v. 68, p. 291–306.

Martin, C., and Dickin, A.P., 2005, Styles of Proterozoic crustal growth on the southeast margin of Laurentia: Evidence from the central Grenville Province northwest of lac St.-Jean, Quebec: Canadian Journal of Earth Sciences, v. 42, p. 1643–1652.

McFarlane, C.R.M., Mavrogenes, J.A., and Tomkins, A.G., 2007, Recognizing hydrothermal alteration through a granulite facies metamorphic overprint at the Challenger Au deposit, South Australia: Chemical Geology, v. 243, p. 64–89.

Ministère des Ressources naturelles et des Forêts (MRNF a), Groupe de Wakeham: Ministère des Ressources naturelles et des Forêts, Lexique stratigraphique du Québec, https://gq.mines.gouv.qc.ca/lexique-stratigraphique/province-de-grenville/groupe-de-wakeham [accessed 23-02-2026].

Ministère des Ressources naturelles et des Forêts (MRNF b), Quebec stratigraphic lexicon: Ministère des Ressources naturelles et des Forêts, Lexique stratigraphique du Québec, https://gq.mines.gouv.qc.ca/lexique-stratigraphique/lexique-stratigraphique_en/ [accessed 16-03-2026].

Ministère des Ressources naturelles et des Forêts (MRNF c), Suite intrusive de Mantuh: Ministère des Ressources naturelles et des Forêts, Lexique stratigraphique du Québec, https://gq.mines.gouv.qc.ca/lexique-stratigraphique/province-de-grenville/suite-intrusive-de-mantuh [accessed 23-02-2026].

Ministère des Ressources naturelles et des Forêts (MRNF d), Intrusion gabbroïque de Musquaro: Ministère des Ressources naturelles et des Forêts, Lexique stratigraphique du Québec, https://gq.mines.gouv.qc.ca/lexique-stratigraphique/province-de-grenville/intrusion-gabbroique-de-musquaro [accessed 11-03-2026].

Ministère des Ressources naturelles et des Forêts (MRNF e), Suite plutonique de La Galissonnière: Ministère des Ressources naturelles et des Forêts, Lexique stratigraphique du Québec, https://gq.mines.gouv.qc.ca/lexique-stratigraphique/province-de-grenville/suite-plutonique-de-la-galissonniere [accessed 23-02-2026].

Morisset, C.-E., Scoates, J.S., Weis, D., and Friedman, R.M., 2009, U–Pb and 40Ar/39Ar geochronology of the Saint-Urbain and Lac Allard (Havre-Saint-Pierre) anorthosites and their associated Fe–Ti oxide ores, Québec: Evidence for emplacement and slow cooling during the collisional Ottawan Orogeny in the Grenville Province: Precambrian Research, v. 174, p. 95–116, doi:10.1016/j.precamres.2009.06.009.

Nabil, H., Barnes, S.-J., and Clark, T., 2003, Distribution du nickel, du cuivre et des éléments du groupe de platine dans les sulfures de l'indice du lac Volant, région de Sept-îles, Québec, *in* Brisebois, D. and Clark, T., eds., Synthèse géologique et métallogénique de la partie est de la Province de Grenville: Ministère des Ressources naturelles, de la Faune et des Parcs, Québec, DV 2002-03, pp. 327–350.

Nägler, T.F., and Kramers, J.D., 1998, Nd isotopic evolution of the upper mantle during the Precambrian: Models, data and the uncertainty of both: Precambrian Research, v. 91, p. 233–252.

Nutman, A.P., and Ehlers, K., 1998, Evidence for multiple Palaeoproterozoic thermal events and magmatism adjacent to the Broken Hill Pb-Zn-Ag orebody, Australia: Precambrian Research, v. 90, p. 203–238.

Parrish, R.R., Roddick, J.C., Loveridge, W.D., and Sullivan, R.W., 1987, Uranium-lead analytical techniques at the Geochronology Laboratory, Geological Survey of Canada: Geological Survey of Canada, Paper 87-2, p. 3–7.

Pelleter, E., Cheilletz, A., Gasquet, D., Mouttaqi, A., Annich, M., El Hakour, A., Deloule, E., and Féraud, G., 2007, Hydrothermal zircons: A tool for ion microprobe U–Pb dating of gold mineralization (Tamlalt–Menhouhou gold deposit, Morocco): Chemical Geology, v. 245, p. 135–161.

Poldervaart, A., 1956, Zircon in rocks: Igneous rocks: American Journal of Science, v. 254, p. 521–554.

Regelous, A., Scharfenberg, L., and De Wall, H., 2021, Origin of S-, A- and I-type granites: Petrogenetic evidence from whole rock Th/U ratio variations: Minerals, v. 11, 672. https://doi.org/10.3390/min11070672

Rivers, T., Culshaw, N., Hynes, A., Indares, A., Jamieson, R., and Martignole, J., 2012, The Grenville Orogen, a post-LITHOPROBE perspective. Chapter 3, *in* Percival, J.A., Cook F.A., and Clowes, R.M., eds., Tectonic styles in Canada: The LITHOPROBE perspective: Geological Association of Canada, Special Paper 49, pp. 97–236.

Robillard, M., 2003, Rapport des travaux 2002, projet rivière Musquaro, Ressources Appalaches inc.: Ministère de l'Énergie et des Ressources naturelles, Québec, GM 61233, 71 p., 3 maps.

Rochín-Bañaga, H., and Davis, D.W., in press, U-Pb LA-ICPMS geochronology of samples collected in 2025 from Québec, Canada. University of Toronto: Ministère des Ressources naturelles et des Forêts (MRNF).

Roddick, J.C., 1987, Generalized numerical error analysis with application to geochronology and thermodynamics: Geochemica et Cosmochemica Acta, v. 51, p. 2129–2135.

Rubatto, D., 2002, Zircon trace element geochemistry: Partitioning with garnet and the link between U-Pb ages and metamorphism: Chemical Geology, v. 184, p. 123–138.

Rubin, J.N., Henry, C.D., and Price, J.G., 1989, Hydrothermal zircons and zircon overgrowths, Sierra Blanca Peaks, Texas: American Mineralogist, v. 74, p. 865–869.

Rubin, J.N., Henry, C.D., and Price, J.G., 1993, The mobility of zirconium and other 'immobile' elements during hydrothermal alteration: Chemical Geology, v. 110, p. 29–47.

Saint-Germain, P., and Corriveau, L., 2003, Évolution magmatique et géochimique du Complexe de gabbronorite et de monzonite de Matamec, *in* Brisebois, D. and Clark, T., eds., Synthèse géologique et métallogénique de la partie est de la Province de Grenville: Ministère des Ressources naturelles, de la Faune et des Parcs, Québec, DV 2002-03, pp. 179–213.

Sawyer, E.W., 1999, Criteria for the recognition of partial melting: Physics and Chemistry of the Earth, v. 24, p. 269–279.

Schärer, U., 1984, The effect of initial ^{230}Th disequilibrium on young U-Pb ages: The Makalu case, Himalaya: Earth and Planetary Science Letters, v. 67, p. 191–204.

Scherrer, G., 2003, Géochimie et pétrogenèse des roches métagabbroïques du domaine de Natashquan, secteur oriental de la Province de Grenville, Québec: Unpublished MSc thesis, Université du Québec, INRS -Eau-Terre-Environnement, 150 p.
https://espace.inrs.ca/id/eprint/373/1/T000325.pdf

Stern, R.A., 1997, The SC sensitive high resolution ion microprobe (SHRIMP): Analytical techniques of zircon U-Th-Pb age determinations and performance evaluation: Geological Survey of Canada, Paper 1997-F, p. 1–31.

Stern, R.A., and Amelin, Y., 2003, Assessment of errors in SIMS zircon U-Pb geochronology using a natural zircon standard and NIST SRM glass: Chemical Geology, v. 197, p. 111–146.

Tollo, R.P., Corriveau, L., McLelland, J., and Bartholomew, M.J., 2004, Proterozoic tectonic evolution of the Grenville orogen in North America: An introduction, *in* Tollo, R.P., Corriveau, L., McLelland, J., and Bartholomew, M., eds., Proterozoic tectonic evolution of the Grenville Orogen in North America: Geological Society of America Memoir, no 197, pp. 1–18.

Tomaschek, F., Kennedy, A.K., Villa, I.M., Lagos, M., and Ballhaus, C., 2003, Zircon from Syros, Cyclades, Greece – recrystallization and mobilization of zircon during high-pressure metamorphism: Journal of Petrology, v. 44, p. 1977–2002.

van Breemen, O., and Corriveau, L., 2005, U-Pb age constraints on arenaceous and volcanic rocks of the Wakeham Group, eastern Grenville Province: Canadian Journal of Earth Sciences, v. 42, p. 1677–1697.

van Breemen, O., and Higgins, M.D., 1993, U- Pb zircon age of the southwest lobe of the Havre-Saint-Pierre Anorthosite Complex, Grenville Province, Canada: Canadian Journal of Earth Sciences, v. 30, p. 1453–1457.

van Breemen, O., Davidson, A., Loveridge, W.D., and Sullivan, R.W., 1986, U-Pb zircon geochronology of Grenville tectonites, granulites and igneous precursors, Parry Sound,

Ontario, *in* Moore, J.M., Davidson, A. and Baer, A.J., eds., The Grenville Province: Geological Association of Canada, Special Paper 31, pp. 191–207.

Vavra, G., Schmid, R., and Gebauer, D., 1999, Internal morphology, habit and U-Th-Pb microanalysis of amphibolite-to-granulite facies zircons: Geochronology of the Ivrea Zone (southern Alps): Contributions to Mineralogy and Petrology, v. 134, p. 380–404.

Verpaelst, P., Madore, L., Brisebois, D., Choinière, J., Dion, D.J., and David, J., 1997a, Géologie de la région du lac Bohier (12N/03): Ministère des Ressources naturelles, Québec, RG 97 -07.

Verpaelst, P., Madore, L., Brisebois, D., Choinière, J., Dion, D.J., and David, J., 1997b, Géologie de la région du lac Le Doré (12N/06): Ministère des Ressources naturelles, Québec, RG 97-02.

Wasteneys, H., Kamo, S., Moser, D., Krogh, T.E., Gower, C.F., and Owen, J.V., 1997, U–Pb geochronological constraints on the geological evolution of the Pinware terrane and adjacent areas, Grenville Province, southeast Labrador, Canada: Precambrian Research, v. 81, p. 101–128.

Williams, I.S., 1998, U-Th-Pb geochronology by ion microprobe, *in* McKibben, M.A., Shanks, W.C., and Ridley, W.I., eds., Applications of microanalytical techniques to understanding mineralizing processes: Reviews in Economic Geology, v. 7, p. 1–35.

Williams, I.S., and Claesson, S., 1987, Isotopic evidence for the Precambrian provenance and Caledonian metamorphism of high grade paragneisses from the Seve Nappes, Scandinavian Caledonides. II. Ion microprobe zircon U–Th–Pb: Contributions to Mineralogy and Petrology, v. 97, p. 205–217.

Williams, I.S., Buick, I.S., and Cartwright, I., 1996, An extended episode of early Mesoproterozoic fluid flow in the Reynolds Ranges, central Australia: Journal of Metamorphic Geology, v. 14, p. 29–47.

Wodicka, N., David, J., Parent, M., Gobeil, A., and Verpaelst, P., 2003, Géochronologie U–Pb et Pb–Pb de la région de Sept-Îles - Natashquan, Province de Grenville, Moyenne-Côte-Nord, *in* Brisebois, D. and Clark, T., eds., Synthèse géologique et métallogénique de la partie est de la Province de Grenville: Ministère des Ressources naturelles, de la Faune et des Parcs, Québec, DV 2002-03, pp. 59–118.

Yeats, C.J., McNaughton, N.J., and Groves, D.I., 1996, SHRIMP U/Pb geochronological constraints on Archean volcanic-hosted massive sulfide and lode gold mineralization at Mount Gibson, Yilgarn Craton, western Australia: Economic Geology, v. 91, p. 1354–1371.

York, D., 1969, Least squares fitting of a straight line with correlated errors: Earth and Planetary Science Letters, v. 5, p. 320–324.

Appendix 1.

Description of lithological units mapped along the shores of the Gulf of St. Lawrence (NTS 12K01, 12K02 and 12K03), at Musquaro and D'Auteuil lakes (NTS 12K10 and 12K11) and Washicoutai and Couillard lakes (NTS 12K07) between 2000 and 2003. These units expanded lithodemic units defined prior to 2003 (e.g. Bourne et al., 1978; Gobeil et al., 2003). Several of these lithodemic units were subsequently modified by the MRNF.

Quaternary (12K01, 12K02, 12K03, 12K06, 12K07, 12K10, 12K11)	
Q	Quaternary sand, gravel, silt and till.
Wapitagun intrusion (12K01)	

mPwap **Syenite and porphyritic quartz monzonite**: pink patina, coarse to very coarse grained; homogeneous; with squared, multi-centimetre phenocrysts of K-feldspar; massive or with magmatic to tectonic foliation; with biotite (<10%) and magnetite (<2%). Local presence of mPcsr enclaves and septa.

Musquaro ultramafic to mafic, sub-vertically layered intrusion (12K03)

mPmqo4 **Dioritic intrusive breccia**: dioritic matrix with a grey patina, medium-grained, massive to foliated; contains rounded to angular mafic enclaves of medium- or fine-grained diorite, amphibolite, gabbro, and locally granite. Eastern border: highly deformed and takes on the appearance of a banded gneiss with fold interference patterns (dome, basin, and crescent morphology).

mPmqo3 **Gabbronorite**: brown to grey patina, medium-grained, mesocratic to leucocratic; sub-ophitic or granular texture; magmatic foliation and local sub-vertical layering; with plagioclase, orthopyroxene, hornblende, biotite, magnetite; locally mineralized in Cu and Ni; mafic enclaves.

mPmqo2 **Troctolite**: grey patina, medium-to-coarse grained, mesocratic to leucocratic; sub-ophitic or granular texture; magmatic foliation and local subvertical layering; with plagioclase, olivine, clinopyroxene, orthopyroxene, amphibole, and biotite; coronitic texture with locally an igneous olivine core preserved and a rim of pyroxene, amphibole, and biotite.

mPmqo1 **Peridotite**: green to black patina, fine-to-medium grained; granular; massive; homogeneous; with olivine, clinopyroxene, and spinel; crisscrossed by serpentine veins.

Lillian mafic suite (12K10, 12K11, 12K14)

mPlil1a **Metagabbro**: dark green patina; medium to fine grained; massive to foliated; with amphibole, plagioclase, locally magnetite or clinopyroxene and garnet; porphyroblastic; relics of igneous texture. Locally intercalated with diabase layers.

mPlil1b **Amphibolite**: black to dark green patina; fine grained; foliated; with amphibole, plagioclase, biotite and quartz.

Robe Noire mafic suite (12K11)

mPrbn **Metagabbro**: dark green patina, medium to fine grained; massive to foliated; with amphibole, plagioclase, locally magnetite or clinopyroxene and garnet; porphyroblastic; relics of a sub-ophitic igneous texture.

Aguanish complex **as mapped in the NTS map sheets 12K01, 12K02, 12K03, 12K06, 12K07, 12K10, and 12K11**

mPagn8 **Amphibolite**. Occurs in NTS sheets 12K01, 12K02, and 12K03.

mPagn7 **Composite granitic unit**: pale pink to salmon-pink or grey patina, fine- to medium-grained, locally coarse-grained; granular; leucocratic; massive (isotropic) to foliated; heterogeneous; biotite (<5%) and magnetite (<3%), locally hornblende (~5%). Includes a mottled granite with white quartz, tectonically laminated granite or syenite, and/or granitic gneiss with disseminated biotite. Locally contains enclaves of anorthosite, grey gneiss, diorite, and amphibolite, as well as Grenvillian sills and dykes of hypidiomorphic salmon-pink K-feldspar granite. Clearly cuts locally the mPcsr and mPagn5a2 units. May include pegmatite. Occurs in NTS sheets 12K01, 12K02, and 12K11.

mPagn6 **Orthopyroxene-bearing granitic to syenitic gneiss**: white to brown patina with a pitted appearance, medium-grained, granoblastic; weakly foliated; homogeneous; leucocratic; with hornblende or biotite (~4%) and orthopyroxene (~2%). Occurs in NTS sheets 12K01 and 12K02.

mPagn5d **Composite unit of grey orthogneiss**: grey patina, fine-grained and granoblastic; foliated; with disseminated biotite and magnetite. Alternates with: granite (mPagn5c), pink granitic gneiss, biotite-magnetite granitic gneiss (mPagn5a2), and tonalitic to dioritic gneiss (mPagn4), giving it a decimetre- to metre-scale layered appearance. Occurs in NTS sheet 12K03.

mPagn5c **Granite with disseminated biotite**: pink patina, fine- to medium-grained and granular; leucocratic and homogeneous; foliated to locally massive (isotropic); with biotite (<5%) and magnetite (1-3%). Local presence of mm phenocrysts of K- feldspar. Occurs in NTS sheets 12K02, 12K03, and 12K07.

mPagn5b2 **Hornblende-biotite granitic gneiss**: medium grey patina, medium-grained; foliated with augen texture to gneissic layered structure; with hornblende (<10%) and biotite (<5%); gneissic equivalent of mPagn5b1. Occurs in NTS sheet 12K11.

mPagn5b1 **Hornblende-biotite porphyritic granite (1.5 Ga)**: pale grey patina, medium-grained; massive (isotropic) to foliated; with hornblende (<10%) and biotite (<5%). Local occurrence of monzodiorite, monzonite, and syenite, zones and dikes with a magma mingling texture, mafic schlieren, and lenticular to angular mafic enclaves. (e.g., mPmqo2a). Occurs in NTS sheet 12K11.

mPagn5a2 **Lenticular biotite-magnetite granitic gneiss**: beige to pinkish patina, medium-grained, granoblastic; foliated with a characteristic augen to lenticular and gneissic texture; biotite (~5%), magnetite (~1%); gneissic equivalent of mPagn5a1. Local occurrence of: monzodioritic phases, mafic schlieren, rounded or angular

microdiorite or amphibolite enclaves, amphibolite boudins, and mPagn7 sill. (e.g., mPmqo1b). Occurs in NTS sheets 12K01, 12K02, 12K03, and 12K07.

mPagn5a1 **Biotite-magnetite porphyritic granite and syenite**: pink patina, medium- to coarse-grained; homogeneous; porphyritic texture with locally deformed K-feldspar phenocrysts; massive (isotropic) to foliated (magmatic or tectonic foliation); with biotite (<5%) and magnetite (1%). Occurs in NTS sheets 12K03 and 12K11.

mPagn4 **Tonalitic to dioritic gneiss**: beige to medium grey patina; medium- to fine-grained; layered; with biotite, hornblende, K-feldspar, locally magnetite and clinopyroxene. Local occurrence of a lesser deformed porphyritic facies, a deformed marginal facies with complex fold interference patterns (dome, basin, and crescent morphology), intrusive breccias, or mPagn7 sills. Occurs in NTS sheets 12K01, 12K02, and 12K03.

mPagn3 **Amphibolite, mafic gneiss, anorthosite**: Amphibolite and mafic gneiss. Anorthosite with a grey patina, medium-grained; massive to foliated or layered; with plagioclase, quartz, and biotite. Occurs in NTS sheets 12K01 (amphibolite and mafic gneiss), 12K02 (amphibolite, mafic gneiss, and anorthosite), 12K03 (amphibolite and mafic gneiss), and 12K07 (amphibolite and mafic gneiss).

mPagn2 **Quartzofeldspathic and siliceous gneiss**: medium grey patina, fine-grained and granoblastic; homogeneous or with weak compositional layering; with biotite and magnetite. Origin of the protolith uncertain but likely sedimentary. Occurs in NTS sheets 12K03 and 12K07.

mPagn1 **Aluminous gneiss with biotite, garnet, sillimanite ± cordierite**: grey patina, medium-grained and granoblastic; foliated; with quartz, feldspar, biotite, garnet, sillimanite (~15%); amoeboid or stromatitic leucosomes locally with garnet and cordierite. Origin of the protolith uncertain (metasedimentary, regolith, hydrothermal?) but likely sedimentary, although the local presence of garnetite points toward a hydrothermal component. Occurs in NTS sheet 12K07.

La Romaine supracrustal belt (mPcsr; NTS 12K01, 12K02, 12K03)

mPcsr4b **Aluminous garnet-sillimanite ± cordierite gneiss with a hydrothermally altered volcanic protolith**: grey to brown patina; medium-grained, granoblastic; heterogeneous; foliated; with quartz, K-feldspar, biotite, garnet, sillimanite (mode ≤30%), locally plagioclase and kyanite (1%); amoeboid or stromatitic leucosomes with garnet-cordierite; local presence of lapilli textures and locally associated with garnetite and atypical quartzitic gneisses, including one with ghost alteration fronts and vein-shaped replacement zones with a vuggy silica texture. Hydrothermal origin from a pyroclastic protolith demonstrable in the field and by lithogeochemical analysis (see Bonnet et al., 2005). Occurs in NTS sheet 12K02.

mPcsr4a **Aluminous, garnet-sillimanite ± cordierite-bearing gneisses with mixed protoliths (sedimentary or hydrothermally altered volcanic)**: grey patina, medium-grained, granoblastic; foliated; with quartz, feldspar, biotite, garnet, sillimanite (~15% in NTS sheet 12K02 and 30% in sheet 12K01) and with or without cordierite; garnet-cordierite amoeboid or stromatitic leucosomes. Locally associated with garnetite, quartz-garnet gneiss, quartz-K-feldspar-biotite-garnet gneiss, and biotitite in sheet 12K01. The hydrothermally altered volcanic versus sedimentary protoliths are difficult to conclusively discriminate in the field. Where gneisses exhibit mineral contents that significantly differ from those typical of metapelites (see Forshaw and Pattison, 2023), the rock is preferentially interpreted as a hydrothermally altered protolith (see hydrothermal origin from a volcaniclastic protolith demonstrated in Bonnet et al., 2005; Bonnet, 2009). Some outcrops exhibit mineral contents typical of metapelites, including that of the aluminous gneiss from outcrop CQA-02-509, which contains potential detrital zircons (this work). Consequently, both protoliths are interpreted to occur in the area. Occurs in NTS sheets 12K01 and 12K02.

mPcsr3c **Composite calc-silicate–mafic unit:** Unit of calc-silicate gneiss, magnetiferous gneiss, metacarbonate, calcic plagioclasite, biotite gneiss, garnetite, and mPcsr3a amphibolite and mPcsr3b metagabbro sills. Calc-silicate rock (including diopsidite, tremolitite, hornblendite): dark to light green patina, very fine to medium grained, foliated, banded to massive; with diopside, carbonate, plagioclase and/or quartz, disseminated sulphides (pyrite, pyrrhotite, and chalcopyrite). Locally epidote and boudinaged veins of massive sulphides in the 12K02 map sheet. Carbonate rocks similar to marble but with a restricted distribution, at an angle to the stratigraphy, and adjacent to interpreted synvolcanic faults are best interpreted as carbonate hydrothermal alteration zones. The varied calc-silicate rocks are interbedded with, or adjacent to, dm to m thick layers of magnetiferous amphibolite, biotite-magnetite gneiss, garnetite, plagioclasite, and biotite-orthopyroxene gneiss in NTS sheet 12K02. In NTS sheets 12K01 and 12K02, these rocks are associated with amphibolite as well as with magnetite-dominant gneisses that are more consistent with metamorphosed stratabound hydrothermal alteration than with the previous interpretation as metamorphosed silicate banded iron formations. The unit also contains amphibolite rich in anastomosing quartz veinlets resembling stockworks and paragneiss (mPcsr1) in sheet 12K01. Fluorite-bearing calc-silicate veins occur locally in NTS sheet 12K02. Occurs in NTS sheets 12K01 and 12K02.

mPcsr3b	**Metagabbro (and metanorite in sheet 12K01) of the composite amphibolite unit**: dark green or medium to dark grey patina, medium to fine-grained (and coarse-grained in sheet 12K01), granoblastic; massive to foliated and/or lineated; with plagioclase, amphibole, orthopyroxene (metamorphic) and locally clinopyroxene, biotite, magnetite; porphyroblastic; morphological relics of a sub-ophitic igneous texture and magmatic layering or bedding; with orthopyroxene-bearing amoeboid leucosomes (in sheet 12K01). Locally cut by garnet, biotite, plagioclase, and fluorite veins in sheet 12K02. Locally in contact with marble in sheet 12K01. In sheet 12K01, these rocks were included in unit mPcsr3a in Corriveau and Bonnet (2009b) and redefined as the mPbak1 unit of the Blacklands Intrusive Suite by Daoudene and Lafrance (2025). Occurs in NTS sheets 12K01 and 12K02.
mPcsr3a	**Amphibolite of the composite amphibolite unit**: black to dark green patina, medium-grained, foliated; locally with a mottled texture in sheet 12K01; in homogeneous to heterogeneous layers ≤10 m in sheet 12K02; with hornblende, plagioclase, orthopyroxene, magnetite, and locally biotite in sheet 12K01; migmatized with orthopyroxene-bearing amoeboid to stromatitic leucosomes that are locally associated with hornblende-rich melanosomes in sheet 12K01. Occurs in NTS sheets 12K01 and 12K02.
mPcsr2c	**Grey quartzofeldspathic gneiss**: medium grey patina, fine-grained, granoblastic; homogeneous or with compositional layering highlighted by a variation in biotite content; locally nodular; with biotite and magnetite. Probable volcanic origin. Occurs in NTS sheet 12K02.
mPcsr2b	**Pink quartzofeldspathic gneiss, commonly nodular**: light pink to beige patina; fine-grained; granoblastic; granitic in composition, with biotite and magnetite. Probable volcanic origin. Contains nodules and aluminous veins of quartz, plagioclase, sillimanite, and muscovite, interpreted as being of pre-metamorphic hydrothermal origin. Occurs in NTS sheet 12K02.
mPcsr2a	**Lapillistone**: light grey to beige patina; fine- to medium-grained; granoblastic; felsic to intermediate in composition; K-feldspar, plagioclase, quartz, and biotite matrix and felsic, intermediate, or mafic lapilli; polygenic; planar fabric. Occurs in NTS sheet 12K02.
mPcsr1	**Arkose and gneissic subarkose**: medium grey patina, fine to very fine-grained; foliated, laminated and layered; quartzofeldspathic and biotite-bearing, locally epidote and garnet. The sedimentary origin is well established for the units shown in Figure 5, which is not the case for unit mPcsr4a. Occurs in NTS sheets 12K01 and 12K02.
Extension of the Wakeham Group into the Musquaro-D'Auteuil lakes region (12K07, 12K10, 12K11, 12K14)	
mPwk12	**Potential meta-exhalite and meta-inhalite and metamorphosed Fe-, Mg- or Ca-rich metasomatites**: laminated to bedded; heterogeneous; fine-to-medium grained; granoblastic; foliated. With layers of garnet-bearing quartzofeldspathic gneiss, olivine and clinopyroxene quartzitic gneiss, chloritoid-calcite or talc schist, tremolitite?, quartz-cummingtonite-plagioclase-biotite schist, biotite schist, coticule (quartz-garnet), potential iron formation (quartz-hornblende-garnet-magnetite), garnetite, garnet and locally clinopyroxene-bearing amphibolite, hornblendite, garnet and magnetite quartzite, garnet-bearing biotitite and a garnet-titanite-zircon and allanite epidosite. Garnet varies from orange with a high spessartine-component in some garnetites and in epidosite, to pink with nearly equal almandine and spessartine components in some garnetites and in amphibolite and to red with a high almandine component in some garnetites, in quartzite and in coticule. Cut by veins of calcic plagioclasite (anorthitite) with grossular and titanite. Pyrite and pyrrhotite can reach 30 vol% locally. Associated with marble and calc-silicate rocks of mPwk7d. Locally occur as enclaves in mPagn5a1 granitoids. Occurs in NTS map sheet 12K11 and 12K14.
mPwk7d	**Marble, and metacarbonate and calc-silicate rocks.** medium-to-fine grained; the metacarbonate rocks are extremely heterogeneous in terms of mafic mineral contents and distribution of calc-silicate rocks; very discontinuous in extent, commonly mylonitized, rarely form typical marble units and are interpreted as metacarbonate rocks resulting from metamorphosed hydrothermal veining and replacement. Occurs in NTS map sheet 12K11 and 12K14.
mPwk7c	**Wacke and varied paragneiss**: medium grey patina; medium- to fine-grained; foliated; with feldspar, quartz, biotite and locally garnet. Includes a localized zone of inhalite of mPwk 12. Occurs in NTS map sheet 12K11.
mPwk7b	**Wacke or nodular paragneiss**: brown or grey patina; medium- to fine-grained; foliated or layered; with feldspar, quartz, biotite, muscovite, locally garnet and sillimanite and with white, lenticular or rectangular, muscovite-rich or fibrolite-rich, K-feldspar-bearing nodules that can amount to 20% of the rock. The nodules can be distributed sporadically within the rocks or form trains of nodules that likely formed through replacement along fractures. Occurs in NTS map sheet 12K11.
mPwk7a	**Muscovite-sillimanite-bearing schist and paragneiss**: brown patina; medium- to fine-grained; foliated; with quartz, feldspar, muscovite, and sillimanite. Locally contains quartzite and other paragneisses and garnet-

	bearing rocks derived from a hydrothermally altered protolith such as garnet-rich amphibolite among quartzite. Occurs in NTS map sheet 12K11.
mPwk4e	**Granitic porphyry**: pink patina, fine-grained, granoblastic; with phenocrysts of quartz or K-feldspar in a matrix of K-feldspar, plagioclase, and quartz. Occurs in NTS map sheet 12K11.
mPwk4d	**Pink gneiss of probable volcanic origin**: pink patina, fine-grained, granoblastic; with K-feldspar, plagioclase, quartz, biotite and magnetite; locally nodular with a dark sillimanite-rich core and a margin of feldspar, muscovite and quartz. Occurs in NTS map sheet 12K11.
mPwk4c	**Banded rhyolite**: pinkish-white patina; medium- to very fine-grained, granoblastic; with quartz, feldspar, biotite, and magnetite; subparallel white and pink lamina. On an outcrop, the rhyolite and its hydrothermal alteration zones are cut by a network of anastomosing veins of varying thickness of granitic porphyry with quartz phenocrysts. Occurs in NTS map sheet 12K11.
mPwk4b	**Lapilli tuff**: pink patina; medium- to fine-grained; with feldspar, quartz, and biotite; coarse lapilli, with local casting of fragments. Locally contains altered fragments rich in epidote and magnetite. Occurs in NTS map sheet 12K11.
mPwk4a	**Lapillistone**: pink or light- to medium-grey patina; medium- to fine-grained; matrix of K-feldspar, plagioclase, quartz, and biotite in varying proportions; with intermediate to mafic lapilli; polygenic or monogenic; locally graded; planar fabric that can be primary or tectonic. Occurs in NTS map sheet 12K11.
mPwk2	**Arkose and subarkose**: pale- to medium-grey patina; fine-grained; with K-feldspar, quartz, biotite, muscovite, locally garnet; locally well-preserved sedimentary structures such as continuous, parallel laminae, convoluted laminae, and modal bedding marked by an increase in biotite content; mineral foliation defined by the preferential orientation of biotite and muscovite. Locally interbedded with arkosic wacke. Occurs in NTS sheet 12K11.
mPwk1	**Quartzitic arenite**: milky white to grey patina; medium- to fine-grained; massive (i.e. isotropic), foliated or layered; with quartz, K-feldspar, biotite; locally interbedded with hornblende-biotite schists. Occurs in NTS map sheet 12K11.

Supplementary file

The supplementary file provides the seven tables of geochronological and isotopic data in Excel spreadsheets.